No Sedimentological Evidence for Deliberate Burial by Homo naledi – A Case Study Highlighting the Need for Best Practices in Geochemical Studies Within Archaeology and Paleoanthropology

Kimberly K Foecke, Alain Queffelec, Robyn Pickering, Katerina Harvati

No Sedimentological Evidence for Deliberate Burial by *Homo naledi* – A Case Study Highlighting the Need for Best Practices in Geochemical Studies Within Archaeology and Paleoanthropology

KIMBERLY K. FOECKE*
Department of Sociology and Anthropology, George Mason University, Fairfax, VA; and, Human Origins Program, Department of Anthropology, Smithsonian Institution National Museum of Natural History, Washington D.C., USA; kfoecke@gmu.edu

ALAIN QUEFFELEC
UMR5199 - PACEA, CNRS, Université Bordeaux, Ministère de la Culture, Pessac, FRANCE; alain.queffelec@u-bordeaux.fr

ROBYN PICKERING
Department of Geological Sciences, Human Evolution Research Institute (HERI), University of Cape Town, Cape Town, SOUTH AFRICA; robyn.pickering@uct.ac.za

*corresponding author: Kimberly K. Foecke; *kfoecke@gmu.edu*

submitted: 15 November 2023; revised: 12 March 2024; revised: 16 March 2024; accepted: 5 June 2024

Handling Editor in Chief: Katerina Harvati

ABSTRACT

In mid-2023, a preprint was uploaded by some of the team working at the Rising Star Cave System in South Africa on new finds regarding the hominin *Homo naledi*. The authors reported what they claim is evidence for deliberate burials by this small-brained species and conducted extensive media engagement presenting this claim to the public, including a Netflix documentary that further amplified the claims made in the preprint. Subsequently, almost unanimously negative publicly available peer-reviews argued that the evidence presented is incomplete and inadequate to support the claims made. The authors are yet to fully address all of the issues raised in the peer-reviews. Here we present a detailed critical assessment and re-analysis of the geochemical and sedimentological data used by the authors as a cornerstone for their assertion. We find that both the theory and experimental design are not supported by the realities of the sedimentary environment and violate all prerequisites for conducting such a study. The authors do not meet minimum reporting standards for their geochemical methods, a problem stretching back to 2015 through the published material from this research team. Based on available information, we surmise that there are likely missteps in data acquisition and quantification leading to inaccurate final data values. We found deep structural issues with data analysis, visualization, and interpretation in addition to mis-characterization and mis-application of statistical methods in assessing data. We show that even if the data provided accurately represent the composition of the samples, when analyzed according to field standards the same data do not support the interpretations, conclusions, and claims made by the authors. We demonstrate that there is insufficient sampling and structured variation in the datasets to allow detection of any difference between the proposed burial features and the surrounding sediment—indeed, all sample groups fully overlap in composition. We believe that the preprint represents an example of where data analysis has been heavily influenced by a presupposed narrative. In the interest of providing broader utility to the archaeological and paleoanthropological community, we offer here an overview of best practices in geochemical data collection and handling for conducting such a study. In conclusion, we argue that from a sedimentological standpoint there is no evidence of deliberate burial of *H. naledi* remains.

INTRODUCTION

Geochemical and sedimentological methods are important tools in the paleo-sciences, widely used in establishing the context of a past event or the formation/disturbance of a site. These analyses are rapidly becoming the standard for the assessment of sedimentary features that may be related to hominin behavior (e.g., Brittingham et al. 2019; Goldberg and Berna 2010; Kanthilatha et al. 2017; Morley et al. 2019; Schlezinger and Howes 2000; Stancampiano et al. 2023; Vos et al. 2018), including investigations of body disposal and/or burial (Martinón-Torres et al. 2021). In June 2023, a preprint was uploaded purporting to show evidence of deliberate burial of the dead by a small-brained hominin, *Homo naledi* (Berger et al. 2023). This work was submitted (along with two additional preprints) to the new peer-reviewed preprint model at eLife (eLife 2022), where peer reviews are solicited and made publicly available by the journal. Prior to completion of the peer review process, the authors presented a press release, the result of which was extensive media coverage of this work. Upon their release several weeks later, the peer reviews and academic response were almost unanimously negative (Callaway 2023; Dibble 2023; Morley et al. 2023; Perry1 2023; Petraglia et al. 2023) but received little publicity. Berger et al. provided a single author response to all three sets of preprint reviews (Berger et al. 2023a). In the time since, one large-scale peer-reviewed comment and assessment of the three preprints has been published (Martinón-Torres et al. 2023) along with a peer-reviewed opinion piece that further highlights the issue (Morley et al. 2023). Here we present a detailed critical assessment of the application of the geochemical and sedimentological methods used by Berger et al. in their preprint suggesting deliberate burial (which were not addressed in depth by reviewers, the author response, or the published comment). Further, we recommend best practices for this type of approach in archaeological contexts. We present this work with the assertion that the preprint released to the media is now functionally the version of record, due to the decisions made by the authors, and is therefore open to published critique. No attempt was made to obtain additional data or records from the authors—we utilize only the information presented in the preprint, as would be the case in any published study. **We wish to be clear that this is an assessment of methods, data handling, and interpretation only, and that we do not inherently object to the idea that a small-brained hominin was capable of this type of behavior.**

Berger et al. present two separate assemblages of *Homo naledi* skeletal remains that they assert were deliberately buried in the Rising Star Cave System of South Africa. One, labeled Feature 1 (Berger et al. 2023: Figure 2), is located in the Dinaledi Chamber and was partially excavated and partly left *in situ*. The other (Berger et al. 2023: Figure 10) is located in the Hill Antechamber and was not fully excavated—rather, the sediment block was placed in plaster and removed from the site for scanning.

We focus our critique on their more complete analyses of Feature 1. Their argument for deliberate burial rests on: a) establishing that the skeletal remains are in a pit that was deliberately created based on field/excavation evidence; b) the positioning and articulation of the skeletal elements; and, c) taphonomic assessment of the skeletal remains. We again focus this critique on the first point and hope other experts in the field will address the others in due course. Berger et al. present the interpretation of intentional interment up front, followed by their evidence. They argue that their geochemical and sedimentological data establish that the chemistry/lithology within the burial features is different from other areas in the cave, following the approach used for the generally accepted burial at Panga ya Saidi (Martinón-Torres et al. 2021).

We approach our critique in three parts. In Section A, we assess the authors' analysis and interpretation of the data provided in the preprint with reference to the research question. This includes an attempt to replicate the authors' results where data are available. In Section B, we assess whether the methodologies and experimental framework selected by Berger et al. were appropriate for the research question. Finally, in Section C we assess whether the data acquisition process followed established standards and offer the community a set of best practices for the use of these methods in this context from a scientific standpoint.

SECTION A
DATA PRESENTATION, ANALYSIS, AND INTERPRETATION

Berger et al. structure their research question regarding identification of intentional burial after Martinón-Torres et al. (2021). In theory, a difference in the physical and chemical properties of the sediment between the 'burial pit' and the surrounding area may reflect digging through adjacent strata and incorporating chemically different material from those strata into the pit or fill. Berger et al. collected geochemical data from the area surrounding Feature 1 to demonstrate that Feature 1 fits this definition of a deliberately created pit. The authors used previously published petrographic analyses (including mineralogy, chemistry, and texture analyses) and newly-collected particle size distribution (PSD) and x-ray fluorescence (XRF) data as the basis for their sedimentological and geochemical assessment of this feature (Berger et al. 2023: page 27). We focus primarily on their XRF data, with some discussion of the PSD data. Berger et al. Supplementary Table 1 provides the weight percent oxide values for 12 major elements analyzed by XRF for each sediment sample, and Berger et al. Supplementary Table 2 presents values for mean, skewness, and kurtosis (PSD data) for each sediment sample. In this section, we assess their analysis, presentation, and interpretation of these two datasets in reference to their research question.

XRF DATA

Berger et al. (2023) primarily utilized principal components analysis (PCA) to analyze the XRF data reported in their Supplementary Table 1. PCA is an exploratory method

through which to present and analyze multidimensional data. It is useful in capturing the variation within datasets with high numbers of attributes per datapoint. PCA utilizes a mathematical transformation to reduce a high number of dimensions/attributes per datapoint to a more accessible number of dimensions, while retaining as much of the original information as possible. PCA is commonly utilized in geochemical analyses where data for many chemical elements is collected for each sample in a dataset.

Berger et al. (2023: Supplementary Table 1) listed the elemental oxide data acquired by XRF as raw percentages, though readers should note that standard procedure would use centered log-ratio transformed data (Aitchison and Greenacre 2002). These values were used in their PCA to assess the variation between samples. **Berger et al. also only utilize major elements to assess differences between sediments, yet it is well established that trace elements are more useful for discriminating between sediments (e.g., Potter et al. 1963; Sun et al. 2019; Vital and Stattegger 2000; Vital et al. 1999; Wang et al. 2019; Živković et al. 2021).**

Two of the elements reported by the authors (Na and S) appear to lack measurements for nearly all samples, despite the interpretation of the results directly relying on at least S (Berger et al. 2023: page 7). Some measurements are lacking for Ba, and one each for Ti and P. This is notated as "-" in their Supplementary Table 1. It is unclear what this notation indicates, other than a lack of data, and it is unclear how these missing data have been incorporated into the calculation of the PCA (in the MATLAB software) since this mathematical transformation requires a complete dataset. There is a standard recommendation for this situation in data analysis—data with more than 10% of values missing (which here would include Na and S) should be removed from the analysis entirely (Aitchison and Greenacre 2002). For rare values missing (<10% in a column), the standard method in compositional analysis would be to replace the missing values with 0.55*LOD (limit of detection) as advised by Martín-Fernandez et al. (2003). This approach is commonly used in archaeological and sedimentological research (Dayet et al. 2019; Martí et al. 2019; Mauran et al. 2021; Sitzia et al. 2017). However, it does not appear to have been implemented in Berger et al. (2023). Because PCA cannot be performed with missing data, it is possible that "-" was substituted with "0" for the PCA under the assumption that there is very little or none of that element in the sample. Testing that assumption ("-" ⟶ 0) with the data provided, we generated the PCA loadings shown in our Figures 1b, 1e, and 1h using the function *prcomp* ('stats' package in base R: R Core Team 2022). Our results were similar to the output presented by Berger et al. We tested several other scenarios, which produced largely dissimilar results. We also ran this PCA function with the standard recommended process; under this protocol, the following elements were removed from the analysis: Ba (16.25% missing data), Na (93.75% missing data), and S (90% missing data). Ideally, we would also employ the recommended replacement of rare missing data with 0.55*LOD, however, neither the instrument LOD nor the raw data with which to calculate it is reported in Berger et al. (or the references they cite for methodology). Therefore, we follow the protocol of Mauran et al. (2021) and replace rare missing values with a value equal to 10% of the lowest value measured on the other samples. This protocol generated the PCA loadings shown in our Figures 1c, 1f, and 1i. Annotated R code and data files are included in our Supplemental Information.

Our Figure 1b (*prcomp*, "-" ⟶ 0) replicates the loading plot Berger et al. present in their Figure 6 for Principal Component 1 (PC1), but we were unable to replicate their most important loading plot (PC2) shown in their Figure 3g and Figure 7. Our loading plot for PC2 (*prcomp*, "-" ⟶ 0) is shown in our Figure 1e. Our analysis also does not replicate the authors' proportions of variance explained by each PC. Berger et al. report that their PC1 explains 51% of the total variance and PC2 8%. In our analysis of these data (*prcomp*, "-" ⟶ 0), we find that PC1 explains ~33% of the total variance and PC2 ~22% (a result reproduced using another package, *FactoMineR,* in R; Lê et al. 2008). Using MATLAB as in Berger et al. with "-" replaced by "0," the PCA function returns PC1 at 80% variance explained and PC2 at 21.4% for unscaled data. Based on our ability to replicate only part of what is presented due to insufficient explanation of process and lack of script, we conclude that the authors assumed a value of zero for their "missing" data and we can only deduce that the data have been scaled in some unexplained way (otherwise the loading of Si on PC1 is very large and this is not what is reported). We suspect that this may reflect the authors' unexplained use of the function *corrplot* ("The data correlations were implemented using the function *corrplot* which uses Pearson's correlation coefficient.": Berger et al. 2023: page 27). We were unable to determine for what purpose this function would be used in relation to these data. We believe that such use is likely either unnecessary or incorrect. All of these data analysis decisions should have been explained in-text, along with the measurement parameters that led to those decisions. **To continue our analysis of this dataset, we utilized our analysis in R that best replicated parts of the results reported by Berger et al. (2023) (*prcomp*, "-" ⟶ 0). We also compared the authors' results and interpretation to our re-analysis of these data using the recommended standard procedure.**

We wish to make some brief comments on data presentation with regard to the use and reporting of PCA. Berger et al. state that "PCA is the standard method for unmixing mixed variables" (Berger et al. 2023: page 24). This appears to be a direct and uncited quote from an April 2017 blog post describing for students the process of using PCA with MATLAB (Trauth 2017). This quote is an incorrect way to describe what PCA does—PCA is used for dimensionality reduction. PCA is primarily a data visualization and data exploration method, in which the data are mathematically transformed into a new coordinate system with fewer dimensions than the initial dataset. It allows for identification of clusters and drivers of variation in the dataset. It does not "unmix" mixed variables. In addition, the plot style

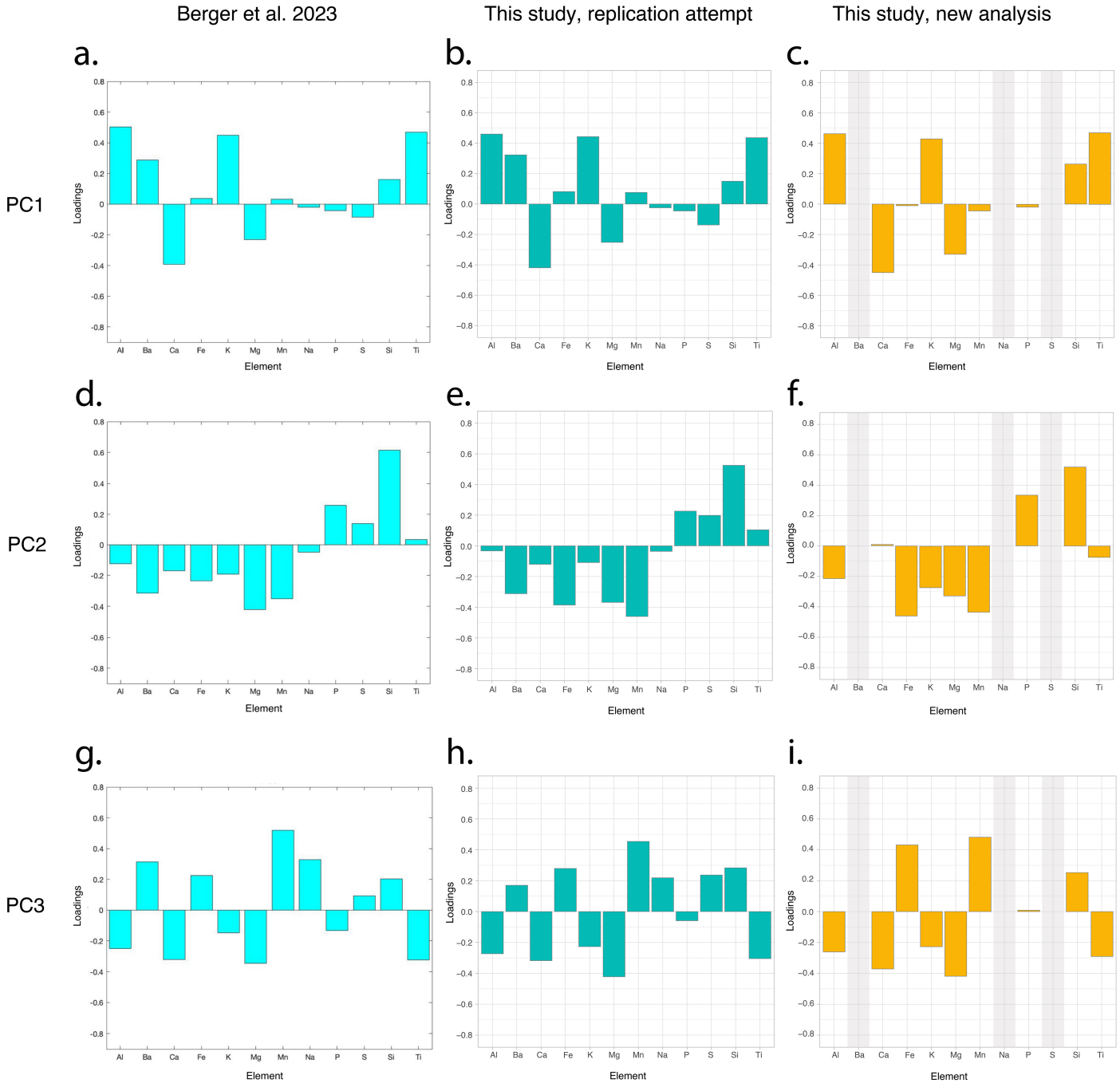

Figure 1. Loading plots for PC1, PC2, and PC3 from Berger et al. (a, d, g) and generated using data provided in Berger et al. in the same plot style. Closest replication of the results presented in Berger et al. was achieved by prcomp *in R where "-" ⟶ 0 in the data table (b, e, h). When subjected to the standard recommended data transformation procedure, our new analysis of the data generated substantially different loading plots (c, f, i).*

that Berger et al. utilize for presenting the PC scores of all samples (their Figures 3f, 6a, 7a, and 8a) appears to also come from the same blog post. This is a non-standard way to plot PC scores and does not help the reader understand the data. **It is incorrect and misleading to use a continuous line plot to connect discrete sample scores.** Score plots are almost always displayed as 2D or 3D plots using two or three PCs and superimposed 95% confidence ellipses. This maximizes the portion of total variation in the data that can be displayed, and leads to the most accurate interpretation (Jolliffe 2002; Jackson 2003). Berger et al. interpret and plot one PC at a time—unless a dataset is overwhelmingly driven by a single variable, one PC is insufficient to capture the variation in the dataset. Fallaciously, if a dataset is overwhelmingly driven by a single variable, PCA is a poor choice for visualization and assessment. The standard way to display the data presented in Berger et al. is shown in our Figure 2, including variable loading biplots, for the

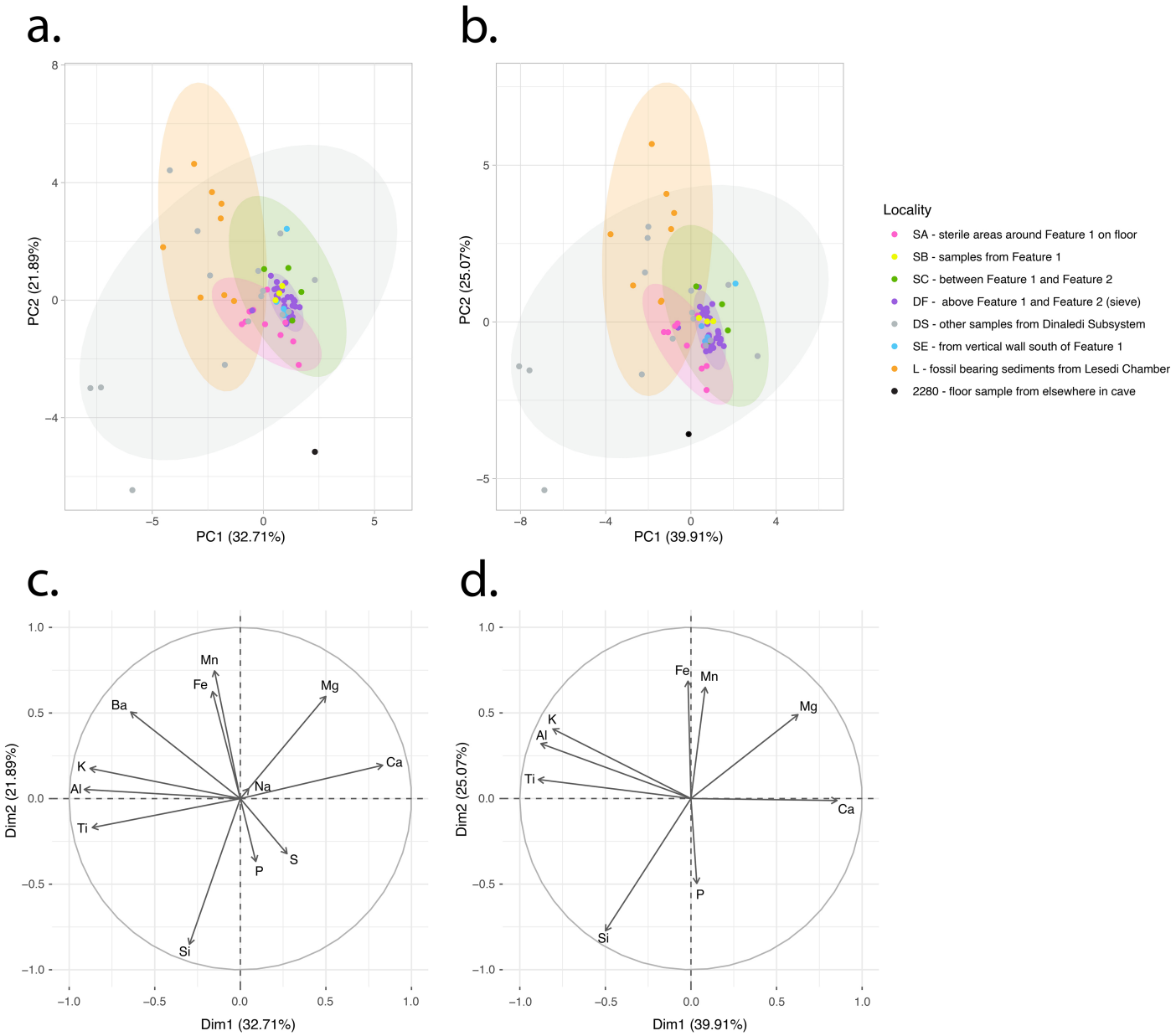

Figure 2. Score plots and variable loading biplots (PC1 and PC2) for the closest replication of the analysis in Berger et al. (prcomp, "-" ⟶ 0; a, c) and for our re-analysis using the recommended standard procedure (b, d).

closest replication of the authors' analysis (*prcomp*, "-" ⟶ 0, see our Figure 2a, 2c) and for our re-analysis using the recommended standard procedure (see our Figure 2b, 2d). We will continue to use 2D biplots with superimposed 95% confidence ellipses in our assessment.

Berger et al. (page 6) primarily utilize PC2 from their PCA to argue that there is a difference in sediment chemistry between the purported burial feature and the surrounding sediment. Though we were not able to exactly replicate their loadings, in both their and our analyses PC2 in the positive direction is driven primarily by Si and then (in order of absolute loading) P, S, and Ti. Importantly, S is only reported for eight samples, none of which are from the Dinaledi Chamber. The authors argue that these four elements are useful to distinguish fossil-bearing sediment from sterile sediment (Berger et al. 2023: page 6). This may or may not be an accurate conclusion—there is not enough information about the sediment or fossil material properties to determine if specific elements represent a fossiliferous signal exclusively. For example, it is well known that P and S are very common in organic sediments or can be inherited from the decay of organic matter present in sediments/soils. In addition, studies have shown that bat guano in caves is very rich in S and P (e.g., Queffelec et al. 2018 and references therein). Multiple scenarios could be responsible for the higher positive loadings for these elements in the Lesedi chamber samples. **It should also be noted that none of the samples taken from Feature 1 (which contains fossils) or the area around it apparently contain any S, further calling into question this element as a distinguishing**

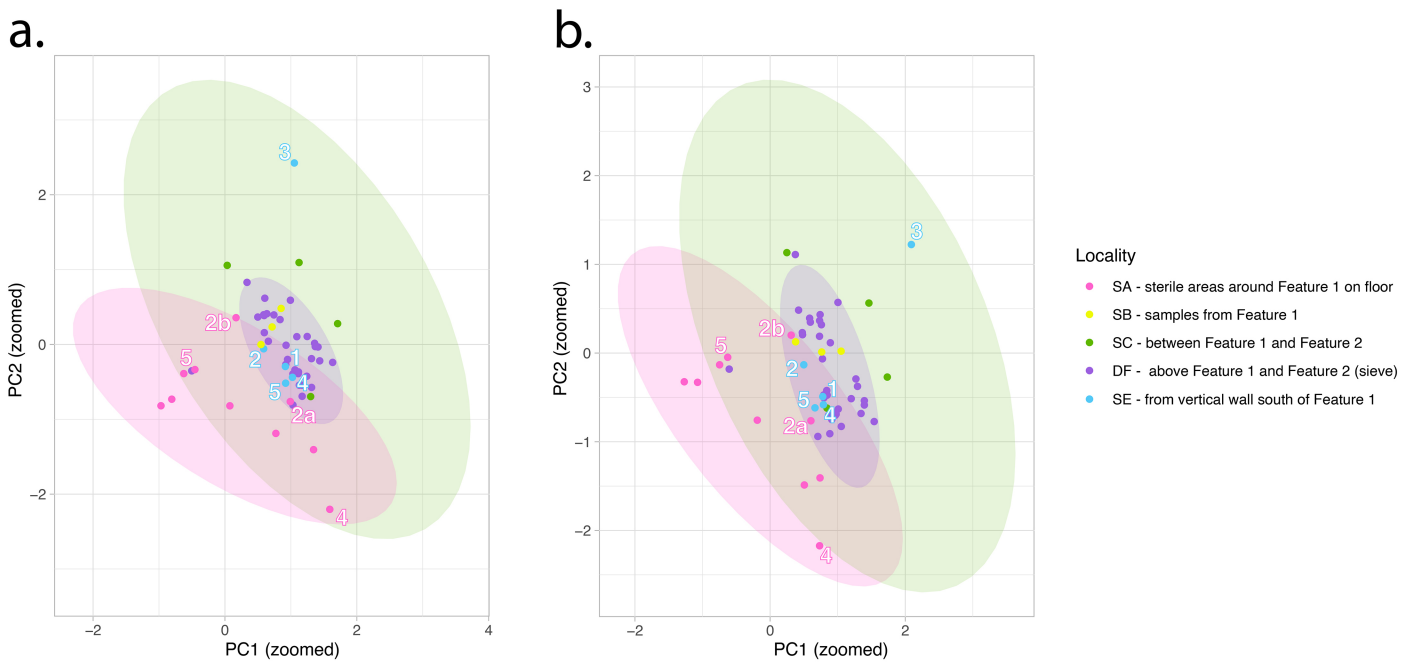

Figure 3. Subset of PCA results shown in Figure 2 (a, b). Data groups irrelevant to the research question have been removed from the visualization only. Sample number as notated in Berger et al. is provided for Localities SA and SE.

character for fossiliferous sediment in this system.

In our re-analysis, PC2 does account for the majority of the separation between Feature 1 and the areas around it. However, when plotted against PC1, this separation is minimal. We have isolated the samples in and around Feature 1 within our two PCA results to better visualize and discuss the trends (our Figure 3) because the comparison with sediments from Lesedi chamber or other chambers in the Dinaledi subsystem is not relevant to identifying a potential burial infilling at Feature 1. **There were only three samples taken within Feature 1 (group SB, with two samples being subsamples of a single sampling location), and they fall entirely within the range of variation of the Dinaledi Floor (DF) samples (samples taken from the sediment above the feature). They are also largely indistinguishable from the sediment between Feature 1 and Feature 2 (locality SC) and the entire range of samples taken from the vertical wall south of Feature 1 (locality SE).** Locality SA separates the best (still with overlap) from the other localities. This locality is described as a sample of the "sterile areas around Feature 1 on floor." Their Supplemental Figure S1a shows the locations of these samples. SA1, SA3, SA5, SA7, and SA8 come from the present-day floor surface. SA2, SA4, and SA5 are taken from some depth below the surface. That depth is not specified, and these samples do not cluster together well within the SA group. Also notice the large difference between samples SA-2a and SA-2b—subsamples of the same spot. This indicates that there may be large variation within samples and localities. This conclusion is supported upon examination of the samples from the SE group—the sample of vertical stratigraphy near the feature. Their Supplemental Figure 1b shows where these samples were taken. SE-5 is closest to the present-day floor surface while SE-1 is the deepest. By our analysis of the data provided there is almost no difference among any of these SE samples with the exception of SE-3, which appears to sample orange sediment. Sample SE-2 also may sample orange sediment but is significantly different from SE-3. **There is no indication that there is sufficient structured variation in this dataset to ask whether or not Feature 1 is different from anything else.** Interestingly, we note that in the Supplementary Information, Berger et al. state that "there are no characteristic differences with all the major elements and loss on ignition (LOI) in terms of concentration range and averages in the geochemistry of the sediments sampled from inside Feature 1, the sterile area around Feature 1, and the sediments removed above Feature 1 (Supplementary Table 1)" (Berger et al. 2023: page 28). This statement runs counter to what is presented in the main text.

As a final assessment, we elected to re-run the PCA using only those samples (groups SA, SB, SC, SE, and DF) directly related to the excavations around Feature 1. If the demonstration of a burial is contingent on establishing a difference between the feature and surrounding sediment, these samples should be the only relevant data for this question. Because these localities all lack measurements for Na and S, we removed those elements. All other data were treated in the same two ways as the above analyses. This re-analysis is presented in our Figure 4. We find the differentiation between Feature 1 and the surrounding material to be even less pronounced in this analysis. In both test cases, PC1 and PC2 each explain ~33% of the variation. The samples from within Feature 1 (SB group) span the ellipses of all other groups. PC2 does not differentiate between sterile and fossiliferous sediments, nor does it drive separation

between these groups. **Per our exhaustive analysis of the data provided (regardless of whether or not its acquisition was methodologically sound), there is no indication that this method of geochemical measurement in any way supports the conclusions of the authors.** All data and commented code for all analyses are provided in our Supplementary Information.

PARTICLE SIZE DATA

Like the XRF results, the particle size results are also presented in a non-standard format by the authors. Despite mentioning that their methodology allows them "to obtain the mean grain size, sorting, skewness and kurtosis in addition to the percentages of clay, silt and sand in each sample," (Berger et al. 2023: page 24), the authors' PSD results (their Supplementary Table 2) only include mean, skewness, and kurtosis and do not include the percentage of clay, silt, and sand. Inclusion of the latter data categories would allow for the generation of a ternary diagram, as is standard practice in sedimentology (Blott and Pye 2012, example in our Figure 5a) and has been implemented with success in burial analysis—most notably in the very study whose methodology Berger et al. claim to be following (Martinón-Torres et al. 2021: ED4). Given that all samples are (as is often the case in caves) bi-, tri-, or polymodal, these summary values are rather unhelpful in describing/defining the complex population of particles. The center of the distribution, its skewness, and kurtosis are useful for marine or river sediments which can be unimodal. In the case of polymodal samples, it is necessary to plot the frequency distribution of the samples to correctly visualize the data. In addition, it would have been more appropriate to establish a multimodal decomposition (example in our Figure 5b), as proposed by many sedimentologists (Bosq et al. 2018; Sitzia et al. 2017; Sun et al. 2002; Varga et al. 2019) and also recently applied in a burial context (Martinon-Torres et al. 2021: ED4). Instead, the authors present their result as a single figure (their Figure S13) showing the mean of the distribution of polymodal samples, making the same error as with the XRF results (discrete samples are connected via a continuous line). Again, this is misleading because there is no stratigraphic order between these samples. The samples taken from within Feature 1 (SB group) only contribute to the variability of samples in the cave —nothing more can be drawn from these data. **The caption of their Figure S13 asserts that patterns can be seen in grain size through the *in situ* stratigraphy, but as explained above, the variation of the mean of the distribution between bi-, tri- and polymodal sediment is a meaningless metric.** We also note that the authors do not integrate the particle size analysis they performed on the same samples as the XRF analysis into the main text, as would be standard practice and important for fully contextualizing geochemical data (see Pye et al. 2007). A more complete reporting of raw data would have allowed us to replicate the results and propose better representation, as we did for XRF, but there is not enough information provided in Berger et al. to achieve this.

SECTION B
CRITICAL ASSESSMENT OF RESEARCH FRAMEWORK

In Section A, we demonstrated that the XRF and PSD data as provided by Berger et al. either do not support their conclusions when analyzed using standard techniques or are not reported completely (impeding replication). In this section, we assess in detail whether the authors' methodological framework was appropriate for this application.

As outlined previously, the authors' objective is to demonstrate a chemical/lithological difference between the sediment within Feature 1 and the sediment surrounding it, under the assumption that such a difference would reflect deliberate digging through adjacent strata and incorporating chemically different material from those strata into the pit or fill. In theory, this would support deliberate burial of the remains rather than natural accumulation. The narrative of deliberate body disposal predates this paper (Dirks et al. 2015) and has been critiqued elsewhere (Egeland et al. 2018, 2022; Pettitt 2022; Val 2016). Dirks et al. (2016) do go on to state that they "recognize that mass mortality of groups of hominins within the Dinaledi Chamber, due to a death trap scenario, is possible" but this hypothesis has not been carried forward. Rather, the 2015 deliberate disposal narrative morphed into one of deliberate burial in the 2023 preprints.

We propose that the logical prerequisites for investigating deliberate burial using these methods are, at minimum, 1) the presence of non-homogeneous, structured stratigraphy in the archaeological site at large; 2) lateral exposure and assessment of stratigraphic continuity surrounding the proposed pit feature; and, 3) complete sampling and assessment of a depth profile near the feature including some distance above and below the proposed pit—this would be necessary to demonstrate that the between-strata variation is greater than the within-stratum variation. **In this section, we will demonstrate that not only does the work presented by Berger et al. not meet minimum methodological standards for this type of analysis but also violates each of these prerequisites for carrying out such a study.**

STRATIGRAPHIC ANALYSIS

Both the authors' study and our assessment rest on previous descriptions of the stratigraphy and depositional context of the cave sediments in the Rising Star Cave System (Dirks et al. 2015, 2017). As such, we begin by addressing this body of work. The Rising Star Cave System is part of the Cradle of Humankind World Heritage Site (known locally as the Cradle), which consists of a concentration of fossil-bearing cave systems hosted in the Paleo-Proterozoic Malamani Dolomites. Much has been written about the cave sediments themselves, their complexity, and how this specific karst setting has made the dating of the deposits and associated fossils more challenging than similarly aged material from the eastern African rift valley (see Edwards et al. 2023 for an overview; we do not aim to provide a detailed review of this topic here). Very simply summarized, the cave de-

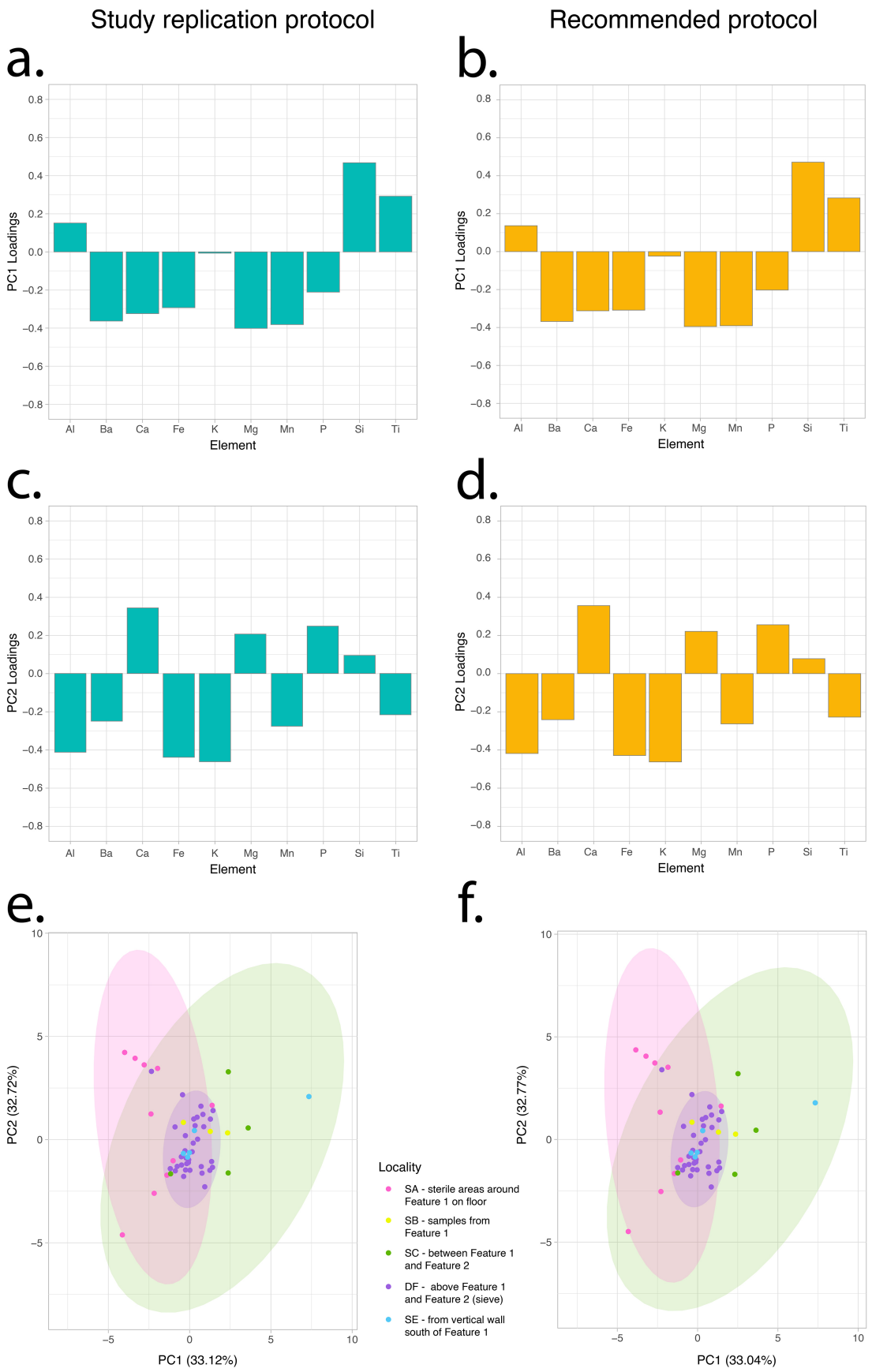

Figure 4. PCA results utilizing only data from Localities SA, SB, SC, SE, and DF presented in Berger et al. PC1 and PC2 loading plots are presented for both the study replication protocol (prcomp, *"-" ⟶ 0; a, c) and the standard recommended procedure (b, d) for data transformation. Score plots resulting from these two conditions (e, f) are presented using PC1 and PC2.*

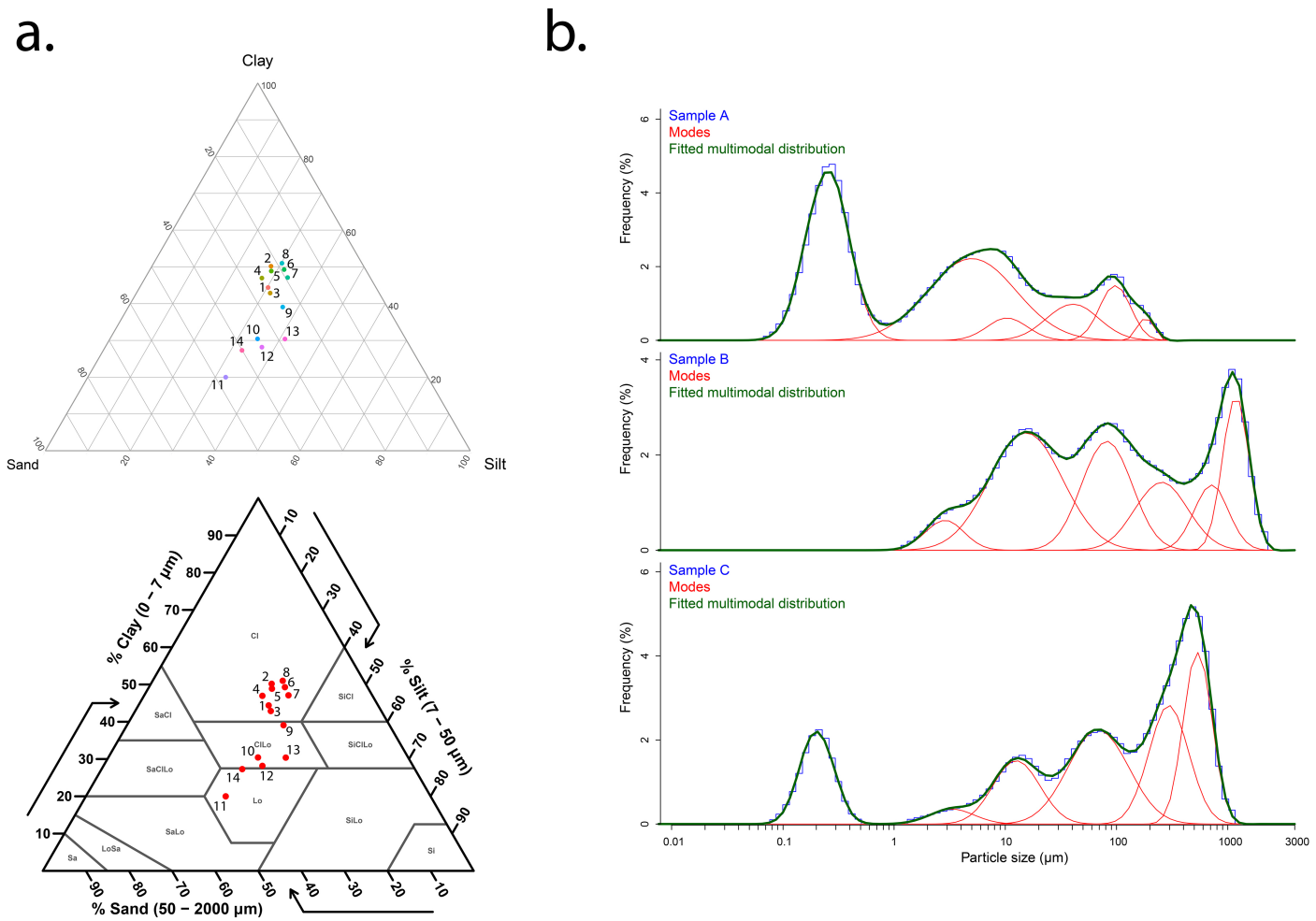

Figure 5. Example of ternary diagrams with samples from Martinón-Torres et al. 2021 (a) and multimodal decomposition of fabricated data (b) generated according to standard procedure in sedimentology for particle size analysis.

posits consist of internally derived/authigenic secondary carbonates (speleothems) and allochthonous, externally derived clastic sediments. The bulk of these sediments are washed into the caves and then hydrodynamically sorted, producing a predictable set of sedimentary facies (e.g., Edwards et al. 2023; Pickering et al. 2007), now recognized at all of the major hominin bearing cave sites across the region (Pickering et al. 2019). The majority of these cave systems have been subject to considerable surface weathering and erosion through time (up to 30m of material removed), and as a result we currently see the 'roots' of much larger cave systems exposed at the surface (Dirks et al. 2010; Edwards et al. 2020). The Rising Star system is in the minority in that the fossil bearing deposits are still underground, in a deep and complex karst system (Dirks et al. 2015). Since the discovery of the *Homo naledi* fossils within the system, these sediments have been the subject of much investigation. Work has focused on sedimentology, geochemistry, and dating (Dirks et al. 2015, 2017; Makhubela et al. 2017, 2019; Robbins et al. 2021; Wiersma et al. 2020). The deposits have been dated to between 241 and 335 ka (Dirks et al. 2017) with detailed work on the flowstones (Robbins et al. 2021), though there is some unpublished debate in the field over these conclusions. We also note that there is no consensus on the proposed history of the cave configuration. Berger et al. imply the antiquity of the inaccessibility of the Dinaledi Chamber, which is indeed central to their argument for deliberate burial through the cave system as we see it today. However, members of their own team (Robbins et al. 2021) argue that "clastic sediments entered the cave through an opening in the roof of the Postbox Chamber from about 600 ka onward, until the opening was choked by coarse breccia blocks, probably sometime after 180 ka. Depositional and erosional events changed the internal morphology of the cave chambers over time, and thereby changed the access route into the Dinaledi Chamber where the bulk of the *H. naledi* fossils were found". Robbins et al. (2021) present compelling evidence that the Rising Star cave system has undergone changes through time, the Dinaledi Chamber has not always been as inaccessible as it is now, and that during the time window during which the *H. naledi* bones were deposited there was an opening in the roof. From a

parsimonious point of view, this alone calls the deliberate disposal and/or burial hypotheses into question. Here we will not go into any more detail about the dating of the deposits, life history of the cave system, or access routes. Instead, we focus on aspects of the geological work relevant to the claims of deliberate burial.

The Rising Star sediments and stratigraphy were first presented in Dirks et al. (2015), with some revision in Dirks et al. (2017). Some additional mapping and visualizations were presented in Kruger et al. (2016). Dirks et al. (2015) presented three sedimentary units, consisting of laminated maroon mudstone (Unit 1), older mud clasts (Unit 2) and the youngest cave floor sediments, which are also mud clast breccia (Unit 3). The majority of the hominin fossils were recovered from Unit 3. Unlike most of the other cave sites in the Cradle, the Rising Star deposits are characterized by clay and silt rich sediments that are mainly attributed to *in situ* production from the weathering of the host rock dolomite. Dirks et al. (2015) argued that the chambers are too deep underground and too inaccessible for coarser grained material to have accumulated. The Proterozoic $^{40}Ar/^{39}Ar$ ages of these mud layers—the same age as the host rock dolomite (Makhubela et al. 2017)—support the hypothesis that the bulk of the sediments are not externally derived. Wiersma et al. (2020) give a detailed account of how the muddy sediments can be brecciated *in situ*.

The role of water in accumulating and reworking the sediments is unclear. Dirks et al. (2015) argued strongly that the fine-grained nature of the sediments and presence of matrix indicate that water played little part in the sediment accumulation. However, they also argued that some of the fossils have been deposited within the cave, and that their positioning (both horizontal and not) suggests a burial history involving multiple geogenic events. Dirks et al. (2015) then used the mineral staining on the bones as further evidence of reworking, erosion, and re-deposition within the cave. The presence alone of flowstones suggests periods of increased precipitation outside the cave (Pickering et al. 2007)—the sediments of Unit 2 and 3 contain multiple intercalated flowstones. Dirks et al. (2015) observed periods of erosion and slumping of the deposits (especially of Unit 2) in between the flowstone accumulation, leading to the sediment of Unit 2 being reworked and spread out along the floor of the Dinaledi Chamber. The agent of this reworking is not specified, but it is difficult to evoke anything other than water, especially given that water-lain deposits have been documented to be present within the cave by Berger et al.'s own analysis (their Figure 3d). Dirks et al. (2017) focused on dating the deposits and fossils, as well as refining their stratigraphy and recognizing sub-units within Units 1 and 3. Therein they argue that all fossils are found in sub-unit 3b and that these sediments were reworked and redistributed across the cave floor. **We argue that the geological configuration within this cave system is not compatible with a deep, well defined, and well characterized stratigraphy within which to discern a disturbance/burial, thus violating prerequisite 1 listed above for the utilization of these methods. In addition, the lack of a clear and standard presentation of the cave stratigraphy (both in detailed cross sections and global geomorphological transects) in this and previous publications complicates our ability to understand the context of any analyses conducted.**

Berger et al. lack an appropriately structured experimental framework for these purported burial features in several demonstrable areas. In excavating Feature 1, they do not sufficiently excavate the area surrounding the feature to allow for complete assessment and structured comparative sampling. **We acknowledge the merit in not fully excavating the deposits, in order to leave room for future advanced methods. However, the authors still did not excavate a large enough section to demonstrate stratigraphic continuity laterally around the feature—prerequisite 2 listed above for their research question.** Their Figures 3A and 3B show what are claimed to be two distinct lithologies in the stratigraphy of the Dinaledi floor. The skeletal remains occur in an unlithified mud clast breccia (denoted in Berger et al. as UMCB) containing laminated orange-red mud clasts (described in Dirks et al. 2015, 2017), and "[a] continuous laminated orange-red mud [LORM] layer beneath unexcavated floor surface dips near the feature, where it becomes fragmented and muddled" (Berger et al. 2023: Figure 3 caption). Their Figure 3B shows that the LORM is continuous to the right (east) of the feature, but the left of the feature was either not excavated or not shown. Their Figures 3A and 3B appear to be the same view taken at different points in the excavation process, during which the profile was advanced toward the skeletal remains from SB, as the same shiny white fragment is visible in both photos above the 5cm scale bar in their Figure 3B (see our Supplementary Figure S1). The LORM layer shown in their Figure 3B (~5cm south of SB) does not appear to be present in their Figure 3A, nor does any semblance of structured stratigraphy. They state that "this layer was not noted during our previous excavations where the clasts were reported (Dirks et al. 2015, 2017), but it is continuous in the profile immediately to the east of the feature; it is disrupted in the sediment profile at the southern extent of the feature" (Berger et al. 2023: page 6). There is no mention or illustration of the extent of the LORM layer which was apparently "continuous" but absent ~5cm to the south.

In other publications (chiefly Wiersma et al. 2020), the incorporation of the LORM layer into the UMCB is noted to be the result of an "auto-brecciation" process in which wet/dry cycles cause cracking and disintegration of the LORM into the orange clasts. **This is described as occurring throughout the cave system in a non-structured way, and would call into question the idea that this particular disturbance of the LORM was due to digging of a pit**. In all previously published work on the area directly adjacent to this feature, such disturbances are pointed to as evidence for the ways in which sediment is naturally re-worked in this system (Dirks et al. 2015, 2017; Wiersma et al. 2020). Berger et al. make no comment on the discrepancy between their description of the LORM and these prior publications. Also relevant to this point is the observation that Berger et

al. appear to have rotated their Figures 3D and 3E relative to their orientation in Figure 3C such that the lamination is oriented horizontally. The orientation of laminations to appear parallel to the floor surface as in Figure 3B implies an undisturbed sedimentary context, whereas the orientations in reality demonstrate that the sediment had been substantially re-worked. This rotation is both unnecessary and misleading.

As a final note on the context of this site and under-engagement with previous work, we assert that singling out these sets of remains as burials without providing any comparative consideration of the other hominin remains in the Dinaledi subsystem seems premature. There is currently no detailed published information on the spatial location or taphonomy for the vast majority of these remains. This same issue occurs in the lack of published information on most of the faunal remains that do occur in the cave, including a juvenile baboon skeleton deeper in the Dinaledi subsystem (Dirks et al. 2017; Elliott et al. 2021; Pettitt 2022) and an owl skeleton yet to be dated (Kruger and Badenhorst 2018).

SAMPLING STRATEGY

In selecting areas to sample for geochemical analysis of Feature 1, the authors do not sample adequately through the stratigraphic profile. Their Supplementary Figure S1 shows the locations of sampling—a photograph taken apparently at the same moment of the excavation as their Figure 3B but later than their Figure 3A. The area to the left of the feature (sample group SC), which was not shown in the profile photographs, is sampled at the depth of the feature. The area to the right of the feature showing a distinct LORM layer in their Figure 3B was not the area sampled for the depth profile. Rather, the depth profile was sampled at a location further east from the feature (profile group E – SE). Their Supplementary Figure S1b shows the locations of those samples through the profile, which appears to lack any kind of structured stratigraphy. In addition, as is the case for their Figure 3B, the allegedly continuous LORM layer, which supposedly was interrupted for the burial pit, is not visible in this profile either. **This degree of sampling would not be sufficient to establish that between-strata variation is greater than within-strata variation, which would be prerequisite 3 listed above for their research question.**

In conjunction with these issues, Berger et al. do not engage with the established literature in chemostratigraphy (Rodrigues 2005). Multiple studies have thoroughly developed and interpreted chemostratigraphic frameworks to establish disturbance (or lack thereof) at archaeological sites using the same category of analytical technique chosen by Berger et al. (Davis et al. 2012; Holcomb 2014; Holcomb and Karkanas 2019; Rowe et al. 2012; Villagran et al. 2009). In this same vein, the authors fail to address the fact that decomposing bodies have effects on surrounding sediment just as sediment composition affects the final composition of fossils. Variation in sediment composition alone may only indicate the presence of a decomposing body. In order to support intentional pit digging and burial, the sediment infill must be shown to either be from lower stratigraphic levels (requiring full comparative sampling) or brought in from another location. **The sampling strategy implemented by Berger et al. is insufficient to address their research question.**

SECTION C
CRITICAL ASSESSMENT OF DATA ACQUISITION, METHODS OVERVIEW, AND PROPOSED BEST PRACTICE GUIDELINES

We have chosen to juxtapose our assessment of the data acquisition reported in Berger et al. (2023) with some basic theory and background on these methods, in hopes that including this information in-text will be of use to other researchers in the field without specific methodological expertise who may wish to employ these methods in their work. As a research community of "method-borrowers," we have a responsibility to be informed enough about the theoretical underpinnings of the methodologies we choose in order to apply them appropriately. We present here a basic but thorough overview of how these methods work, how quantitative data can be obtained, and highlight where these topics intersect our critique. Including this section in the main text, rather than a supplemental section or reference to other literature, is a choice we are making that places these issues front and center. We believe that this inclusion provides broader utility of this work to the research community in archaeology and paleoanthropology.

X-RAY FLUORESCENCE SPECTROMETRY (XRF)

XRF is a type of spectroscopic analysis that measures secondary emitted characteristic X-rays to identify, and in some cases quantify, chemical elements. Secondary characteristic X-rays are generated following photoelectric ionization of a sample's atoms by an incident X-ray beam. Ionization by the incident beam ejects an electron from an inner electron shell, leaving a vacancy. This vacancy de-stabilizes the atom. An electron from an outer shell spontaneously releases energy to enable it to drop to a lower shell and fill the vacant spot. The amount of energy it must lose is proportional to the distance it must "fall." The distance between the shells is different for each atomic element, and therefore the energy loss required for an electron to move from outer to inner shell is unique to each element. The energy lost is emitted as an X-ray with a specific energy and wavelength. In typically analyzed elements, an atom can emit up to three series of characteristic X-rays (termed K, L, and M series in Siegbahn notation) depending upon which shells the vacancy and fill electrons occupy and how many shells they drop. The atom will continue to undergo electron shell transitions until there are only vacancies in the outer shell, resulting in a set of K, L, and M emissions that are diagnostic to the atom. The process that generates characteristic X-rays is illustrated in our Figure 6a. K, L, and M series emissions are illustrated in our Figure 6b.

There are two varieties of XRF spectrometers that col-

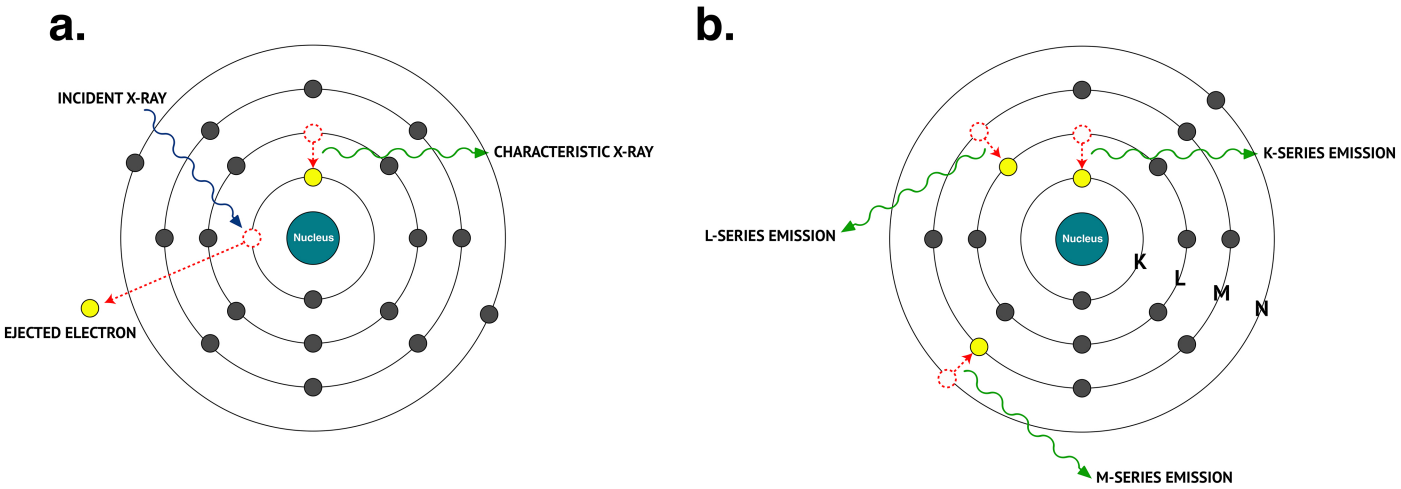

Figure 6. Schematic diagram of the generation of characteristic x-rays within an atom (a) and illustration of the three types of shell transitions that result in K, L, and M series emissions (b).

lect and measure sample-emitted characteristic X-rays in slightly different ways. Energy dispersive XRF (EDXRF) spectrometers collect all of the secondary radiation emitted from the sample and the detector separates (disperses) it by energy. This is the most common type of system, and it is generally the measurement method selected for most archaeological/cultural heritage applications. In fact, it is rare for EDXRF to be notated as anything other than "XRF" in archaeological literature. Raw data from characteristic X-rays are collected as a spectrum. Peaks in the spectrum correspond to diagnostic characteristic X-rays (K, L, and M series) for different elements. An example spectrum is shown in our Figure 7. The second possible system configuration is a wavelength dispersive XRF (WDXRF) spectrom-

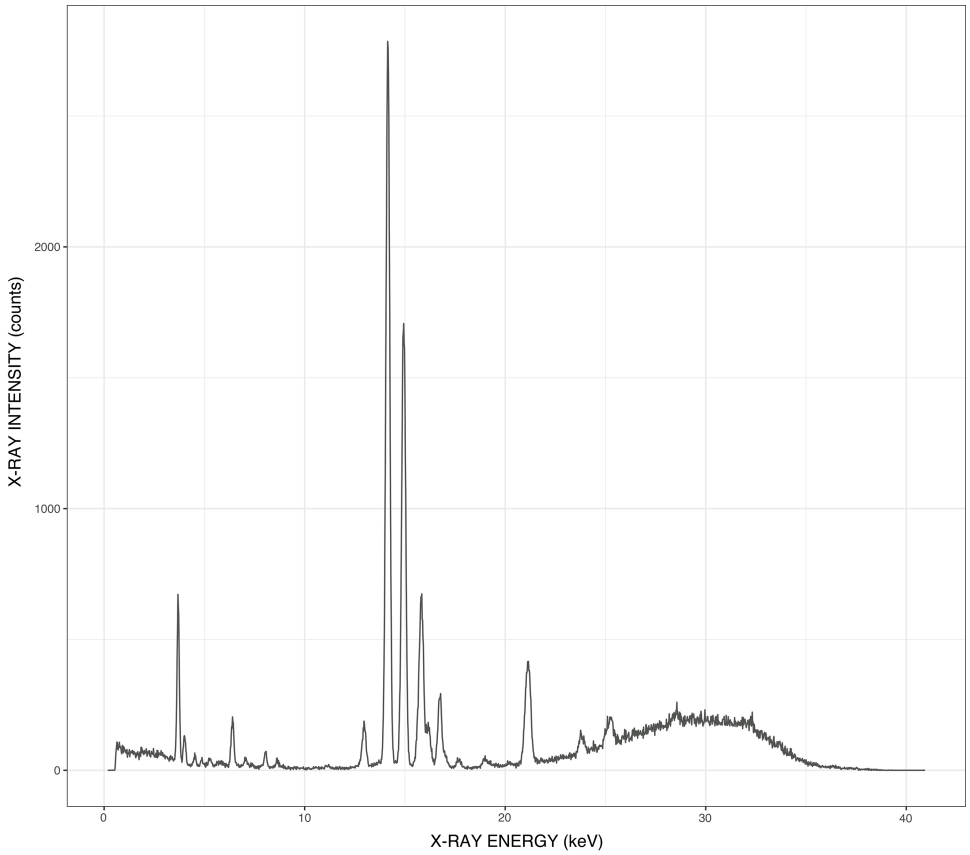

Figure 7. Example EDXRF spectrum. Data from an unpublished unidentifiable faunal fossil fragment used in start-up testing of pXRF instrumentation (Foecke et al. 2022).

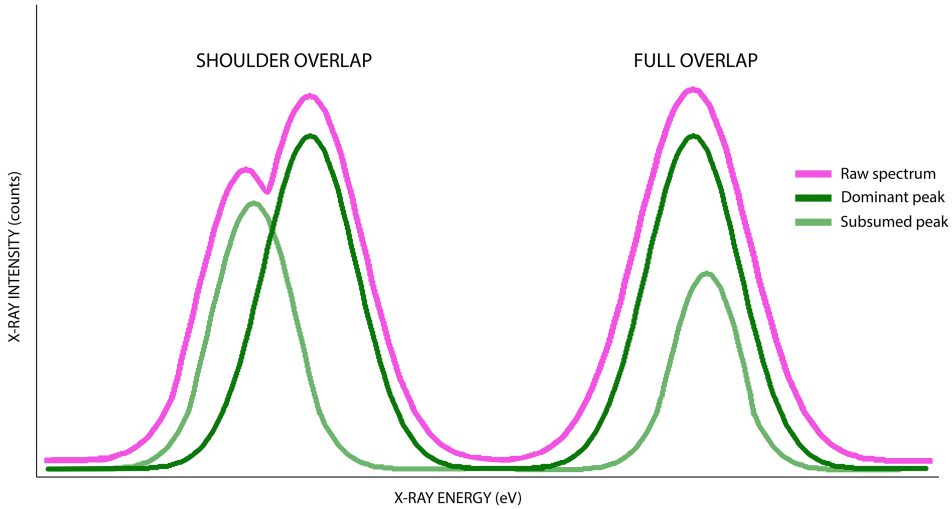

Figure 8. Schematic representation of the types of peak overlap that can occur in an XRF spectrum.

eter. WDXRF spectrometers can have specifically calibrated crystals placed between the sample and the detector. Emitted radiation from the sample hits the crystal, which diffracts X-rays of different wavelengths in different directions. By placing the detector and crystal at a specific angle, it is possible to isolate a narrow range of wavelengths (elements) of interest to enter the detector.

The raw data from both configurations is a spectrum with intensity (counts per second) on the y-axis and either X-ray energy (EDXRF) or wavelength (WDXRF) on the x-axis. WDXRF is a less common setup but has advantages in a slightly larger range of detectable elements and increased signal-to-noise ratio for elements of interest. However, the sample preparation is more involved and the system more expensive. WDXRF also does not currently have a portable version—EDXRF does, but the portability may come at a slight cost of accuracy and precision in relation to the benchtop EDXRF systems (reviewed in Kim et al. 2023) and typically removes the ability to modify calibrations (see Frahm 2013; reply by Speakman and Shackley 2013). For recent open-source resources regarding calibrations relevant to common archaeological materials, see Frahm et al. (2016) and Frahm (2019).

In terms of data acquisition methodology, Berger et al. cite Dirks et al. (2015), the first geological and taphonomic characterization of the Rising Star Cave System after the announcement of *Homo naledi*. Dirks et al. (2015) at minimum do not meet methodological reporting standards for geochemical analysis. That article contains very little information regarding analytical methods used. There is no explicit statement as to the specific variety (energy dispersive or wavelength dispersive) of XRF utilized, only that "[b]ulk chemical analyses of 4 samples were carried out by X-ray fluorescence (XRF)…" (Dirks et al. 2015). Based on the mention of the instrument used (PANalytical MagicX Pro) and a comment on "standard borate fusion," it is probable that Dirks et al. (2015) were following a protocol similar to that outlined in Taggart, Jr. and Siems (2002) (and references therein) to acquire weight percent oxides for major elements by wavelength dispersive XRF. This information should always be specified and measurement parameters outlined when reporting XRF data.

In raw form, an XRF spectrum is largely qualitative in nature—it indicates the presence of specific elements in the sample. A multi-step processing protocol is required to extract quantitative information from the spectrum.

Element Identification

Qualitative identification processes differ between EDXRF and WDXRF. Multiple factors complicate the apparently simple task of identifying the elements present in an EDXRF sample spectrum. Firstly, some elements' characteristic X-ray energies overlap (L and M series emissions of higher atomic weight elements with K series emissions of lower atomic weight elements). Smaller peaks can become subsumed by larger peaks in the spectrum, as illustrated in our Figure 8. Peak deconvolution can sometimes be performed in order to extract quantitative data from the overlapping peaks (Newbury and Ritchie 2019; Schamber 1973), but this is not always successful or recommended (Flude et al. 2017). The existence of overlaps and whether or not they are problematic for analysis is entirely dependent on the composition of the sample and which elements are of interest to the research question. In addition to overlaps, peaks can occur in a spectrum that do not correspond to a diagnostic X-ray. Interaction with the materials the detector is made of can happen (escape peaks), two X-rays can arrive almost simultaneously on the detector and be counted as a single X-ray with the sum of both energies (sum peaks), etc. These additional peaks may overlap with diagnostic sample peaks and can also be mis-identified as elements present in the sample. WDXRF, with the ability to collect a single wavelength at a time (and in theory a single peak at a time), removes some of these difficulties. However, the issue of overlapping peaks remains—while WDXRF filters which emissions are recorded by the detector, the source

generates the full spectrum of emissions. Any emissions within the wavelength range of interest will be detected, whether they come from the same element or not. WDXRF spectrometers can minimize peak overlap issues for certain elements through careful selection of the crystal and collimator configuration. When utilizing WDXRF, we recommend a procedure be implemented to assess whether a peak overlap issue is present in a given sample of unknown composition. Wavelength overlaps for all detectable elements are known (common examples listed in Feret et al. 2003: Tables 1 and 2). Selection and measurement of diagnostic L and M emissions with no overlaps can confirm the presence of elements that may have an overlap with a primary K emission. Alternatively, EDXRF can be employed to identify all elements present in the sample, thus ensuring any overlaps are accounted for in any subsequent quantitative WDXRF analysis. If overlaps occur, we recommend a conservative approach in excluding those elements from analyses. If an overlapping element is critical to analysis, assessment should be made as to whether an attempt at peak de-convolution is robust. Otherwise, a conservative approach would be to select a different analytical method for the research question. In methodological reporting for WDXRF analysis, we recommend inclusion of a comment on assessment and mitigation of peak overlaps. This information is not included in Dirks et al. (2015) (and therefore nor Berger et al. 2023).

Computation of Quantitative Data

Extraction of quantitative data from the spectrum rests on computation of the net intensity of each diagnostic elemental peak. Net intensity in EDXRF analysis is computed by integrating the area under the curve of each peak. In WDXRF analysis, net intensity corresponds to peak height with no integration necessary. An element is generally assumed to be at or above the detection limit in the sample if the net intensity is 3 times greater than the standard deviation of the background (but see Rousseau 2001). A common misconception about XRF data is that the higher the intensity, the more of that element in the sample. However, intensity does not correlate directly with the quantity of the element in the sample but is rather a complicated function of the sample matrix. True accurate quantitative XRF analysis requires the use of standard reference materials for this reason. Standard reference materials are materials for which the precise composition and material properties are known and/or manufactured. They are measured alongside the sample to calibrate the relationship between the concentrations of elements and the intensity of the emissions within a certain material for a particular spectrometer. These measurements are critical to the calculation of the concentration of different elements in the sample. Numerous standard reference materials are available for many elements and materials and must be carefully selected to complement the sample to be analyzed. Many software packages (often those sold in conjunction with instruments) include automatic peak identification and net intensity extraction functions that may or may not permit the incorporation of measured standard reference materials. Multiple studies have shown that these functions are prone to error, and that manual identification and data extraction are the recommended procedure for best results (Newbury 2005, 2007). Additionally, we wish to note here that PANalytical, the manufacturer of the instrument used by Berger et al., has an associated data analysis software that offers "standardless" analysis, the goal of which is to make the calibration independent of the compounds in the sample. "Standardless" analysis within instrument software is usually based on a set of general calibrations and does not require the user to measure standard reference materials. This is not generally advisable and tends to lead to inaccurate quantitative values (Flude et al. 2017; Newbury and Ritchie 2015), however, other procedural modifications have been shown to be effective given careful construction of the research question and assessment of methodological limitations (Hammond et al. 2019; Foecke et al. 2022; Frahm et al. 2016). Methodological reporting should always include standard reference materials utilized for each element and any relevant software parameters input for the calculation of quantitative values. This is key to reproducibility and is not reported in either Berger et al. (2023) or Dirks et al. (2015).

Sample Preparation

Sample preparation for XRF analysis can vary, with associated implications for performing quantitative analysis. XRF, in which the incident beam is an X-ray, is a non-destructive analytical technique and thus has been an appealing option for the paleo-community. Samples or objects may be analyzed intact without any preparatory procedures in many cases by EDXRF. However, unmodified bulk samples or intact objects are subject to matrix effects within the resultant data. Objects or samples containing multiple compounds or materials absorb X-rays differently, and the depth that the incident X-rays reach within the sample (and subsequently secondary X-rays escape) is dependent on the absorption qualities of the matrix. It is for this reason that researchers utilizing XRF on intact heterogeneous samples must be mindful of the interaction volume (our Figure 9) of the incident beam and where in the sample the emissions are coming from. When destructive sample preparation is an option, material may be mechanically ground into powder and pressed into pellets to homogenize the texture of the matrix and mitigate some of these effects. The most extreme option for sample homogenization is the "fusion" method, wherein the powdered sample is melted at extremely high temperatures in the presence of a binding additive to create a homogenous glass. As noted in Section A, Berger et al. collected data for major elements only, and mention the use of borate fusion (via Dirks et al. 2015). The use of a time-consuming and expensive sample preparation method like a fusion method and conducting the analysis by WDXRF would have allowed for excellent quantitative analysis of many trace elements that are often very useful in discriminating sediment origin for silica-rich sediments or similar samples like ceramics. Measurement of many

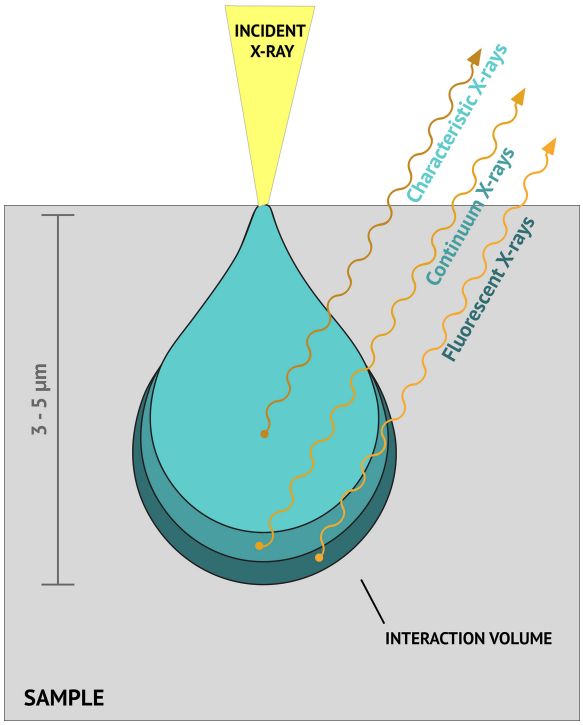

Figure 9. Illustration of X-ray interaction volume within the upper depth of a solid sample.

trace elements is possible under this methodology, including V, Cr, Ni, Cu, Zn, Ga, As, Rb, Sr, Y, Zr, Pb, and Th (e.g., Živković et al. 2021). Elements within this category are also detectable and quantifiable (with a slightly reduced degree of precision) using the more accessible EDXRF method on bulk samples or intact objects (e.g., Foecke et al. 2022; Hammond et al. 2019).

In including the above overview, we hope to emphasize the need for studies utilizing XRF to report detailed methodological parameters—especially if quantitative data are generated. This is a standard expectation for publications in this area (Holmqvist 2016; Rousseau 2001). Berger et al. (2023: page 24) state that "the methodologies, software, and measurement parameters/conditions for XRD, XRF and SEM were as used for Dirks et al. (2015) at the Spectrum Analytical Facility of the University of Johannesburg (UJ)." No other information on sample preparation, data acquisition, data processing, or standard reference materials is provided. None of this information is reported in the reference cited (Dirks et al. 2015). As demonstrated in this paper, this information is necessary in order for the analysis to be accurately reviewed and replicated.

PARTICLE-SIZE DISTRIBUTION (PSD)

Berger et al. primarily rely on their XRF analysis for their conclusions, but also collected particle size distribution data for the relevant sediments. This type of analysis is generally complementary to geochemical data (e.g., Guagliardi et al. 2013; Spagnoli et al. 2008; Wu et al. 2022) but is not addressed or integrated with any other data in their analysis. As in the XRF analysis, the methodology reported by Berger et al. for particle-size analysis is very sparse. No information on sample preparation is provided—the authors only describe the instrument that was used and in which laboratory the analyses were carried out (Berger et al. 2023: page 24) and make a brief mention of field sampling (Berger et al. 2023: page 29). For broader utility to the research community, here we provide a limited overview and critique, and underscore that thorough methodological reporting is key to analytical reproducibility.

PSD measures the size of particles in a sample and quantifies their frequency. It is used in several disciplines, but is especially common in sedimentology where particle size of sediments is informative of origin, process of deposition, energy of the deposition media, and (potentially) of post-depositional processes (Bieganowski et al. 2018; López 2017). The main measurement method utilized in sedimentological analysis is currently the light diffraction method that allows for high reproducibility of the distribution of a large range of size of particles, from several nanometers to several millimeters in a single measurement (Yang et al. 2019). Particle size analysis by laser-diffraction analyzer relies on: 1) the sample selection and preparation; 2) the measurement of the diffraction pattern in the instrument; and, 3) the mathematical reconstruction of the distribution based on the measured diffraction pattern (our Figure 10). All these parameters are key to achieve reliable measurements of the PSD of a sample (Bieganowski et al. 2018).

Field Sampling

Samples for PSD, as for any other sedimentological analysis, must be selected following a specific strategy. This strategy depends on the sediment and the stratigraphy of the site and must be adapted to the conditions and context present. In cases of well-defined strata it may be one sample for each layer, or samples could be taken at intervals (2cm/5cm/10cm) for thick layers, very simple stratigraphy, or in cores. The volume of the sample should also be dependent on the size of the particles of which it is composed, to ensure that the sample is representative. Unfortunately, it is not possible to put a large quantity of sediment into a laser particle-sizer because the light scattering would be induced by multiple particles before arriving at the detector. In cave systems, mixing of very fine particles (clays) with sandy elements makes this analysis even more complicated, as in order to achieve a representative sample for the coarse particles it is necessary to increase the sample volume. Particle-sizers with large water containers are therefore favored for these kinds of samples, allowing for dispersion of clays even if the total sample volume is larger. In a cave system such as Rising Star, reporting sampling parameters is crucial for assessment of the resultant PSD data. The only mention of field sampling protocol states that "the SA and SE groups were sampled in situ at various depths and so their mean grain sizes show patterns of upward fining sequences (Figure S13). The DF group of samples are also from various depths of 0 to 15 cm, but the sediments of each sample were mixed during sieving" (Berger et al.

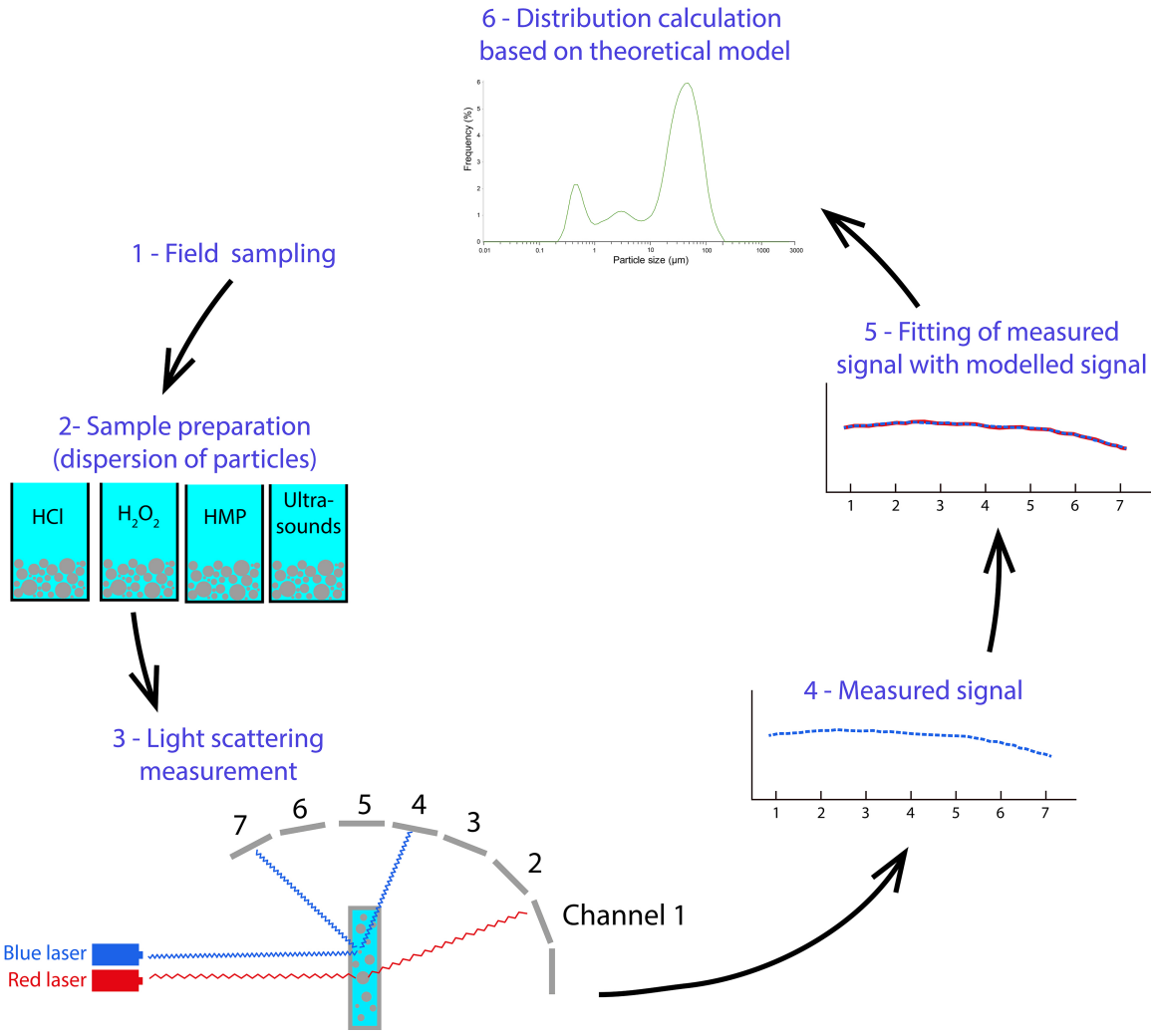

Figure 10. Schematic workflow for measurement and calculation of sample particle size distribution.

2023: page 29). This information is insufficient, and the latter statement calls into question the representative nature of the samples.

Preparation of Sedimentological Samples

After careful selection of sediment samples in the field, sample preparation is key before undertaking any analysis (Makó et al. 2014). Particles in sediment agglomerate rapidly due to organic matter content, compaction, concretions, and other factors and therefore must be dis-aggregated prior to measurement. Publications having undertaken analysis by this method should clearly explain the sample preparation procedure, which varies but can include dissolution of carbonates with hydrochloric acid, destruction of organic matter with hydrogen peroxide, chemical dispersion with sodium hexametaphosphate, and physical dispersion in ultrasonic baths. Sample preparation strongly impacts reproducibility with this technique and is important to report in detail, especially when practices may vary between laboratories. The choice of whether or not to disintegrate agglomerated particles (e.g., mud clasts), authigenic concretions (e.g., manganese oxides, carbonated concretions) is important for the interpretation of the result—whether the aim is to describe the original sediment or the current state of the deposit. Methodological reporting should include this information.

Measurement of Particle Size

Laser particle sizers utilize the diffraction of light by particles in a sample, which depends (for constant refractive index) on the size of the particles—smaller particles diffract at higher angles than large particles. To improve the measurement of a large range of particle sizes, recent instruments use two (or more) different wavelengths—a long wavelength (red laser) for large particles and a short wavelength (blue laser) for small particles. The diffracted light is collected by detectors located at different angles around the measurement cell in which the sample, diluted in water, continuously passes. These detectors measure the amount of light they receive and subtract the background light when no sample is flowing in the measurement cell (blank correction). The pattern and intensity of light received by the various detectors form the raw data that is then processed to obtain the particle size distribution of the sample.

Berger et al. do not report which emissions were used for the measurement, but the system used (Microtrac S3500 – Berger et al. 2023: page 24) apparently possesses three different red lasers (Microtrac 2023).

Computation of the Size Distribution

The mathematical computation of the frequency distribution of particles in the sample based on the measured light pattern relies on Maxwell's equations. These equations have two different possible solutions that are used in the case of light diffraction, and are both implemented in all modern particle sizer software. The first possible solution to Maxwell's equation is from Fraunhofer, which is simpler in its assumption that the particles in the sample are spherical and opaque. This solution works extremely well for large particles. The second possible solution is the Lorenz–Mie–Debye solution (better known as the Mie solution) and does not assume that the particles are opaque but rather uses their refractive index to calculate the diffraction of light. This solution, which is more sophisticated and has been integrated in particle sizer software for decades, provides optimal results for smaller particles that are mainly non-opaque to light. It is of tremendous importance to know which solution was used, and, if the Mie solution was applied, to know the refractive index used for the calculation. This is key to the final calculated distribution (our Figure 11). The solution to Maxwell's equation used is not indicated in Berger et al. and none of the mathematical parameters for the calculation of the distribution are given. It is important to stress that the result of such an analysis is the volumetric distribution of spherical particles that would have theoretically given the measured light diffraction pattern if analyzed. This is not perfect, as sedimentologists may be interested in the number of particles rather than the volume each size fraction represents. Additionally, in reality, particles (especially small ones) are likely not spherical. Nonetheless, the method allows for robust inter-comparison of samples. Berger et al. do report that "the obtained results were reduced using GRADISTAT, the grain size and statistics package (Blott and Pye 2001), and selecting the Folk and Ward Method to obtain the mean grain size, sorting, skewness and kurtosis in addition to the percentages of clay, silt and sand in each sample" (Berger et al. 2023: page 24). This information is relevant only to the statistical computation of the listed metrics and implies nothing regarding the actual data acquisition.

We offer Section C of this paper as both a critique and a simple and targeted guide to precise decision making in study design. These analytical methods are powerful tools in archaeological science but must be applied within their own constraints with full understanding of the data that they generate.

CONCLUSIONS

In this paper, we endeavored to not only provide a scientific critique of a specific body of research but also to illustrate the need for adherence to methodological and reporting best practices when utilizing geochemical and sedimentological techniques. The application of these methods to paleoanthropology is becoming progressively more important and offers the opportunity to investigate in more detail archaeological, paleoanthropological, and even genetic aspects of hominins. Through juxtaposition of detailed critique with theoretical background, we show that the preprint released by Berger et al. does not meet established scientific standards. The problems identified are cumulative, resulting in unsupported conclusions. At the highest level, the research question as stated has three prerequisites—each of which are not met. First, this work (and previous work by this team) does not demonstrate that the site contains sufficiently structured and non-homogeneous stratigraphy to enable the analysis attempted. Second, this area of the site does not preserve lateral stratigraphic continuity around the feature of interest, eliminating the ability to detect, let alone measure, disturbance of strata. Lastly, the sampling strategy was insufficient to demonstrate that between-strata variation is greater than within-stratum variation. This would be necessary to identify disturbance of one stratum into another, as proposed by the authors for the digging and infill of a burial pit. Many methodologies exist other than those chosen by Berger et al. for the analysis of the types of features present in the Rising Star system. Though unsystematic petrographic thin sections are included, particularly conspicuous in its absence is a thorough micromorphological analysis (noted by multiple peer-reviewers), which has been applied to archaeological and natural sediments in cave contexts and has solidly demonstrated its ability to distinguish the sedimentary processes driving the formation of deposits, the effects of human actions (including digging into natural sediments), and post-depositional (weathering) events that modified sediments and archaeological materials (bones and artifacts) buried within them.

At the level of data acquisition, we show that, at minimum, the work presented does not provide sufficient methodological reporting. Through detailed assessment, we hypothesize the existence of methodological errors relating to sample preparation, the use of standard reference materials, and quantitative data transformations that call into question the accuracy of the reported XRF and PSD data. Even if these data are reliable, our analysis revealed missteps in data analysis, presentation, and interpretation. The authors incorrectly utilized PCA in identification of purported differences between samples, which were the foundation of their argument for a deliberately dug burial pit. Our re-analysis shows these proposed differences to be non-existent.

We wish to conclude with some general comments on scientific procedure in the field of paleoanthropology. To be clear—we do not dispute that it is possible that a small-brained hominin engaged in "complex" behavior, and are quite open to and excited by that prospect and its broader implications for human evolution. An ever-increasing body of work indicates a need to re-orient old frameworks in light of new data. This is expected and welcomed, and is a key component in how science functions. Presenting and

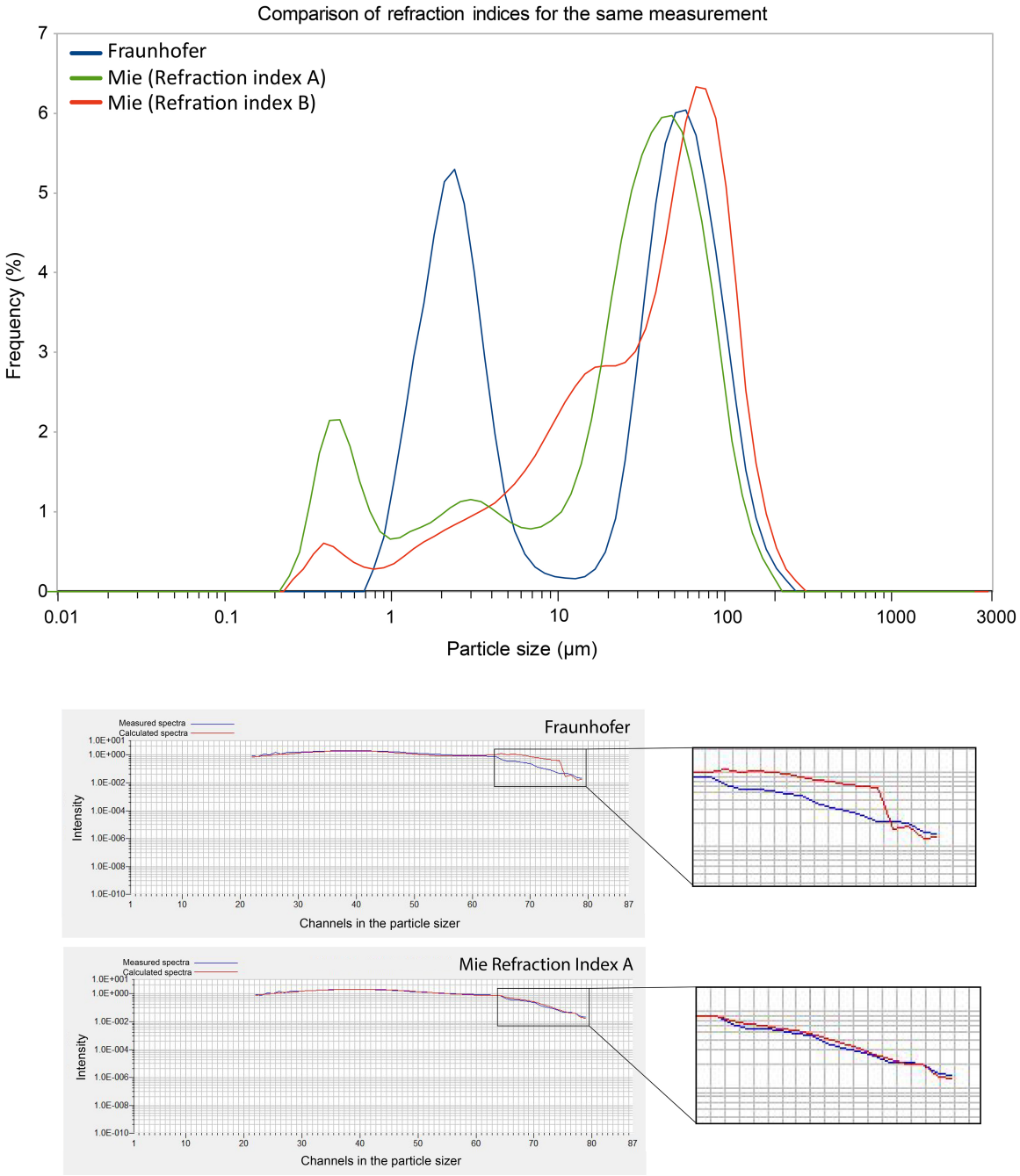

Figure 11. Illustration of the effect of mathematical solution to Maxwell's equations as applied to the same sample (loess sediment from Lautagne, SE France). Note that the Fraunhofer and Mie solutions produce different particle size distributions (top) and different success at fitting the measured spectra (bottom).

testing bold ideas pushes our field forward and is a necessary part of the scientific process. The critique we present here is not of an idea, but purely of scientific procedure—an assessment of method, data, and what those data do and do not support. **Here the interpretations, the narrative, and the data are not aligned.**

As a field, we must reflect on how we structure research questions and consider the balance between exploratory research and hypothesis testing that is so central to what we do. In the author response to the public peer reviews, the following is stated: "We suggest that it may be damaging to take "natural accumulation" as the standard null hypothesis for paleoanthropology, and that it is more conservative in practice to engage remains with the null hypothesis of possible cultural formation." The data presented by Berger et al., on our re-analysis, do not support cultural formation, so calling for such a radical change in approach is both unwarranted and premature. We categorically reject this statement and wish to emphasize the central importance of natural accumulation as the null hypothesis in paleoanthropological research on possible interments.

ACKNOWLEDGEMENTS

We have chosen to expand involvement in this work beyond the established norms due to the unusual situation resulting from the events leading to submission of our response to Berger et al. We define here a group of Endorsing Scholars who were invited to assess this work prior to manuscript submission and present comments, suggestions, and additions. These individuals were then offered the opportunity to sign their name to this work in support of this critique. We thank (in alphabetical order): Stefano Costanzo, Flint Dibble, Tara Edwards, Ellery Frahm, Kim Genuite, Huw Groucutt, Andy I.R. Herries, Jamie Hodgkins, Justin A. Holcomb, Makarius Itambu, Dipuo Winnie Kgotleng, George M. Leader, Guilhem Mauran, Ryan McRae, Kathleen Nicoll, Robert Patalano, Paul Pettitt, Michael Petraglia, Travis Rayne Pickering, Luca Sitzia, Chris Stantis, Mathew Stewart, Chris Stringer, Benjamin Utting, E. Grace Veatch, Manuel Will, Rebecca Wragg Sykes, and Andrea Zerboni. We also thank Mike Morley and two anonymous reviewers, whose thoughtful and thorough feedback enhanced this work.

DATA AVAILABILITY STATEMENT

All data and commented code for all analyses are provided in the Supplementary Information.

REFERENCES

Aitchison, J., Greenacre, M., 2002. Biplots of compositional data. J. R. Stat. Soc. Ser. C Appl. Stat. 51, 375–392.

Berger, L.R., Fuentes, A., Hawks, J., Makhubela, T., 2023a. Author response to peer-reviews of "Evidence for deliberate burial of the dead by *Homo naledi*" [WWW Document]. eLife. https://elifesciences.org/reviewed-preprints/89106/reviews#author-response

Berger, L.R., Makhubela, T., Molopyane, K., Krüger, A., Randolph-Quinney, P., Elliott, M., Peixotto, B., Fuentes, A., Tafforeau, P., Beyrand, V., Dollman, K., Jinnah, Z., Gillham, A.B., Broad, K., Brophy, J., Chinamatira, G., Dirks, P.H.M., Feuerriegel, E., Gurtov, A., Hlophe, N., Hunter, L., Hunter, R., Jakata, K., Jaskolski, C., Morris, H., Pryor, E., Ramaphela, M., Roberts, E., Smilg, J.S., Tsikoane, M., Tucker, S., Rooyen, D. van, Warren, K., Wren, C.D., Kissel, M., Spikins, P., Hawks, J., 2023b. Evidence for deliberate burial of the dead by *Homo naledi*. eLife 12, RP89106.

Bieganowski, A., Ryżak, M., Sochan, A., Barna, G., Hernádi, H., Beczek, M., Polakowski, C., Makó, A., 2018. Chapter Five - Laser diffractometry in the measurements of soil and sediment particle size distribution. In: Sparks, D.L. (Ed.), Advances in Agronomy. Academic Press, Cambridge, MA, pp. 215–279.

Blott, S.J., Pye, K., 2012. Particle size scales and classification of sediment types based on particle size distributions: review and recommended procedures. Sedimentology 59, 2071–2096.

Bosq, M., Bertran, P., Degeai, J.-P., Kreutzer, S., Queffelec, A., Moine, O., Morin, E., 2018. Last Glacial aeolian landforms and deposits in the Rhône Valley (SE France): spatial distribution and grain-size characterization. Geomorphology 318, 250–269.

Brittingham, A., Hren, M.T., Hartman, G., Wilkinson, K.N., Mallol, C., Gasparyan, B., Adler, D.S., 2019. Geochemical evidence for the control of fire by Middle Palaeolithic hominins. Sci. Rep. 9, 15368.

Callaway, E., 2023. Sharp criticism of controversial ancient-human claims tests eLife's revamped peer-review model. Nature 620, 13–14.

Davis, L.G., Macfarlan, S.J., Henrickson, C.N., 2012. A PXRF-based chemostratigraphy and provenience system for the Cooper's Ferry site, Idaho. J. Archaeol. Sci. 39, 663–671.

Dayet, L., Faivre, J.-P., Le Bourdonnec, F.-X., Discamps, E., Royer, A., Claud, E., Lahaye, C., Cantin, N., Tartar, E., Queffelec, A., Gravina, B., Turq, A., d'Errico, F., 2019. Manganese and iron oxide use at Combe-Grenal (Dordogne, France): a proxy for cultural change in Neanderthal communities. J. Archaeol. Sci. Rep. 25, 239–256.

Dibble, F., 2023. *Homo naledi* burial? A public peer review of the evidence [WWW Document]. Archaeology with Flint Dibble. https://www.youtube.com/watch?v=9iN9t393QQI (accessed 11.8.23).

Dirks, P.H., Roberts, E.M., Hilbert-Wolf, H., Kramers, J.D., Hawks, J., Dosseto, A., Duval, M., Elliott, M., Evans, M., Grün, R., Hellstrom, J., Herries, A.I., Joannes-Boyau, R., Makhubela, T.V., Placzek, C.J., Robbins, J., Spandler, C., Wiersma, J., Woodhead, J., Berger, L.R., 2017. The age of *Homo naledi* and associated sediments in the Rising Star Cave, South Africa. eLife 6, e24231.

Dirks, P.H.G.M., Berger, L.R., Hawks, J., Randolph-Quinney, P.S., Backwell, L.R., Roberts, E.M., 2016. Comment on "Deliberate body disposal by hominins in the Dinaledi Chamber, Cradle of Humankind, South Africa?" [J. Hum. Evol. 96 (2016) 145–148]. J. Hum. Evol. 96, 149–153.

Dirks, P.H.G.M., Berger, L.R., Roberts, E.M., Kramers, J.D., Hawks, J., Randolph-Quinney, P.S., Elliott, M., Musiba, C.M., Churchill, S.E., De Ruiter, D.J., Schmid, P., Backwell, L.R., Belyanin, G.A., Boshoff, P., Hunter, K.L., Feuerriegel, E.M., Gurtov, A., Harrison, J.D.G., Hunter, R., Kruger, A., Morris, H., Makhubela, T.V., Peixotto, B., Tucker, S., 2015. Geological and taphonomic context for the new hominin species *Homo naledi* from the Dinaledi Chamber, South Africa. eLife 4, e09561.

Dirks, P.H.G.M., Kibii, J.M., Kuhn, B.F., Steininger, C., Churchill, S.E., Kramers, J.D., Pickering, R., Farber, D.L., Mériaux, A.-S., Herries, A.I.R., King, G.C.P., Berger, L.R., 2010. Geological setting and age of *Australopithecus sediba* from southern Africa. Science 328, 205–208.

Edwards, T.R., Pickering, R., Mallett, T.L., Herries, A.I.R., 2020. Reconstructing the depositional history and age of fossil-bearing palaeokarst: a multidisciplinary ex-

ample from the terminal Pliocene Aves Cave Complex, Bolt's farm, South Africa. Results Geophys. Sci. 1–4, 100005.

Edwards, T.R., Pickering, R., Mallett, T.L., Herries, A.I.R., 2023. Challenging the antiquity of the Cradle of Humankind, South Africa: geochronological evidence restricts the age of *Eurotomys bolti* and *Parapapio* to less than 2.3 Ma at Waypoint 160, Bolt's Farm. J. Hum. Evol. 178, 103334.

Egeland, C.P., Domínguez-Rodrigo, M., Pickering, T.R., Menter, C.G., Heaton, J.L., 2018. Hominin skeletal part abundances and claims of deliberate disposal of corpses in the Middle Pleistocene. Proc. Nat. Acad. Sci. U.S.A. 115, 4601–4606.

Egeland, C.P., Pickering, T.R., Fadem, C.M., Domínguez-Rodrigo, M., 2022. Back from the dead: another response to the contextual bases of the Rising Star "deliberate body disposal" hypothesis. S. Afr. J. Sci. 118, 1–2.

eLife, 2022. eLife's new model: changing the way you share your research | Inside eLife | eLife [WWW Document]. https://elifesciences.org/inside-elife/54d63486/elife-s-new-model-changing-the-way-you-share-your-research (accessed 11.5.23).

Elliott, M., Makhubela, T., Brophy, J., Churchill, S., Peixotto, B., Feuerriegel, E., Morris, H., Van Rooyen, D., Ramalepa, M., Tsikoane, M., Kruger, A., Spandler, C., Kramers, J., Roberts, E., Dirks, P., Hawks, J., Berger, L., 2021. Expanded explorations of the Dinaledi subsystem, Rising Star Cave system, South Africa. PaleoAnthropology 2021, 15–22.

Feret, F.R., Hamouche, H., Boissonneault, Y., 2003. Spectral interference in X-ray fluorescence analysis of common materials. In: JCPDS (Ed.), Proceedings of the Denver X-Ray Conference. Presented at the Advances in X-Ray Analysis, International Center for Diffraction Data, Denver, CO, pp. 381–387.

Flude, S., Haschke, M., Storey, M., 2017. Application of benchtop micro-XRF to geological materials. Mineral. Mag. 81, 923–948.

Foecke, K.K., Hammond, A.S., Kelley, J., 2022. Portable x-ray fluorescence spectroscopy geochemical sourcing of Miocene primate fossils from Kenya. J. Hum. Evol. 170, 103234.

Frahm, E., 2013. Validity of "off-the-shelf" handheld portable XRF for sourcing Near Eastern obsidian chip debris. J. Archaeol. Sci. 40, 1080–1092.

Frahm, E., 2019. Introducing the Peabody-Yale Reference Obsidians (PYRO) sets: open-source calibration and evaluation standards for quantitative X-ray fluorescence analysis. J. Archaeol. Sci. Rep. 27, 101957.

Frahm, E., Monnier, G.F., Jelinski, N.A., Fleming, E.P., Barber, B.L., Lambon, J.B., 2016. Chemical soil surveys at the Bremer Site (Dakota county, Minnesota, USA): measuring phosphorous content of sediment by portable XRF and ICP-OES. J. Archaeol. Sci. 75, 115–138.

Goldberg, P., Berna, F., 2010. Micromorphology and context. Quatern. Int. 214, 56–62.

Guagliardi, I., Apollaro, C., Scarciglia, F., De Rosa, R., 2013. Influence of particle-size on geochemical distribution of stream sediments in the Lese river catchment, southern Italy. Biotechnol. Agron. Soc. Environ. 17, 43–55.

Hammond, A.S., Foecke, K.K., Kelley, J., 2019. Hominoid anterior teeth from the late Oligocene site of Losodok, Kenya. J. Hum. Evol. 128, 59–75.

Holcomb, J.A., 2014. Expanding the Chemostratigraphic Framework of the Cooper's Ferry Site (10IH73) Using Portable X-Ray Fluorescence Spectrometry. M.A. Thesis. Oregon State University.

Holcomb, J.A., Karkanas, P., 2019. Elemental mapping of micromorphological block samples using portable X-ray fluorescence spectrometry (pXRF): integrating a geochemical line of evidence. Geoarchaeology 34, 613–624.

Holmqvist, E., 2016. Handheld portable Energy-Dispersive X-Ray Fluorescence spectrometry (pXRF). In: Hunt, A. (Ed.), The Oxford Handbook of Archaeological Ceramic Analysis. Oxford University Press, New York, pp. 363–381.

Jackson, J.E., 2003. A User's Guide to Principal Components, Wiley series in probability and statistics. Wiley, Hoboken, N.J.

Jolliffe, I.T. (Ed.), 2002. Graphical srepresentation of data using principal components. In: Joliffe, I.T. (Ed.), Principal Component Analysis. Springer Series in Statistics. Springer, New York, pp. 78–110.

Kanthilatha, N., Boyd, W., Chang, N., 2017. Multi-element characterization of archaeological floors at the prehistoric archaeological sites at Ban Non Wat and Nong Hua Raet in Northeast Thailand. Quatern. Int. 432, 66–78.

Kim, Junkyu, Park, J.-W., Kim, H., Oh, Y., Park, J., Conte, M., Kim, J., 2023. Selecting reproducible elements in non-destructive portable X-ray fluorescence analysis of prehistoric and early historical ceramics from Korea. J. Archaeol. Sci. Rep. 47, 103788.

Kruger, A., Badenhorst, S., 2018. Remains of a barn owl (*Tyto alba*) from the Dinaledi Chamber, Rising Star Cave, South Africa. S. Afr. J. Sci. 114, 1–5.

Kruger, A., Randolph-Quinney, P., Elliott, M., 2016. Multimodal spatial mapping and visualisation of Dinaledi Chamber and Rising Star Cave. S. Afr. J. Sci. 112, 1–11.

Lê, S., Josse, J., Husson, F., 2008. FactoMineR: an R package for multivariate analysis. J. Stat. Softw. 25, 1–18.

López, G.I., 2017. Grain size analysis. In: Gilbert, A.S. (Ed.), Encyclopedia of Geoarchaeology. Encyclopedia of Earth Sciences Series. Springer Netherlands, Dordrecht, pp. 341–348.

Makhubela, T.V., Kramers, J.D., Scherler, D., Wittmann, H., Dirks, P.H.G.M., Winkler, S.R., 2019. Effects of long soil surface residence times on apparent cosmogenic nuclide denudation rates and burial ages in the Cradle of Humankind, South Africa. Earth Surf. Process. Landf. 44, 2968–2981.

Makhubela, T.V., Kramers, J.D., Belyanin, G.A., Dirks, P.H.G.M., Roberts, E.M., 2017. Proterozoic $^{40}Ar/^{39}Ar$ ages from cave deposits of the Malapa, Sterkfontein

and Dinaledi fossil sites, Cradle of Humankind, South Africa. S. Afr. J. Geol. 120, 21–44.

Makó, A., Rajkai, K., Hernádi, H., Hauk, G., 2014. Comparison of different settings and pre-treatments in soil particle-size distribution measurement by laser-diffraction method. Agrokémia és Talajtan 63, 19–28.

Martí, A.P., d'Errico, F., Turq, A., Lebraud, E., Discamps, E., Gravina, B., 2019. Provenance, modification and use of manganese-rich rocks at Le Moustier (Dordogne, France). PLoS One 14, e0218568.

Martinón-Torres, M., d'Errico, F., Santos, E., Álvaro Gallo, A., Amano, N., Archer, W., Armitage, S.J., Arsuaga, J.L., Bermúdez de Castro, J.M., Blinkhorn, J., Crowther, A., Douka, K., Dubernet, S., Faulkner, P., Fernández-Colón, P., Kourampas, N., González García, J., Larreina, D., Le Bourdonnec, F.-X., MacLeod, G., Martín-Francés, L., Massilani, D., Mercader, J., Miller, J.M., Ndiema, E., Notario, B., Pitarch Martí, A., Prendergast, M.E., Queffelec, A., Rigaud, S., Roberts, P., Shoaee, M.J., Shipton, C., Simpson, I., Boivin, N., Petraglia, M.D., 2021. Earliest known human burial in Africa. Nature 593, 95–100.

Martinón-Torres, M., Garate, D., Herries, A.I.R., Petraglia, M.D., 2023. No scientific evidence that *Homo naledi* buried their dead and produced rock art. J. Hum. Evol., 103464.

Martın-Fernandez, J.A., Barcelo-Vidal, C., Pawlowsky-Glahn, V., 2003. Dealing with zeros and missing values in compositional data sets using nonparametric imputation. Math. Geol. 35, 253–278.

Mauran, G., Caron, B., Détroit, F., Nankela, A., Bahain, J.-J., Pleurdeau, D., Lebon, M., 2021. Data pretreatment and multivariate analyses for ochre sourcing: application to Leopard Cave (Erongo, Namibia). J. Archaeol. Sci. Rep. 35, 102757.

Microtrac, 2023. Laser diffraction particle size analyzer S3500 Microtrac [WWW Document]. https://www.microtrac.com/products/particle-size-shape-analysis/laser-diffraction/s3500/

Morley, M.W., Goldberg, P., Uliyanov, V.A., Kozlikin, M.B., Shunkov, M.V., Derevianko, A.P., Jacobs, Z., Roberts, R.G., 2019. Hominin and animal activities in the microstratigraphic record from Denisova Cave (Altai Mountains, Russia). Sci. Rep. 9, 13785.

Morley, M.W., Moffat, I., Kotarba-Morley, A.M., Hernandez, V.C., Zerboni, A., Herries, A.I.R., Joannes-Boyau, R., Westaway, K., 2023. Why the geosciences are becoming increasingly vital to the interpretation of the human evolutionary record. Nature Ecol. Evol. 7, 1971–1977.

Newbury, D.E., 2005. Misidentification of major constituents by automatic qualitative energy dispersive X-ray microanalysis: a problem that threatens the credibility of the analytical community. Microsc. Microanal. 11, 545–561.

Newbury, D.E., 2007. Mistakes encountered during automatic peak identification in low beam energy X-ray microanalysis. Scanning 29, 137–151.

Newbury, D.E., Ritchie, N.W.M., 2015. Performing elemental microanalysis with high accuracy and high precision by scanning electron microscopy/silicon drift detector energy-dispersive X-ray spectrometry (SEM/SDD-EDS). J. Mater. Sci. 50, 493–518.

Newbury, D.E., Ritchie, N.W.M., 2019. Using the EDS clues: peak fitting residual spectrum and analytical total. Microsc. Microanal. 25, 446–447.

Perry, G.R. (Ed.), 2023. Public peer reviews of "Evidence for deliberate burial of the dead by *Homo naledi*." [WWW Document]. eLife. https://elifesciences.org/reviewed-preprints/89106/reviews#peer-review-3

Petraglia, M.D., Ndiema, E., Martinón-Torres, M., Boivin, N., 2023. Major new research claims smaller-brained *Homo naledi* made rock art and buried the dead. But the evidence is lacking [WWW Document]. The Conversation. http://theconversation.com/major-new-research-claims-smaller-brained-homo-naledi-made-rock-art-and-buried-the-dead-but-the-evidence-is-lacking-207000 (accessed 11.8.23).

Pettitt, P., 2022. Did *Homo naledi* dispose of their dead in the Rising Star Cave system? S. Afr. J. Sci. 118.

Pickering, R., Hancox, P.J., Lee-Thorp, J.A., Grün, R., Mortimer, G.E., McCulloch, M., Berger, L.R., 2007. Stratigraphy, U-Th chronology, and paleoenvironments at Gladysvale Cave: insights into the climatic control of South African hominin-bearing cave deposits. J. Hum. Evol. 53, 602–619.

Pickering, R., Herries, A.I.R., Woodhead, J.D., Hellstrom, J.C., Green, H.E., Paul, B., Ritzman, T., Strait, D.S., Schoville, B.J., Hancox, P.J., 2019. U–Pb-dated flowstones restrict South African early hominin record to dry climate phases. Nature 565, 226–229.

Potter, P.E., Shimp, N.F., Witters, J., 1963. Trace elements in marine and fresh-water argillaceous sediments. Geochim. Cosmochim. Acta 27, 669–694.

Pye, K., Blott, S.J., Croft, D.J., Witton, S.J., 2007. Discrimination between sediment and soil samples for forensic purposes using elemental data: an investigation of particle size effects. Forensic Sci. Int. 167, 30–42.

Queffelec, A., Bertran, P., Bos, T., Lemée, L., 2018. Mineralogical and organic study of bat and chough guano: implications for guano identification in ancient context.J. Cave Karst Stud. 80, 1–17.

R Core Team, 2022. R: The R Project for Statistical Computing [WWW Document]. R Foundation for Statistical Computing. https://www.r-project.org/ (accessed 11.8.23).

Robbins, J.L., Dirks, P.H.G.M., Roberts, E.M., Kramers, J.D., Makhubela, T.V., Hilbert-Wolf, H.L., Elliott, M., Wiersma, J.P., Placzek, C.J., Evans, M., Berger, L.R., 2021. Providing context to the *Homo naledi* fossils: constraints from flowstones on the age of sediment deposits in Rising Star Cave, South Africa. Chem. Geol. 567, 120108.

Rodrigues, R., 2005. Chemostratigraphy. In: Koutsoukos, E.A.M. (Ed.), Applied Stratigraphy. Topics in Geobiology. Springer Netherlands, Dordrecht, pp. 165–178.

Rousseau, R., 2001. Detection limit and estimate of uncertainty of analytical XRF results. Rigaku J. 18, 33–47.

Rowe, H., Hughes, N., Robinson, K., 2012. The quantification and application of handheld energy-dispersive x-ray fluorescence (ED-XRF) in mudrock chemostratigraphy and geochemistry. Chem. Geol. (Special Issue Recent Advances in Trace Metal Applications to Paleoceanographic Studies) 324–325, 122–131.

Schamber, F.C., 1973. A new technique for deconvolution of complex X-ray energy spectra. In: Proceedings of the 8th National Conference on Electron Probe Analysis. Presented at the Electron Probe Analysis Society of America, New Orleans, LA.

Schlezinger, D.R., Howes, B.L., 2000. Organic phosphorus and elemental ratios as indicators of prehistoric human occupation. J. Archaeol. Sci. 27, 479–492.

Sitzia, L., Bertran, P., Sima, A., Chery, P., Queffelec, A., Rousseau, D.-D., 2017. Dynamics and sources of last glacial aeolian deposition in southwest France derived from dune patterns, grain-size gradients and geochemistry, and reconstruction of efficient wind directions. Quatern. Sci. Rev. 170, 250–268.

Spagnoli, F., Bartholini, G., Dinelli, E., Giordano, P., 2008. Geochemistry and particle size of surface sediments of Gulf of Manfredonia (Southern Adriatic sea). Estuar. Coast. Shelf Sci. 80, 21–30.

Speakman, R.J., Shackley, S.M., 2013. Silo science and portable XRF in archaeology: a response to Frahm. J. Archaeol. Sci. 40, 1435–1443.

Stancampiano, L.M., Rubio-Jara, S., Panera, J., Uribelarrea, D., Pérez-González, A., Magill, C.R., 2023. Organic geochemical evidence of human-controlled fires at Acheulean site of Valdocarros II (Spain, 245 kya). Sci. Rep. 13, 7119.

Sun, D., Bloemendal, J., Rea, D.K., Vandenberghe, J., Jiang, F., An, Z., Su, R., 2002. Grain-size distribution function of polymodal sediments in hydraulic and aeolian environments, and numerical partitioning of the sedimentary components. Sediment. Geol. 152, 263–277.

Sun, X., Liu, S., Li, J., Zhang, H., Zhu, A., Cao, P., Chen, M.-T., Zhao, G., Khokiattiwong, S., Kornkanitnan, N., Shi, X., 2019. Major and trace element compositions of surface sediments from the lower Bengal Fan: implications for provenance discrimination and sedimentary environment. J. Asian Earth Sci. 184, 104000.

Taggart Jr., J.E., Siems, D.F., 2002. Major element analysis by wavelength dispersive X-ray fluorescence spectrometry. In: Analytical Methods for Chemical Analysis of Geologic and Other Materials. U.S. Geological Survey, U.S. Geological Survey Open File Report 02-223-T.

Trauth, M.H., 2017. Linear Unmixing Variables Using the PCA with MATLAB. MATLAB and Python Recipes for Earth Sciences. http://mres.uni-potsdam.de/index.php/2017/04/10/linear-unmixing-variables-using-the-pca-with-matlab/

Val, A., 2016. Deliberate body disposal by hominins in the Dinaledi Chamber, Cradle of Humankind, South Africa? J. Hum. Evol. 96, 145–148.

Varga, G., Újvári, G., Kovács, J., 2019. Interpretation of sedimentary (sub)populations extracted from grain size distributions of Central European loess-paleosol series. Quatern. Int. 502, 60–70.

Villagran, X.S., Giannini, P.C.F., DeBlasis, P., 2009. Archaeofacies analysis: using depositional attributes to identify anthropic processes of deposition in a monumental shell mound of Santa Catarina State, southern Brazil. Geoarchaeology 24, 311–335.

Vital, H., Stattegger, K., 2000. Major and trace elements of stream sediments from the lowermost Amazon River. Chem. Geol. 168, 151–168.

Vital, H., Stattegger, K., Garbe-Schoenberg, C.-D., 1999. Composition and trace-element geochemistry of detrital clay and heavy-mineral suites of the lowermost Amazon River; a provenance study. J. Sed. Res. 69, 563–575.

Vos, D., Jenkins, E., Palmer, C., 2018. A dual geochemical-phytolith methodology for studying activity areas in ephemeral sites: insights from an ethnographic case study from Jordan. Geoarchaeology 33, 680–694.

Wang, L., Han, X., Ding, S., Liang, T., Zhang, Y., Xiao, J., Dong, L., Zhang, H., 2019. Combining multiple methods for provenance discrimination based on rare earth element geochemistry in lake sediment. Sci. Total Environ. 672, 264–274.

Wiersma, J.P., Roberts, E.M., Dirks, P.H.G.M., 2020. Formation of mud clast breccias and the process of sedimentary autobrecciation in the hominin-bearing (*Homo naledi*) Rising Star Cave system, South Africa. Sedimentology 67, 897–919.

Wu, K., Liu, S., Shi, X., Colin, C., Bassinot, F., Lou, Z., Zhang, H., Zhu, A., Fang, X., Mohamed, C.Abd.R., 2022. The effect of size distribution on the geochemistry and mineralogy of tropical river sediments and its implications regarding chemical weathering and fractionation of alkali elements. Lithosphere 2022, 8425818.

Yang, Y., Wang, L., Wendroth, O., Liu, B., Cheng, C., Huang, T., Shi, Y., 2019. Is the laser diffraction method reliable for soil particle size distribution analysis? Soil Sci. Soc. Am. J. 83, 276–287.

Živković, J., Bikić, V., Georgakopoulou, M., Carvajal López, J.C., 2021. Archaeology of craft and artisans in the Ottoman Empire: a case of ceramic production in Belgrade during the sixteenth and seventeenth centuries. Archaeol. Anthropol. Sci. 13, 63.

Supplement 1: No Sedimentological Evidence for Deliberate Burial by *Homo naledi* – A Case Study Highlighting the Need for Best Practices in Geochemical Studies Within Archaeology and Paleoanthropology

KIMBERLY K. FOECKE
Department of Sociology and Anthropology, George Mason University, Fairfax, VA; and, Human Origins Program, Department of Anthropology, Smithsonian Institution National Museum of Natural History, Washington D.C., USA; kfoecke@gmu.edu

ALAIN QUEFFELEC
UMR5199 - PACEA, CNRS, Université Bordeaux, Ministère de la Culture, Pessac, FRANCE; alain.queffelec@u-bordeaux.fr

ROBYN PICKERING
Department of Geological Sciences, Human Evolution Research Institute (HERI), University of Cape Town, Cape Town, SOUTH AFRICA; robyn.pickering@uct.ac.za

SUPPLEMENT 1

This supplement includes: Supplementary Figure S1, R code, FactoMineR code, and eleven data files. The data files are replication_data (contains transcribed XRF data as reported in the Berger et al. pre-print), RepPCA (contains the PCA loadings for the *prcomp*, "-"⟶ 0 test condition), new_data (contains transcribed XRF data processed with the standard recommended protocol), NewPCA (contains the PCA loadings for the standard recommended protocol test condition), RepScores (contains the PCA scores for the *prcomp*, "-"⟶ 0 test condition), NewScores contains the PCA scores for the standard recommended protocol test condition), extradata (contains transcribed XRF data isolated to Feature 1 using the standard recommended protocol test condition), ExtraPCARep (contains the PCA loadings for the Feature 1 only PCA test condition), ExtraRepScores (contains the PCA scores for the Feature 1 only PCA test condition), ExtraNewScores (contains the PCA scores for the Feature 1 only PCA test condition), and ExtraPCANew (contains the PCA loadings for the Feature 1 only PCA test condition).

Paleoanthropology Society & European Society for the study of Human Evolution.
OPEN ACCESS
ISSN 1545-0031
Early View available online 23 July 2024

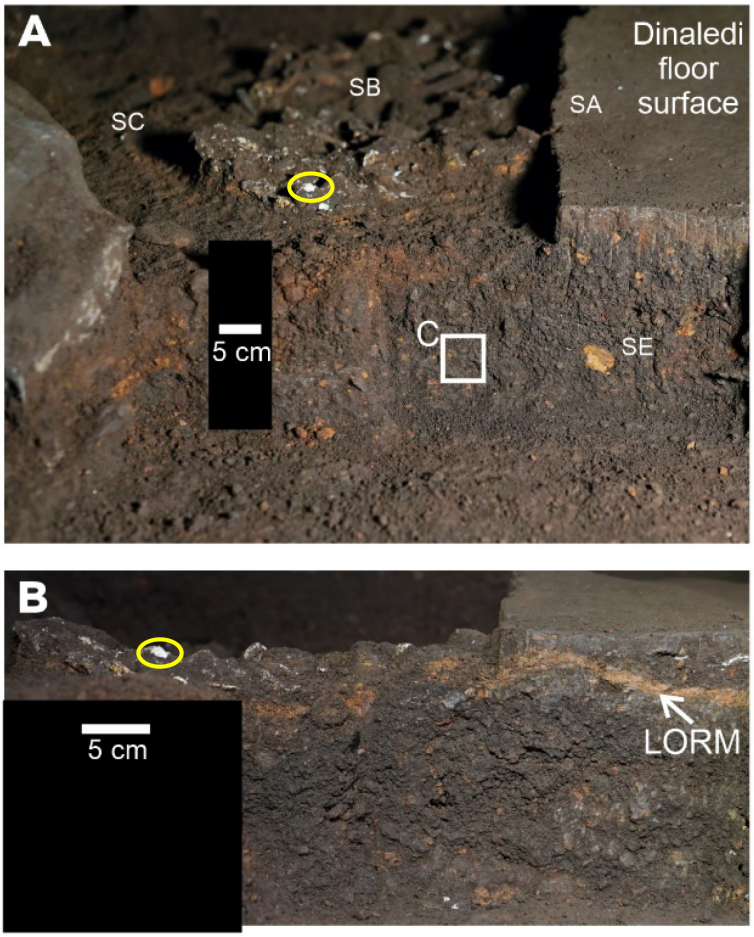

Figure S1. Modified from Berger et al. 2023 Figure 3. Yellow circles show the same white fragment connecting the views in Berger et al. 2023 Figure 3B and 3B.

Foecke et al. 2023 R Code

2023-11-08

#PCA using prcomp

#Load packages

```
library(ggplot2)
library(plyr)
library(dplyr)

##
## Attaching package: 'dplyr'

## The following objects are masked from 'package:plyr':
##
##     arrange, count, desc, failwith, id, mutate, rename, summarise,
##     summarize

## The following objects are masked from 'package:stats':
##
##     filter, lag

## The following objects are masked from 'package:base':
##
##     intersect, setdiff, setequal, union

library(factoextra)

## Welcome! Want to learn more? See two factoextra-related books at
https://goo.gl/ve3WBa
```

#Replicate Berger et al PCA using prcomp, "-" -> 0

```
data <- read.csv("~/Desktop/replication_data.csv")
pca <- prcomp(data[,c(4:15)], center = TRUE, scale. = TRUE)
summary(pca)

## Importance of components:
##                           PC1    PC2    PC3    PC4     PC5     PC6     PC7
## Standard deviation     1.9811 1.6208 1.2563 1.1122 0.98259 0.85639 0.72649
## Proportion of Variance 0.3271 0.2189 0.1315 0.1031 0.08046 0.06112 0.04398
## Cumulative Proportion  0.3271 0.5460 0.6775 0.7806 0.86105 0.92217 0.96615
##                           PC8     PC9    PC10    PC11    PC12
## Standard deviation     0.42441 0.36257 0.25357 0.16585 0.05283
## Proportion of Variance 0.01501 0.01095 0.00536 0.00229 0.00023
## Cumulative Proportion  0.98116 0.99212 0.99748 0.99977 1.00000

RepPCA <- pca$rotation[,1:5]
```

##Create .csv file of output RepPCA, invert loading signs for PC1 and PC2 re Berger (column noted with "F") and load into R as a dataframe:

```
RepPCAloadings <- read.csv("~/Desktop/RepPCA.csv")
```

##Replicate Berger loading plots using prcomp, "-" -> 0

```
PC1loadingplot <- ggplot(RepPCAloadings) + geom_col(aes(x=Element, y=PC1F)) +
  theme_light() + labs(y="PC1 Loadings") +
  scale_y_continuous(breaks=c(-0.8,-0.6,-0.4,-0.2,0,0.2,0.4,0.6,0.8),
limits=c(-0.8, 0.8))
PC1loadingplot
```

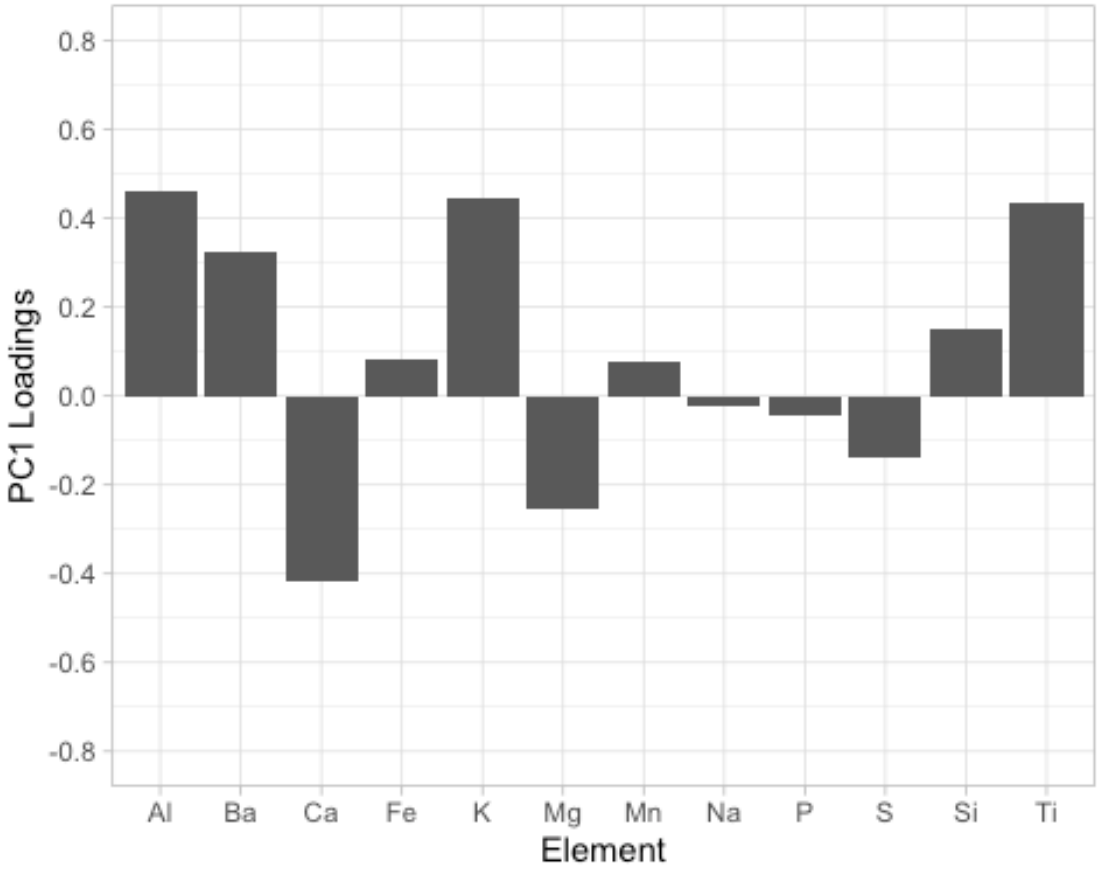


```
PC2loadingplot <- ggplot(RepPCAloadings) + geom_col(aes(x=Element, y=PC2F)) +
  theme_light() + labs(y="PC2 Loadings") +
  scale_y_continuous(breaks=c(-0.8,-0.6,-0.4,-0.2,0,0.2,0.4,0.6,0.8),
limits=c(-0.8, 0.8))
PC2loadingplot
```

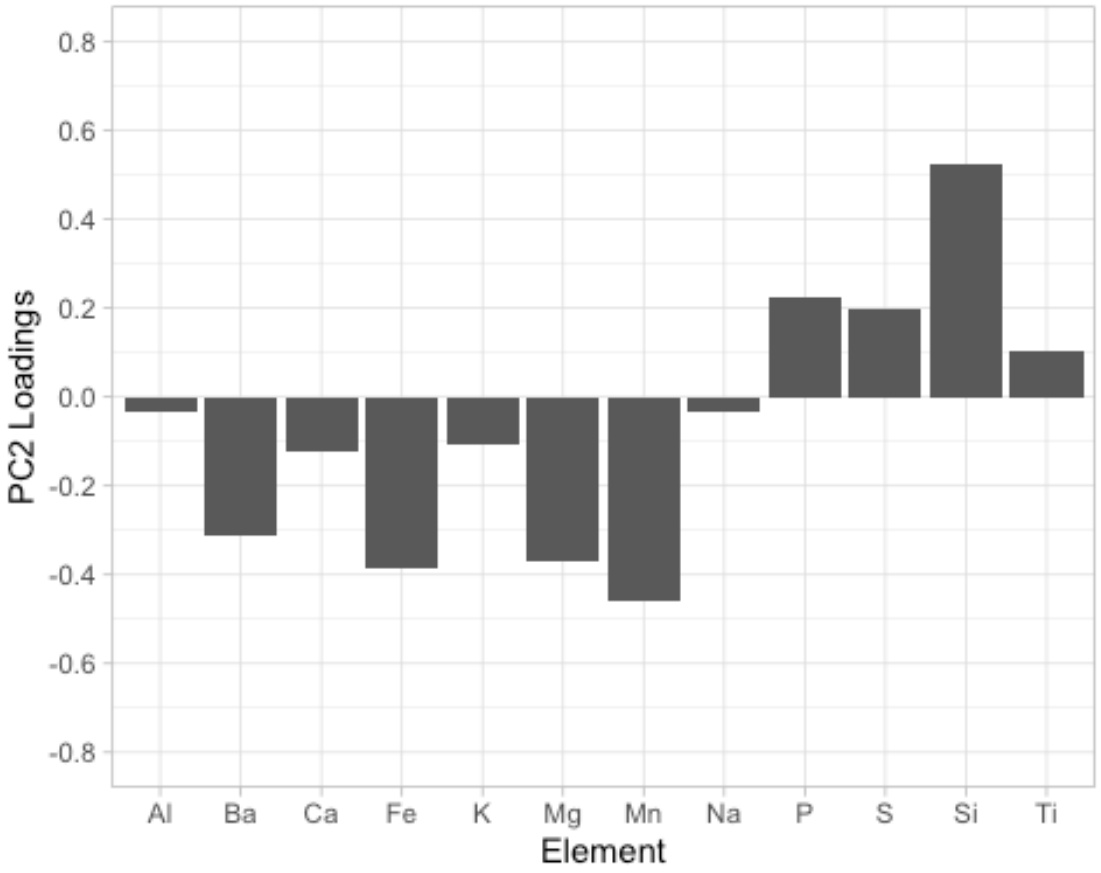


```
PC3loadingplot <- ggplot(RepPCAloadings) + geom_col(aes(x=Element, y=PC3)) +
  theme_light() + labs(y="PC3 Loadings") +
  scale_y_continuous(breaks=c(-0.8,-0.6,-0.4,-0.2,0,0.2,0.4,0.6,0.8),
limits=c(-0.8, 0.8))
PC3loadingplot
```

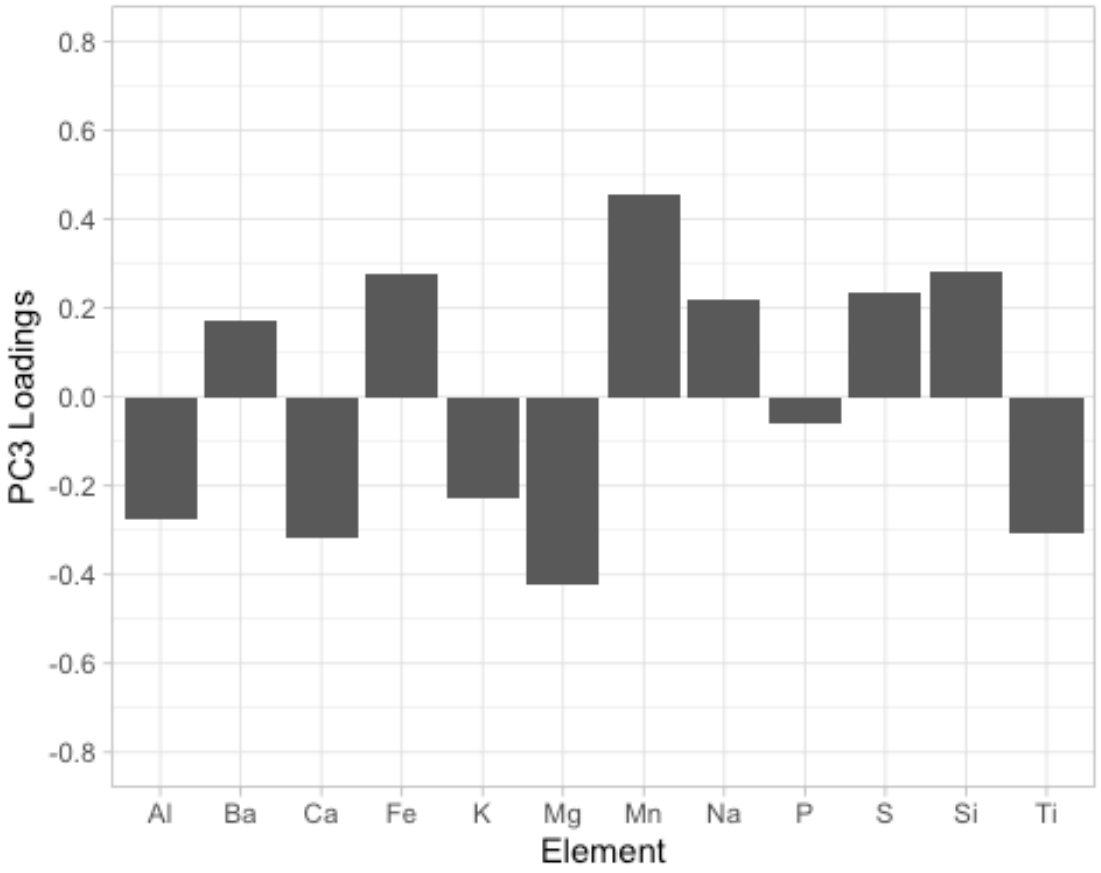

##Create variable correlation circle for PC1 and PC2

```
fviz_pca_var(pca, col.var = "black")
```

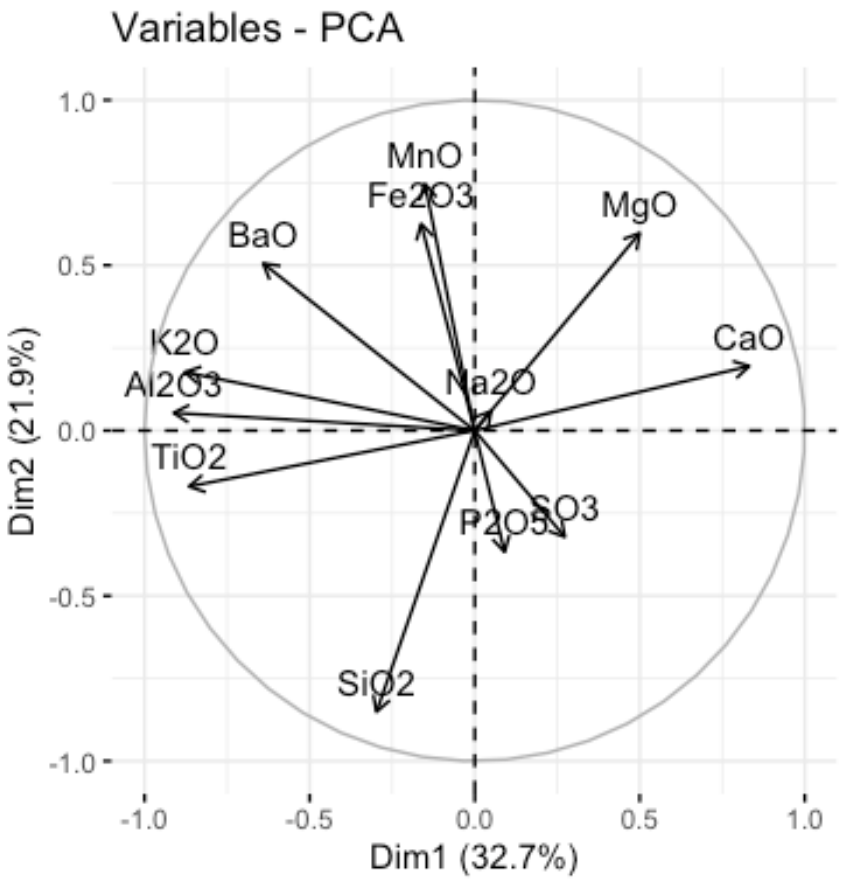

#Data re-analysis with recommended standard data processing methodology - prcomp, elements with >10% data missing removed re Martín-Fernández et al 2003, rare missing values replaced with 10% of lowest value measured re Mauran et al 2021

```
newdata <- read.csv("~/Desktop/new_data.csv")
newpca <- prcomp(newdata[,c(4:12)], center = TRUE, scale. = TRUE)
summary(newpca)

## Importance of components:
##                           PC1    PC2    PC3     PC4    PC5     PC6     PC7
## Standard deviation     1.8953 1.5021 1.2200 0.92159 0.6978 0.42631 0.33310
## Proportion of Variance 0.3991 0.2507 0.1654 0.09437 0.0541 0.02019 0.01233
## Cumulative Proportion  0.3991 0.6498 0.8152 0.90955 0.9636 0.98384 0.99617
##                           PC8     PC9
## Standard deviation     0.17594 0.05948
## Proportion of Variance 0.00344 0.00039
## Cumulative Proportion  0.99961 1.00000

NewPCA <- newpca$rotation[,1:5]
```

##Create .csv file of output NewPCA, invert loading signs for PC1 and PC2 re Berger (column noted with "F") and load into R as a dataframe:

```
NewPCAloadings <- read.csv("~/Desktop/NewPCA.csv")
```

##New loading plots recommended standard data processing methodology

```
NewPC1loadingplot <- ggplot(NewPCAloadings) + geom_col(aes(x=Element,
y=PC1F)) +
  theme_light() + labs(y="PC1 Loadings") +
  scale_y_continuous(breaks=c(-0.8,-0.6,-0.4,-0.2,0,0.2,0.4,0.6,0.8),
limits=c(-0.8, 0.8))
NewPC1loadingplot
```

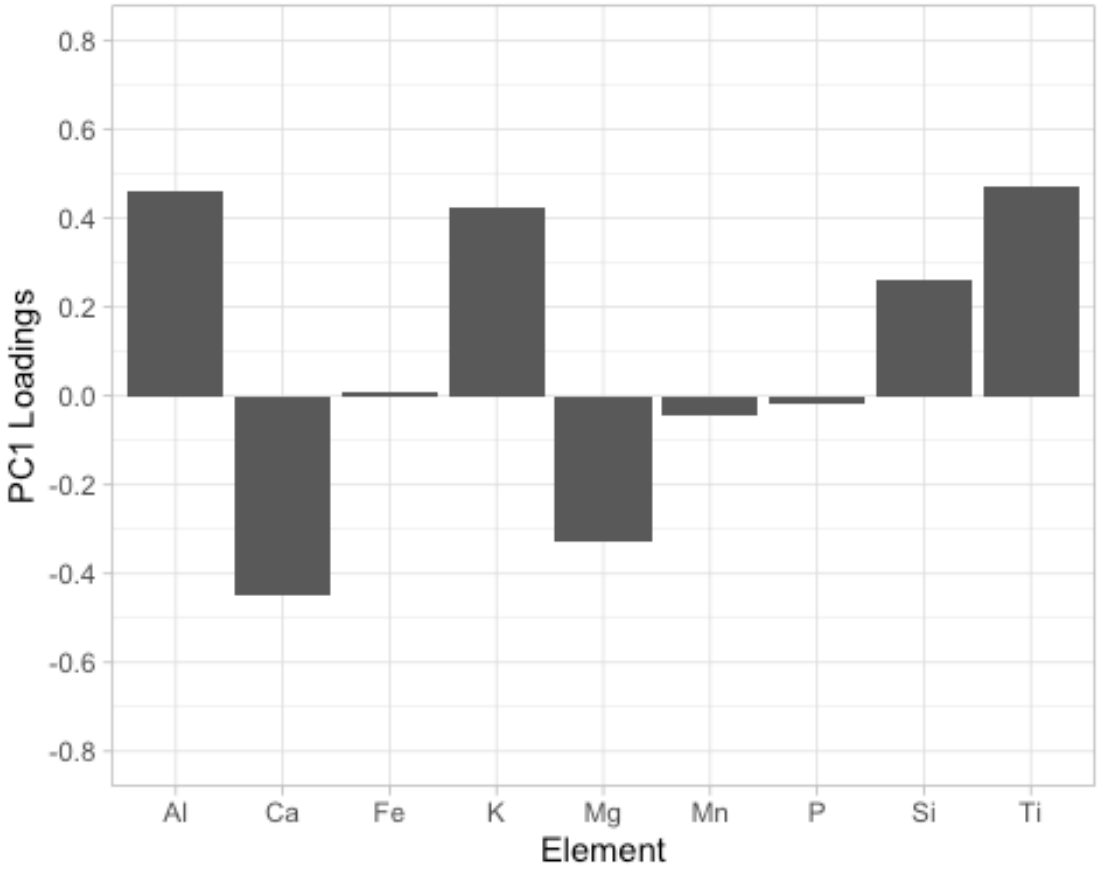


```
NewPC2loadingplot <- ggplot(NewPCAloadings) + geom_col(aes(x=Element,
y=PC2F)) +
  theme_light() + labs(y="PC2 Loadings") +
  scale_y_continuous(breaks=c(-0.8,-0.6,-0.4,-0.2,0,0.2,0.4,0.6,0.8),
limits=c(-0.8, 0.8))
NewPC2loadingplot
```

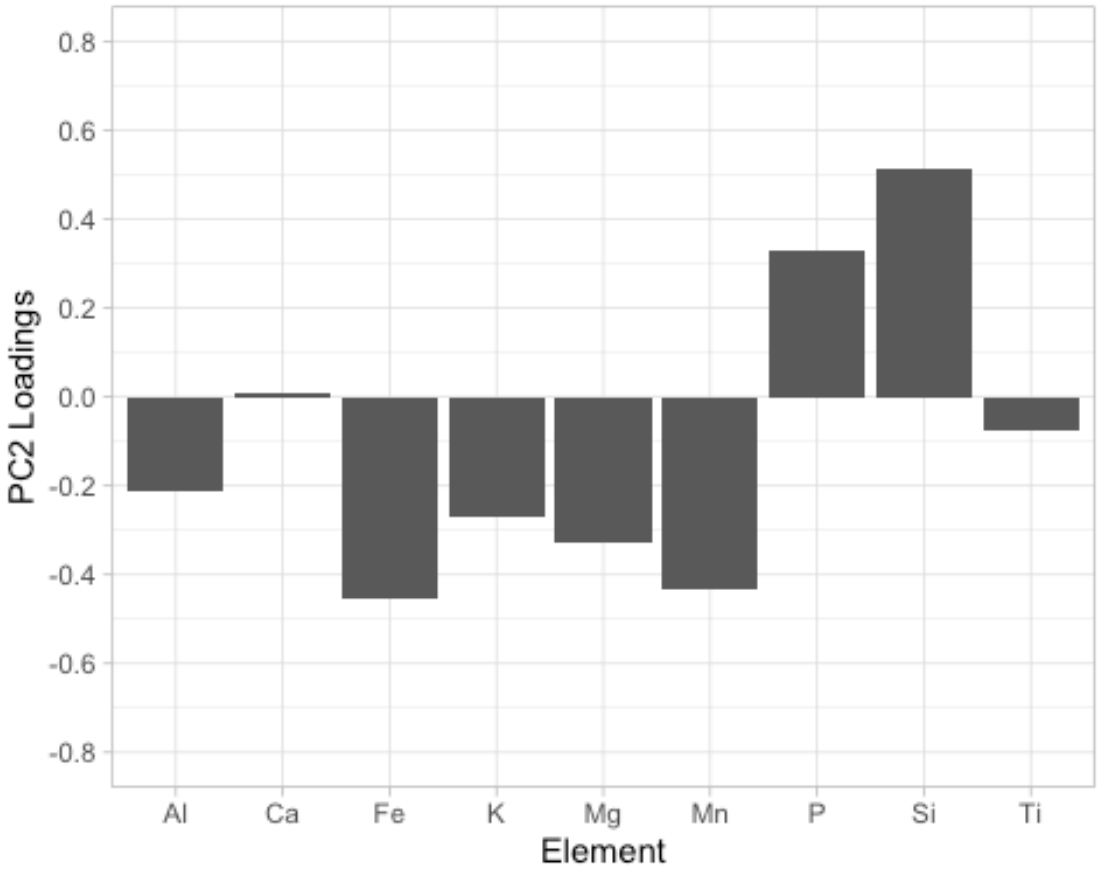


```
NewPC3loadingplot <- ggplot(NewPCAloadings) + geom_col(aes(x=Element, y=PC3))
+
  theme_light() + labs(y="PC3 Loadings") +
  scale_y_continuous(breaks=c(-0.8,-0.6,-0.4,-0.2,0,0.2,0.4,0.6,0.8),
limits=c(-0.8, 0.8))
NewPC3loadingplot
```

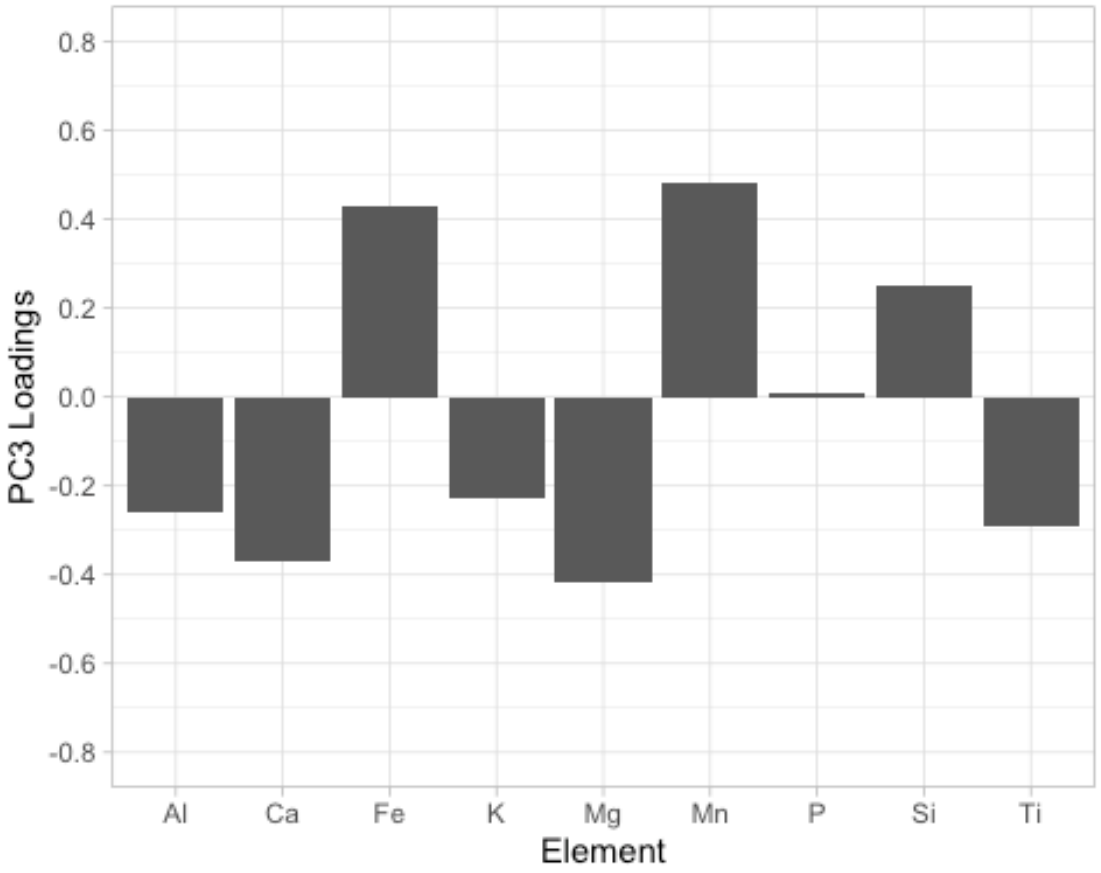

##Create variable correlation circle for PC1 and PC2

```
fviz_pca_var(newpca, col.var = "black")
```

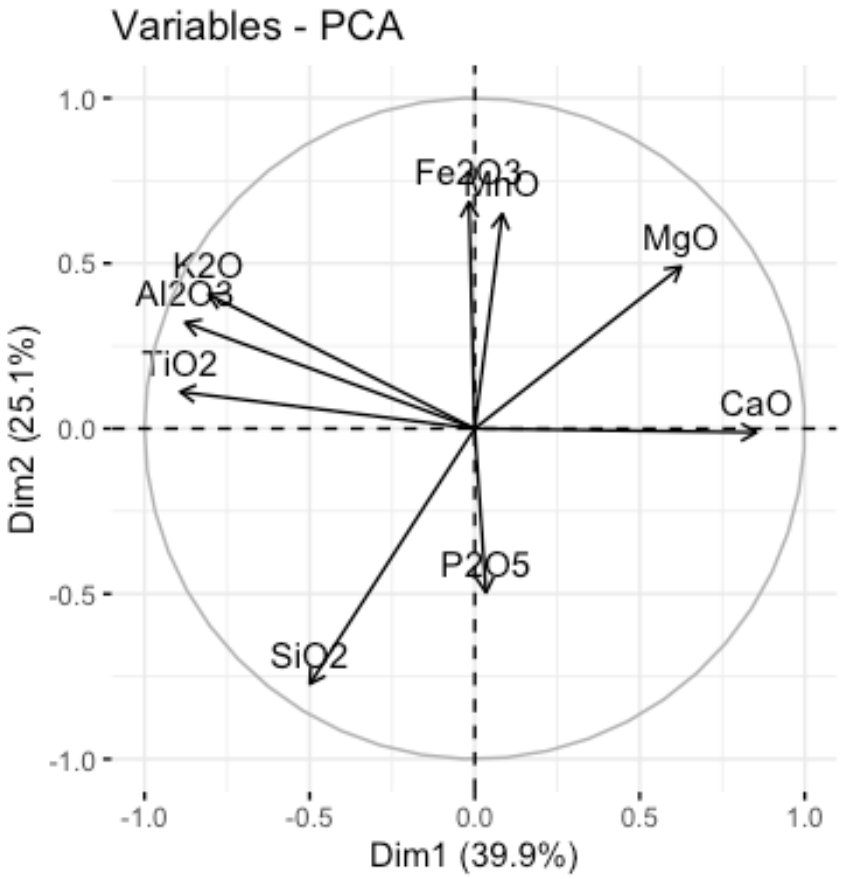

#Extract PCA scores from replication attempt and new re-analysis, generate .csv files, invert loading signs for PC1 and PC2 re Berger (column noted with "F") and load into R as a dataframe

```
RepScores <- pca$x[,1:2]
NewScores <- newpca$x[,1:2]
RepScoreData <- read.csv("~/Desktop/RepScores.csv")
NewScoreData <- read.csv("~/Desktop/NewScores.csv")
```

##Plot PCA scores from replication attempt and new re-analysis with 95% confidence ellipses

```
RepScorePlot <- ggplot(data = RepScoreData, aes(x =PC1F, y = PC2F, colour=
Locality, fill = Locality)) +
  theme_light() + geom_point() + stat_ellipse(geom="polygon", aes(fill =
Locality), alpha = 0.2, show.legend = FALSE, level = 0.95)
RepScorePlot

## Too few points to calculate an ellipse
## Too few points to calculate an ellipse
```

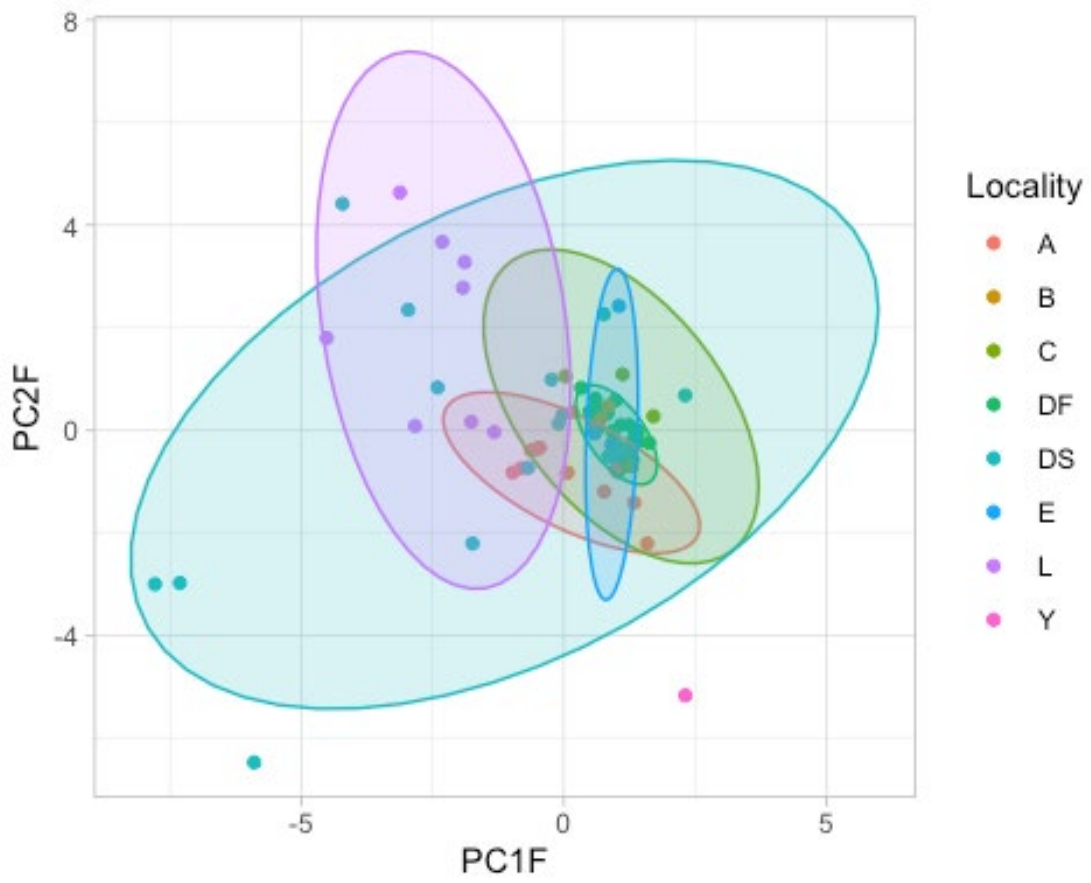


```
NewScorePlot <- ggplot(data = NewScoreData, aes(x =PC1F, y = PC2F, colour=
Locality, fill = Locality)) +
  theme_light() + geom_point() + stat_ellipse(geom="polygon", aes(fill =
Locality), alpha = 0.2, show.legend = FALSE, level = 0.95)
NewScorePlot

## Too few points to calculate an ellipse
## Too few points to calculate an ellipse
```

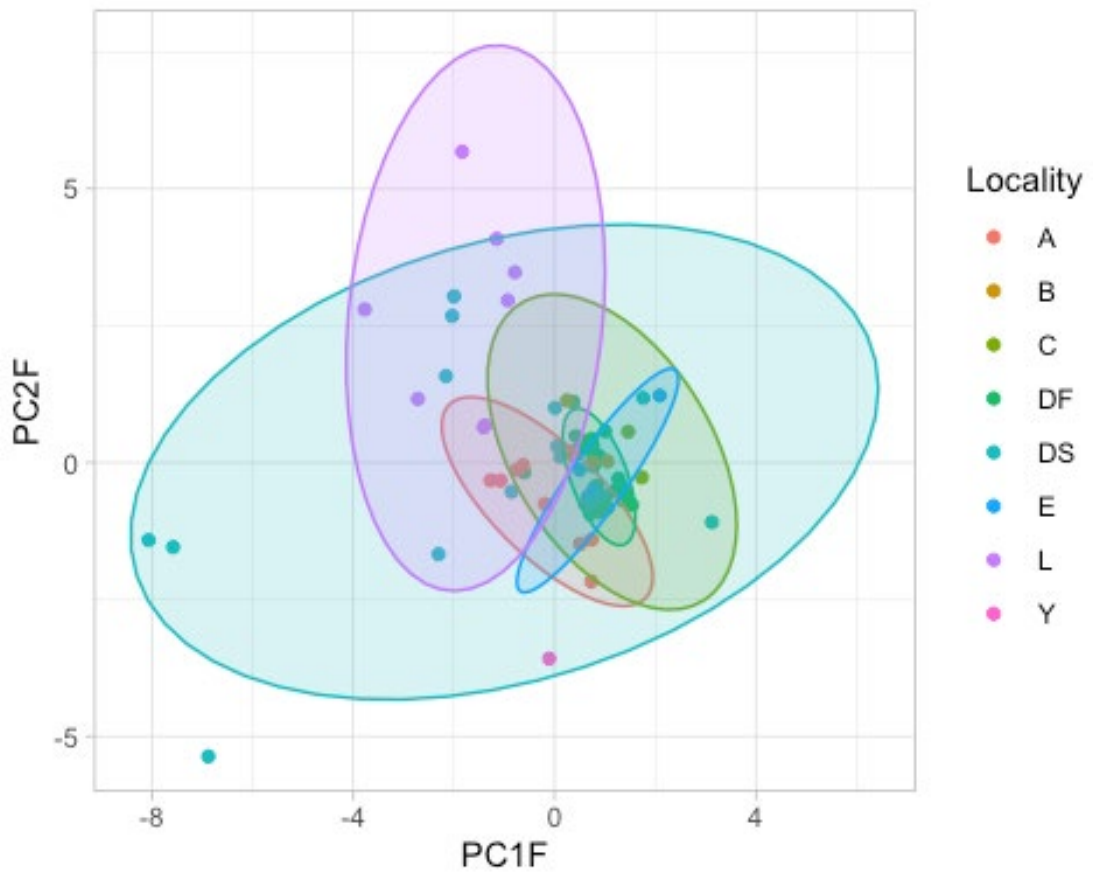

##Isolate PCA scores for localities relevant to Feature 1 from RepScorePlot and NewScorePlot

```
ReducedRepScoreData <- filter(RepScoreData, Locality %in%
c("A","B","C","DF","E"))
ReducedNewScoreData <- filter(NewScoreData, Locality %in%
c("A","B","C","DF","E"))

RedRepScorePlot <- ggplot(data = ReducedRepScoreData, aes(x =PC1F, y = PC2F,
colour= Locality, fill = Locality)) +
  theme_light() + geom_point() + stat_ellipse(geom="polygon", aes(fill =
Locality), alpha = 0.2, show.legend = FALSE, level = 0.95)
RedRepScorePlot

## Too few points to calculate an ellipse
```

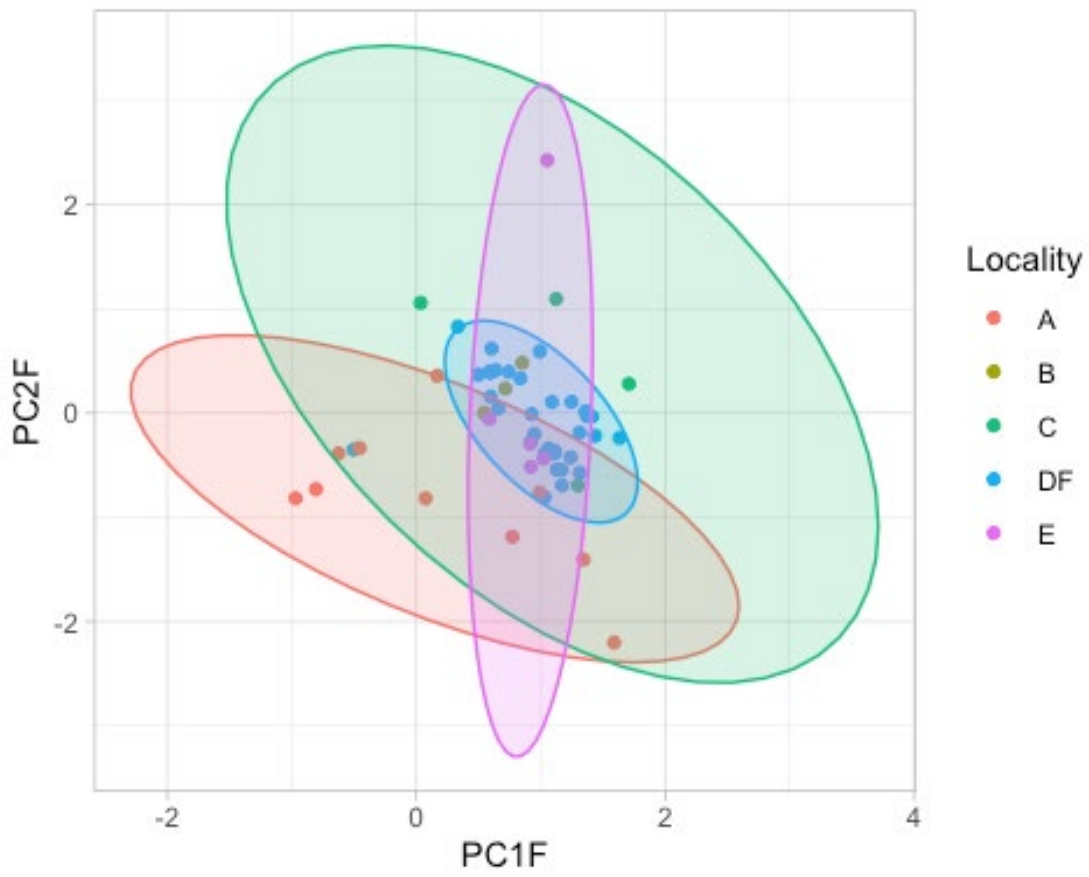


```
RedNewScorePlot <- ggplot(data = ReducedNewScoreData, aes(x =PC1F, y = PC2F,
colour= Locality, fill = Locality)) +
  theme_light() + geom_point() + stat_ellipse(geom="polygon", aes(fill =
Locality), alpha = 0.2, show.legend = FALSE, level = 0.95)
RedNewScorePlot

## Too few points to calculate an ellipse
```

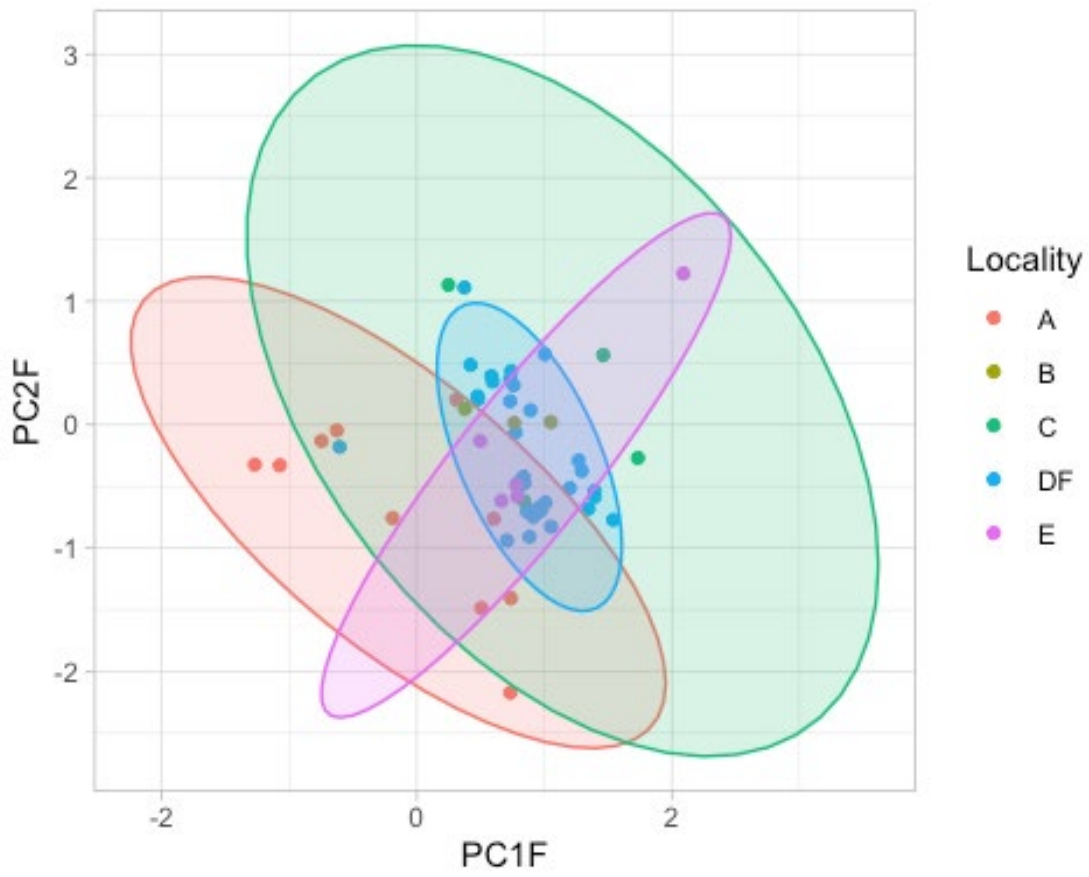

#Re-run PCAs as above including only localities relevant to Feature 1, only PC1 and PC2, prcomp, "-" -> "0"

```
ExtraPCARep <- prcomp(data[c(1:56),c(4:10,12,13,15)], center = TRUE, scale. =
TRUE)
summary(ExtraPCARep)

## Importance of components:
##                           PC1    PC2    PC3     PC4     PC5     PC6
PC7
## Standard deviation     1.8198 1.8088 1.2768 0.89495 0.65911 0.53057
0.38321
## Proportion of Variance 0.3312 0.3272 0.1630 0.08009 0.04344 0.02815
0.01468
## Cumulative Proportion  0.3312 0.6583 0.8214 0.90148 0.94492 0.97307
0.98775
##                           PC8     PC9    PC10
## Standard deviation     0.2775 0.20085 0.07158
## Proportion of Variance 0.0077 0.00403 0.00051
## Cumulative Proportion  0.9954 0.99949 1.00000

ExtraPCAR <- ExtraPCARep$rotation[,1:5]
ExtraPCAReploadings <- read.csv("~/Desktop/ExtraPCARep.csv")
```

```
ExtraPC1Rloadingplot <- ggplot(ExtraPCAReploadings) + geom_col(aes(x=Element,
y=PC1F)) +
  theme_light() + labs(y="PC1 Loadings") +
  scale_y_continuous(breaks=c(-0.8,-0.6,-0.4,-0.2,0,0.2,0.4,0.6,0.8),
limits=c(-0.8, 0.8))
ExtraPC1Rloadingplot
```

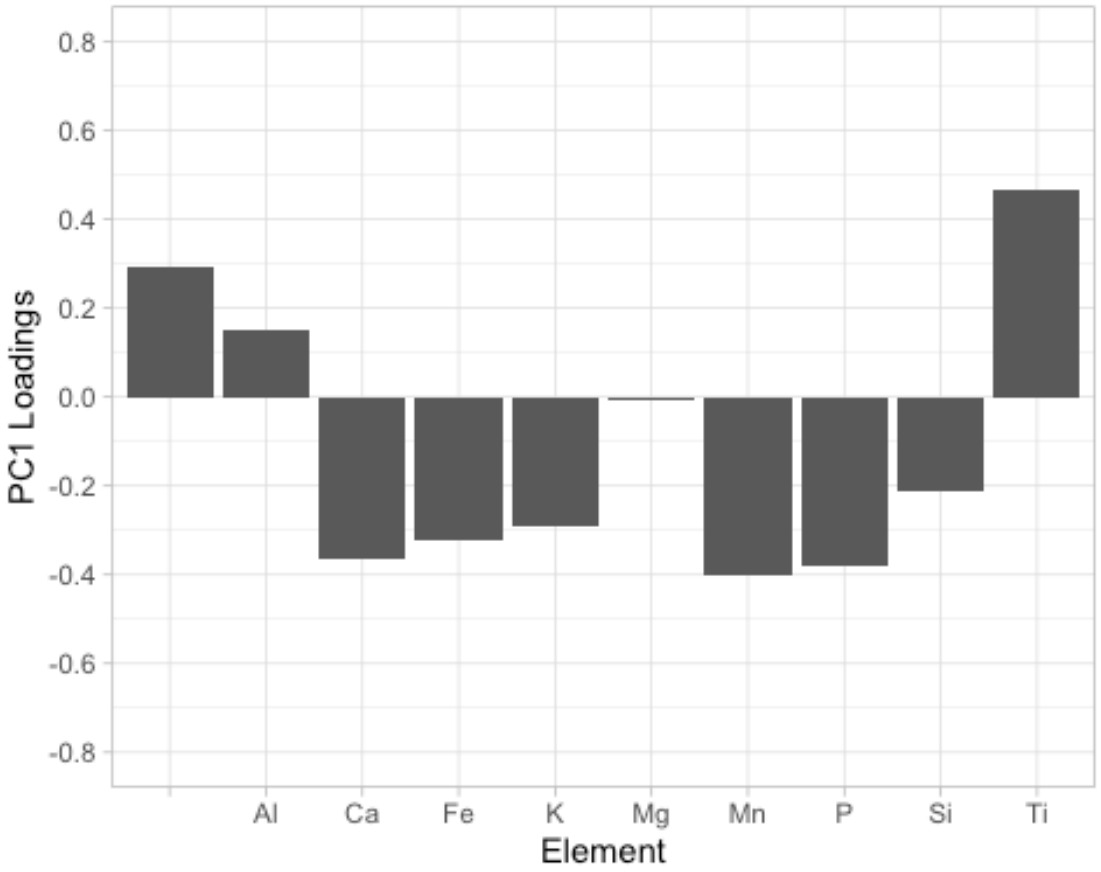


```
ExtraPC2Rloadingplot <- ggplot(ExtraPCAReploadings) + geom_col(aes(x=Element,
y=PC2F)) +
  theme_light() + labs(y="PC2 Loadings") +
  scale_y_continuous(breaks=c(-0.8,-0.6,-0.4,-0.2,0,0.2,0.4,0.6,0.8),
limits=c(-0.8, 0.8))
ExtraPC2Rloadingplot
```

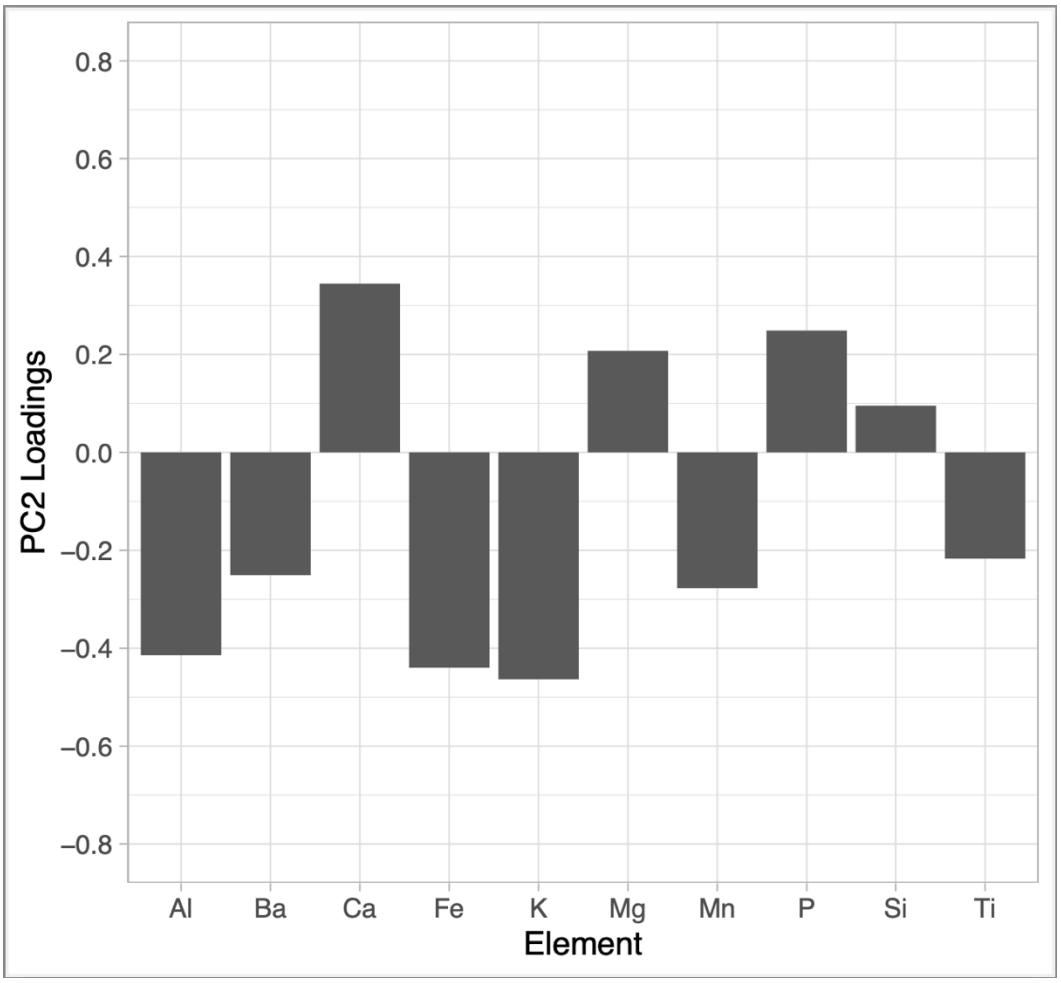


```
ExtraRepScores <- ExtraPCARep$x[,1:2]
ExtraRepScoreData <- read.csv("~/Desktop/ExtraRepScores.csv")
ExtraScorePlotR <- ggplot(data = ExtraRepScoreData, aes(x =PC1F, y = PC2F,
colour= Locality, fill = Locality)) +
  theme_light() + geom_point() + stat_ellipse(geom="polygon", aes(fill =
Locality), alpha = 0.2, show.legend = FALSE, level = 0.95)
ExtraScorePlotR

## Too few points to calculate an ellipse
```

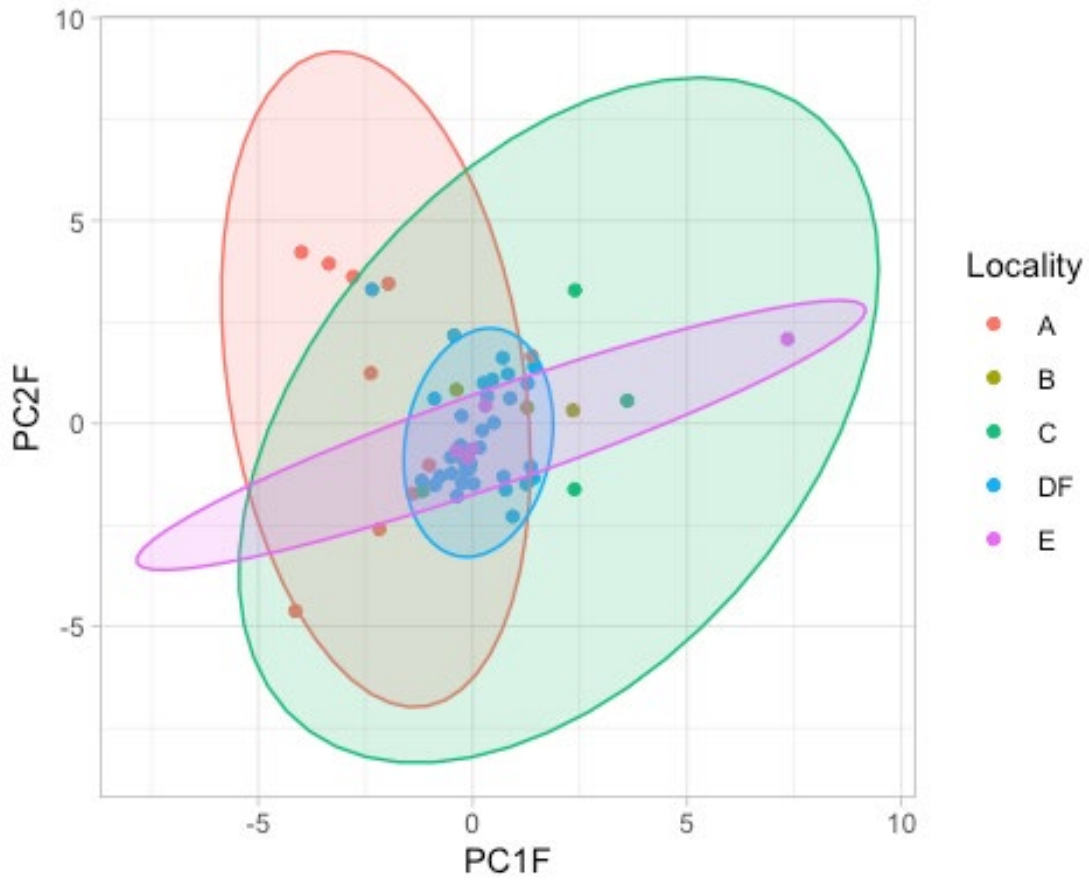

#Re-run PCAs as above including only localities relevant to Feature 1, only PC1 and PC2, standard recommended protocol

```
extradata <- read.csv("~/Desktop/extradata.csv")
ExtraPCANew <- prcomp(extradata[,c(4:13)], center = TRUE, scale. = TRUE)
summary(ExtraPCANew)

## Importance of components:
##                           PC1    PC2    PC3     PC4     PC5     PC6
PC7
## Standard deviation     1.8176 1.8102 1.2758 0.89646 0.66415 0.53063
0.37919
## Proportion of Variance 0.3304 0.3277 0.1628 0.08036 0.04411 0.02816
0.01438
## Cumulative Proportion  0.3304 0.6581 0.8208 0.90120 0.94531 0.97346
0.98784
##                           PC8     PC9    PC10
## Standard deviation     0.2756 0.20118 0.07149
## Proportion of Variance 0.0076 0.00405 0.00051
## Cumulative Proportion  0.9954 0.99949 1.00000

ExtraPCAN <- ExtraPCANew$rotation[,1:5]
ExtraPCANewloadings <- read.csv("~/Desktop/ExtraPCANew.csv")
```

```
ExtraPC1Nloadingplot <- ggplot(ExtraPCANewloadings) + geom_col(aes(x=Element,
y=PC1F)) +
  theme_light() + labs(y="PC1 Loadings") +
  scale_y_continuous(breaks=c(-0.8,-0.6,-0.4,-0.2,0,0.2,0.4,0.6,0.8),
limits=c(-0.8, 0.8))
ExtraPC1Nloadingplot
```

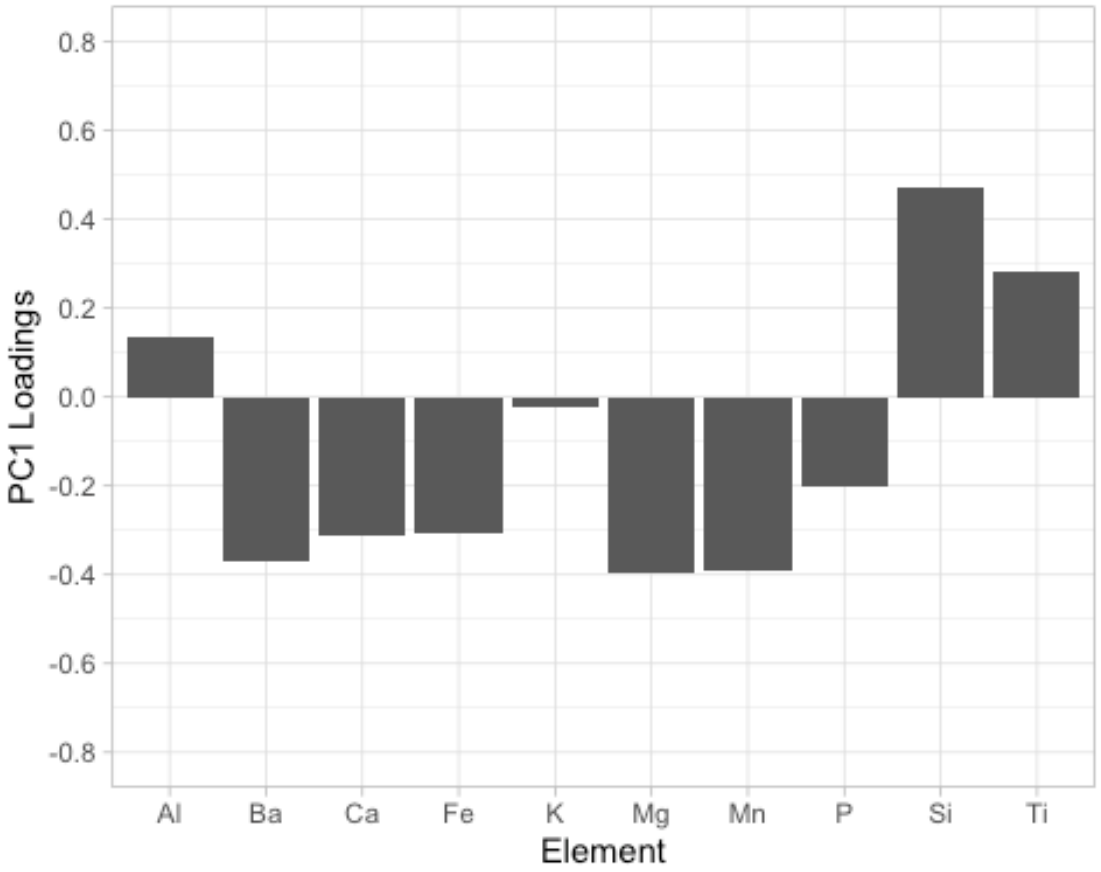


```
ExtraPC2Nloadingplot <- ggplot(ExtraPCANewloadings) + geom_col(aes(x=Element,
y=PC2F)) +
  theme_light() + labs(y="PC2 Loadings") +
  scale_y_continuous(breaks=c(-0.8,-0.6,-0.4,-0.2,0,0.2,0.4,0.6,0.8),
limits=c(-0.8, 0.8))
ExtraPC2Nloadingplot
```

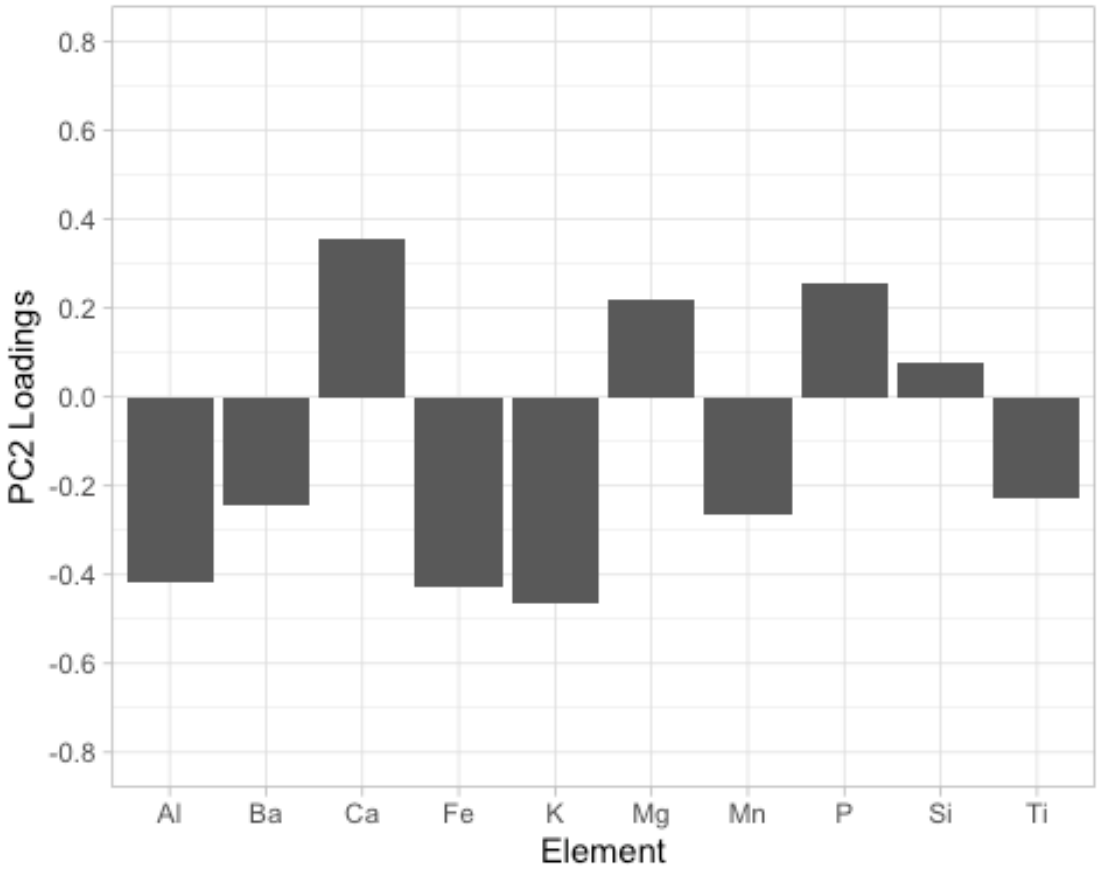


```
ExtraNewScores <- ExtraPCANew$x[,1:2]
ExtraNewScoreData <- read.csv("~/Desktop/ExtraNewScores.csv")
ExtraScorePlotN <- ggplot(data = ExtraNewScoreData, aes(x =PC1F, y = PC2F,
colour= Locality, fill = Locality)) +
  theme_light() + geom_point() + stat_ellipse(geom="polygon", aes(fill =
Locality), alpha = 0.2, show.legend = FALSE, level = 0.95)
ExtraScorePlotN

## Too few points to calculate an ellipse
```

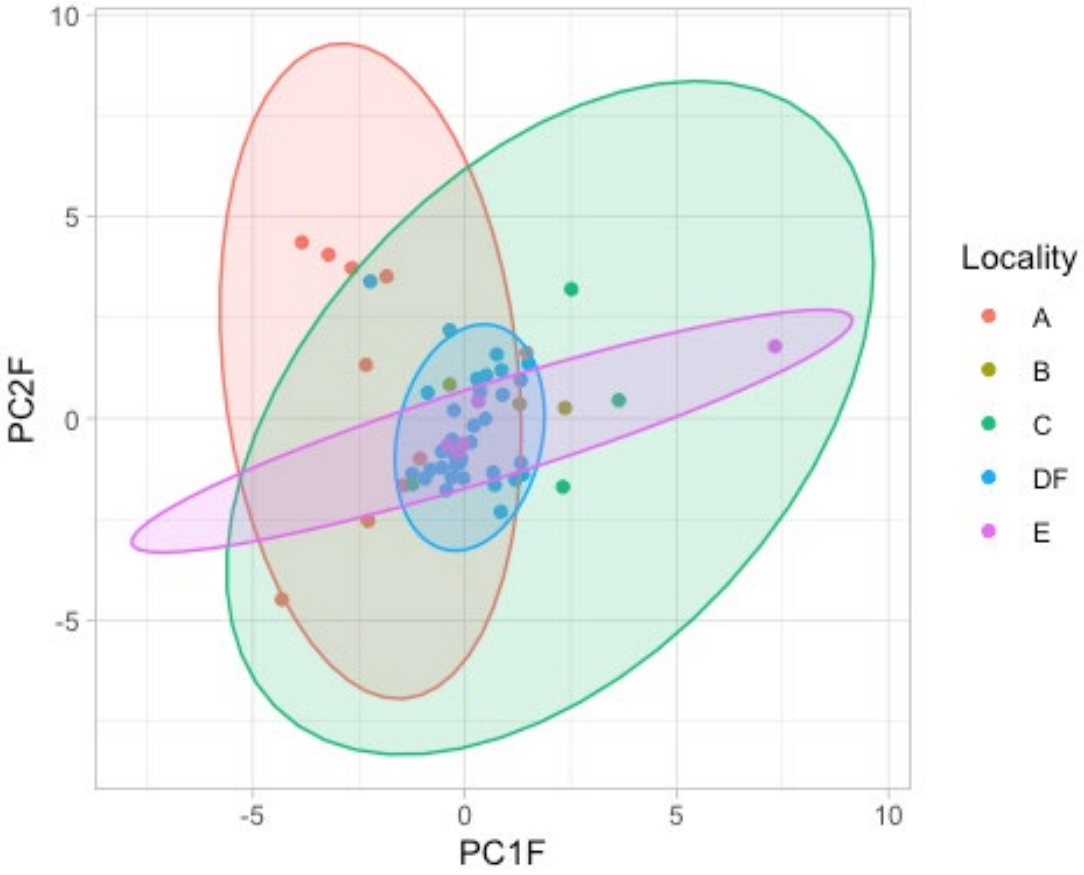
10
5
0
-5
PC2F
-5
0
5
10
PC1F
Locality
A
B
C
DF
E

---
title: "Foecke et al. 2023 FactoMineR Code"
output:
  word_document: default
  html_document: default
  pdf_document: default
date: "2023-11-08"

```{r setup, include=FALSE}
knitr::opts_chunk$set(echo = TRUE)
```

#PCA using FactoMineR

#Load packages
```{r}
library(FactoMineR)
library(ggplot2)
```
#Make the PCA with FactoMineR with missing values (will be replaced by the mean of the column)
##Quite different from the PCA in Berger et al. 2023 fig. 5.
```{r}
Berger = PCA(Berger_etal_2023_PCA[,1:15],
         quali.sup = c(1:3))
```
###Attempt at alternate plotting method
```{r}
plot.PCA(Berger,
       choix = c("ind"),
       axes = c(1,2),
       invisible = "quali",
       habillage = "Locality",
       graph.type= "ggplot",
       ggoptions = list(size = 8),
       label = "none")
```
#Make the PCA with FactoMineR with missing values replaced by 0.
##Makes a PCA apparently very similar to the one from Berger et al. 2023 fig. 5
```{r}
Berger_0 = PCA(Berger_etal_2023_PCA_0[,1:15],
         quali.sup = c(1:3),axes = c(1,2))
```

###Attempt at alternate plotting method
```{r}
barplot(Berger_0$var$coord[,1],main="Eigenvalues",names.arg=names(Berger_0$var$coo
rd[,1]))
barplot(-
Berger_0$var$coord[,2],main="Eigenvalues",names.arg=names(Berger_0$var$coord[,1]))
```
###Biplot of samples on the first two dimensions
```{r}
plot.PCA(Berger_0,
      choix = c("ind"),
      axes = c(1,2),
      invisible = "quali",
      habillage = "Locality",
      graph.type= "ggplot",
      ggoptions = list(size = 8),
      label = "none")
```

---
title: "Foecke et al. 2023 R Code"
output:
  word_document: default
  html_document: default
  pdf_document: default
date: '2023-11-08'

```{r setup, include=FALSE}
knitr::opts_chunk$set(echo = TRUE)
```
#PCA using prcomp

#Load packages
```{r}
library(ggplot2)
library(plyr)
library(dplyr)
library(factoextra)
```
#Replicate Berger et al PCA using prcomp, "-" -> 0
```{r}
data <- read.csv("~/Desktop/replication_data.csv")
pca <- prcomp(data[,c(4:15)], center = TRUE, scale. = TRUE)
```

```
summary(pca)
RepPCA <- pca$rotation[,1:5]
```
##Create .csv file of output RepPCA, invert loading signs for PC1 and PC2 re Berger (column noted with "F") and load into R as a dataframe:
```{r}
RepPCAloadings <- read.csv("~/Desktop/RepPCA.csv")
```
##Replicate Berger loading plots using prcomp, "-" -> 0
```{r}
PC1loadingplot <- ggplot(RepPCAloadings) + geom_col(aes(x=Element, y=PC1F)) +
  theme_light() + labs(y="PC1 Loadings") +
  scale_y_continuous(breaks=c(-0.8,-0.6,-0.4,-0.2,0,0.2,0.4,0.6,0.8), limits=c(-0.8, 0.8))
PC1loadingplot

PC2loadingplot <- ggplot(RepPCAloadings) + geom_col(aes(x=Element, y=PC2F)) +
  theme_light() + labs(y="PC2 Loadings") +
  scale_y_continuous(breaks=c(-0.8,-0.6,-0.4,-0.2,0,0.2,0.4,0.6,0.8), limits=c(-0.8, 0.8))
PC2loadingplot

PC3loadingplot <- ggplot(RepPCAloadings) + geom_col(aes(x=Element, y=PC3)) +
  theme_light() + labs(y="PC3 Loadings") +
  scale_y_continuous(breaks=c(-0.8,-0.6,-0.4,-0.2,0,0.2,0.4,0.6,0.8), limits=c(-0.8, 0.8))
PC3loadingplot
```
##Create variable correlation circle for PC1 and PC2
```{r}
fviz_pca_var(pca, col.var = "black")
```
#Data re-analysis with recommended standard data processing methodology - prcomp, elements with >10% data missing removed re Martín-Fernández et al 2003, rare missing values replaced with 10% of lowest value measured re Mauran et al 2021
```{r}
newdata <- read.csv("~/Desktop/new_data.csv")
newpca <- prcomp(newdata[,c(4:12)], center = TRUE, scale. = TRUE)
summary(newpca)
NewPCA <- newpca$rotation[,1:5]
```
##Create .csv file of output NewPCA, invert loading signs for PC1 and PC2 re Berger (column noted with "F") and load into R as a dataframe:
```{r}
NewPCAloadings <- read.csv("~/Desktop/NewPCA.csv")
```
##New loading plots recommended standard data processing methodology

```{r}
NewPC1loadingplot <- ggplot(NewPCAloadings) + geom_col(aes(x=Element, y=PC1F)) +
  theme_light() + labs(y="PC1 Loadings") +
  scale_y_continuous(breaks=c(-0.8,-0.6,-0.4,-0.2,0,0.2,0.4,0.6,0.8), limits=c(-0.8, 0.8))
NewPC1loadingplot

NewPC2loadingplot <- ggplot(NewPCAloadings) + geom_col(aes(x=Element, y=PC2F)) +
  theme_light() + labs(y="PC2 Loadings") +
  scale_y_continuous(breaks=c(-0.8,-0.6,-0.4,-0.2,0,0.2,0.4,0.6,0.8), limits=c(-0.8, 0.8))
NewPC2loadingplot

NewPC3loadingplot <- ggplot(NewPCAloadings) + geom_col(aes(x=Element, y=PC3)) +
  theme_light() + labs(y="PC3 Loadings") +
  scale_y_continuous(breaks=c(-0.8,-0.6,-0.4,-0.2,0,0.2,0.4,0.6,0.8), limits=c(-0.8, 0.8))
NewPC3loadingplot
```
##Create variable correlation circle for PC1 and PC2
```{r}
fviz_pca_var(newpca, col.var = "black")
```
#Extract PCA scores from replication attempt and new re-analysis, generate .csv files, invert loading signs for PC1 and PC2 re Berger (column noted with "F") and load into R as a dataframe
```{r}
RepScores <- pca$x[,1:2]
NewScores <- newpca$x[,1:2]
RepScoreData <- read.csv("~/Desktop/RepScores.csv")
NewScoreData <- read.csv("~/Desktop/NewScores.csv")
```
##Plot PCA scores from replication attempt and new re-analysis with 95% confidence ellipses
```{r}
RepScorePlot <- ggplot(data = RepScoreData, aes(x =PC1F, y = PC2F, colour= Locality, fill = Locality)) +
  theme_light() + geom_point() + stat_ellipse(geom="polygon", aes(fill = Locality), alpha = 0.2, show.legend = FALSE, level = 0.95)
RepScorePlot

NewScorePlot <- ggplot(data = NewScoreData, aes(x =PC1F, y = PC2F, colour= Locality, fill = Locality)) +
  theme_light() + geom_point() + stat_ellipse(geom="polygon", aes(fill = Locality), alpha = 0.2, show.legend = FALSE, level = 0.95)
NewScorePlot
```

##Isolate PCA scores for localities relevant to Feature 1 from RepScorePlot and NewScorePlot

```{r}
ReducedRepScoreData <- filter(RepScoreData, Locality %in% c("A","B","C","DF","E"))
ReducedNewScoreData <- filter(NewScoreData, Locality %in% c("A","B","C","DF","E"))

RedRepScorePlot <- ggplot(data = ReducedRepScoreData, aes(x =PC1F, y = PC2F, colour= Locality, fill = Locality)) +
  theme_light() + geom_point() + stat_ellipse(geom="polygon", aes(fill = Locality), alpha = 0.2, show.legend = FALSE, level = 0.95)
RedRepScorePlot

RedNewScorePlot <- ggplot(data = ReducedNewScoreData, aes(x =PC1F, y = PC2F, colour= Locality, fill = Locality)) +
  theme_light() + geom_point() + stat_ellipse(geom="polygon", aes(fill = Locality), alpha = 0.2, show.legend = FALSE, level = 0.95)
RedNewScorePlot
```

#Re-run PCAs as above including only localities relevant to Feature 1, only PC1 and PC2, prcomp, "-" -> "0"

```{r}
ExtraPCARep <- prcomp(data[c(1:56),c(4:10,12,13,15)], center = TRUE, scale. = TRUE)
summary(ExtraPCARep)
ExtraPCAR <- ExtraPCARep$rotation[,1:5]
ExtraPCAReploadings <- read.csv("~/Desktop/ExtraPCARep.csv")

ExtraPC1Rloadingplot <- ggplot(ExtraPCAReploadings) + geom_col(aes(x=Element, y=PC1F)) +
  theme_light() + labs(y="PC1 Loadings") +
  scale_y_continuous(breaks=c(-0.8,-0.6,-0.4,-0.2,0,0.2,0.4,0.6,0.8), limits=c(-0.8, 0.8))
ExtraPC1Rloadingplot

ExtraPC2Rloadingplot <- ggplot(ExtraPCAReploadings) + geom_col(aes(x=Element, y=PC2F)) +
  theme_light() + labs(y="PC2 Loadings") +
  scale_y_continuous(breaks=c(-0.8,-0.6,-0.4,-0.2,0,0.2,0.4,0.6,0.8), limits=c(-0.8, 0.8))
ExtraPC2Rloadingplot

ExtraRepScores <- ExtraPCARep$x[,1:2]
ExtraRepScoreData <- read.csv("~/Desktop/ExtraRepScores.csv")
ExtraScorePlotR <- ggplot(data = ExtraRepScoreData, aes(x =PC1F, y = PC2F, colour= Locality, fill = Locality)) +
  theme_light() + geom_point() + stat_ellipse(geom="polygon", aes(fill = Locality), alpha = 0.2, show.legend = FALSE, level = 0.95)
```

ExtraScorePlotR
```
#Re-run PCAs as above including only localities relevant to Feature 1, only PC1 and PC2, standard recommended protocol
```{r}
extradata <- read.csv("~/Desktop/extradata.csv")
ExtraPCANew <- prcomp(extradata[,c(4:13)], center = TRUE, scale. = TRUE)
summary(ExtraPCANew)
ExtraPCAN <- ExtraPCANew$rotation[,1:5]
ExtraPCANewloadings <- read.csv("~/Desktop/ExtraPCANew.csv")

ExtraPC1Nloadingplot <- ggplot(ExtraPCANewloadings) + geom_col(aes(x=Element, y=PC1F)) +
  theme_light() + labs(y="PC1 Loadings") +
  scale_y_continuous(breaks=c(-0.8,-0.6,-0.4,-0.2,0,0.2,0.4,0.6,0.8), limits=c(-0.8, 0.8))
ExtraPC1Nloadingplot

ExtraPC2Nloadingplot <- ggplot(ExtraPCANewloadings) + geom_col(aes(x=Element, y=PC2F)) +
  theme_light() + labs(y="PC2 Loadings") +
  scale_y_continuous(breaks=c(-0.8,-0.6,-0.4,-0.2,0,0.2,0.4,0.6,0.8), limits=c(-0.8, 0.8))
ExtraPC2Nloadingplot

ExtraNewScores <- ExtraPCANew$x[,1:2]
ExtraNewScoreData <- read.csv("~/Desktop/ExtraNewScores.csv")
ExtraScorePlotN <- ggplot(data = ExtraNewScoreData, aes(x =PC1F, y = PC2F, colour= Locality, fill = Locality)) +
  theme_light() + geom_point() + stat_ellipse(geom="polygon", aes(fill = Locality), alpha = 0.2, show.legend = FALSE, level = 0.95)
ExtraScorePlotN
```
```

replication_data

Number	Sample Name	Locality	Al2O3	BaO	CaO	Fe2O3	K2O	MgO	MnO	Na2O	P2O5	SiO2	SO3	TiO2
1	DF1	DF	16.39	0.08	1.55	10.69	1.72	2.79	4.41	0	0.27	52.67	0	0.75
2	DF2	DF	16.97	0.07	1.18	10.15	1.75	2.42	3.66	0	0.19	54.23	0	0.81
3	DF3	DF	15.65	0.07	1.22	10.49	1.61	2.66	4.25	0	0.37	54.69	0	0.75
4	DF4	DF	16.09	0.08	1.17	10.33	1.68	2.67	4.32	0	0.27	53.11	0	0.76
5	DF5	DF	16.23	0.07	1.21	10.51	1.68	2.51	4.3	0	0.29	53.89	0	0.75
6	DF6	DF	16.02	0.07	1.21	10.46	1.67	2.59	4.29	0	0.25	54.1	0	0.77
7	DF7	DF	16.47	0.07	1.58	10.09	1.71	2.73	3.98	0	0.27	53.34	0	0.77
8	DF8	DF	14.38	0.06	6.9	8.95	1.52	3.08	3.45	0	0.57	48.09	0	0.69
9	DF9	DF	15.63	0.08	1.04	10.42	1.62	2.51	4.51	0	0.34	54.9	0	0.73
10	DF10	DF	16.09	0.08	1.17	10.66	1.67	2.56	4.53	0	0.35	53.33	0	0.74
11	DF11	DF	17.45	0.07	0.86	10.38	1.8	2.13	3.7	0	0.18	53.75	0	0.81
12	DF12	DF	16.91	0.07	1.3	10.42	1.74	2.2	4.09	0	0.48	52.89	0	0.78
13	DF13	DF	15.82	0.08	0.92	10.7	1.68	2.31	4.52	0	0.27	55.15	0	0.75
14	DF14	DF	16.45	0.06	0.76	10.08	1.68	2.08	3.7	0	0.21	56.3	0	0.78
15	DF15	DF	15.15	0.08	1	10.79	1.7	2.61	5.28	0	0.23	53.78	0	0.71
16	DF16	DF	16.09	0.08	0.88	10.69	1.71	2.39	4.6	0	0.23	53.82	0	0.76
17	DF17	DF	15.35	0.07	0.88	10.36	1.6	2.33	4.35	0	0.25	56.1	0	0.73
18	DF18	DF	15.48	0.08	0.95	10.46	1.61	2.27	4.41	0	0.27	55.39	0	0.73
19	DF19	DF	16.73	0.06	0.8	10.07	1.71	2.25	3.62	0	0.16	55.6	0	0.81
20	DF20	DF	17.3	0.06	0.97	10.13	1.72	2.22	3.49	0	0.2	54.3	0	0.8
21	DF21	DF	14.57	0.08	0.89	9.55	1.49	2	3.59	0	0.33	59.28	0	0.72
22	DF22	DF	14.85	0.08	0.89	10.22	1.54	2.07	4.13	0	0.32	57.61	0	0.72
23	DF23	DF	14.13	0.08	0.96	9.78	1.42	2.32	3.86	0	0.34	58.71	0	0.7
24	DF24	DF	14.69	0.07	1	9.5	1.42	2.33	3.45	0	0.39	58.44	0	0.72
25	DF25	DF	15.02	0.06	0.91	9.51	1.44	2.36	3.5	0	0.29	58.57	0	0.74
26	DF26	DF	14.78	0.06	1.08	9.28	1.43	2.32	3.2	0	0.4	58.76	0	0.76
27	DF27	DF	15.18	0.09	0.98	9.54	1.52	2.12	3.74	0	0.36	57.51	0	0.76
28	DF28	DF	13.71	0.08	1.01	9.31	1.35	2.18	3.78	0	0.31	60.38	0	0.7
29	DF29	DF	14.8	0.08	1.55	9.96	1.52	2.22	4.6	0	0.75	55.51	0	0.7
30	DF30	DF	14.26	0.07	1.18	9.64	1.47	2.02	4.02	0	0.51	58.44	0	0.71
31	DF31	DF	16.19	0.08	0.88	10.1	1.69	1.95	3.88	0	0.3	56.21	0	0.78
32	DF32	DF	14.88	0.07	1.36	9.8	1.53	1.94	3.9	0	0.63	57.03	0	0.73
33	DF33	DF	14.1	0.07	2.11	9.45	1.49	1.91	3.92	0	1.16	57.55	0	0.69
34	DF34	DF	16.09	0.07	2.03	10.19	1.68	2.01	3.54	0	1.14	54.58	0	0.78
35	A1a	A	14.02	0.06	4.7	9.12	1.44	4.29	3.6	0	0.75	48.99	0	0.67
36	A1b	A	17.95	0.06	1.18	10.77	1.44	2.08	6.57	0	0.12	48.76	0	0.65
37	A2a	A	15.12	0.09	0.81	10.52	1.56	2.48	5.14	0	0.16	54.71	0	0.7
38	A2b	A	15.69	0.05	0.82	8.53	1.35	1.69	4.34	0	0.09	59.01	0	0.55
39	A3	A	13	0.07	5.05	9.03	1.36	4.67	4.19	0	0.68	47.76	0	0.62
40	A4	A	15.46	0.11	0.88	12.84	2.01	2.59	7.06	0	0.19	48.44	0	0.65
41	A5	A	13.34	0.07	3.71	8.88	1.37	3.94	3.75	0	0.47	52.66	0	0.66
42	A6	A	15.32	0.1	0.81	10.99	1.76	2.45	6.24	0	0.14	51.72	0	0.7
43	A7	A	13.19	0.07	4.85	8.99	1.37	4.52	3.94	0	0.55	48.99	0	0.64
44	A8	A	14.29	0.07	3.16	10.22	1.52	3.75	4.4	0	0.41	49.87	0	0.71
45	B1a	B	14.85	0.06	0.82	8.99	1.58	1.52	4.53	0	0.14	58.77	0	0.65
46	B1b	B	14.49	0.08	1.2	9.92	1.42	2.18	4.31	0	0.46	56.52	0	0.68
47	B2	B	16.65	0.05	0.72	8.83	1.5	1.68	3.48	0	0.09	57.65	0	0.71
48	C1	C	15.32	0.05	0.76	8.25	1.69	1.38	2.68	0	0.14	61.98	0	0.77
49	C2a	C	17.1	0.07	0.54	9.3	1.74	1.59	3.24	0	0.1	56.77	0	0.83
50	C2b	C	12.03	0.06	0.69	7.45	1.42	1.37	3.72	0	0.1	65.79	0	0.56

51	C3	C	15.43	0.1	0.95	10.57	1.64	1.86	5.24	0	0.35	53.63	0	0.72
52	E1	E	15.03	0.07	0.86	10.31	1.59	2.11	4.83	0	0.23	55.68	0	0.72
53	E2	E	14.17	0.07	0.76	10.03	1.47	2.08	4.5	0	0.17	58.16	0	0.67
54	E3	E	16.01	0	0.33	7.35	1.54	1.58	0.5	0	0.1	65.01	0	0.96
55	E4	E	15.3	0.08	0.73	10.36	1.55	2.28	4.7	0	0.15	55.66	0	0.73
56	E5	E	15	0.08	0.69	10.27	1.55	2.39	4.88	0	0.15	55.38	0	0.71
57	LBL1	L	9.87	0.05	4.33	7.16	1.25	2.14	4.89	0.21	0.1	58.93	0.79	0.44
58	LBL2	L	6.15	0.05	6.22	6.51	1.05	1.59	6.16	0.09	0.09	60.83	0.19	0.25
59	LBL3	L	7.66	0.06	1.62	7.42	1.35	2.08	7.13	0	0.11	64.47	0	0.33
60	LFP1a	L	6.84	0	14.1	4.18	0.68	1.61	1.43	0	0.76	51.82	0.07	0.4
61	LFP1b	L	7.53	0	2.01	4.75	0.66	0.72	1.35	0	0.77	72.56	0	0.5
62	LFP2	L	6.49	0	3.61	4.19	0.56	0.63	1.35	0	2.05	71.92	0.1	0.44
63	LFP3	L	8.57	0	1.76	5.49	0.76	0.78	1.63	0	0.65	70.14	0	0.56
64	LFP-cmp	L	8.97	0	2.29	5.84	0.96	1.13	2.46	0	0.67	68.2	0.1	0.49
65	2280	Y	15.16	0.23	1.17	9.07	1.6	2.17	16.05	0.07	0.17	41.21	0	0.66
66	HAP1	DS	16.57	0	0.28	8.67	1.23	0.68	0.95	0	0.08	63.08	0	0.9
67	HD01	DS	12.82	0.06	0.54	9.07	0.88	3.2	1.89	0	0.07	63.48	0	0.77
68	HD02	DS	12.74	0.06	0.87	9.88	1.24	2.45	3.59	0	0.12	59.79	0	0.67
69	HD03	DS	5.47	0	16.79	5.05	0.56	12.66	2.48	0	0.08	28.41	0	0.27
70	LO1	DS	15.38	0.08	0.62	9.96	1.65	2.36	4.48	0	0.11	55.96	0	0.73
71	LO2	DS	12.11	0.07	6.1	9.14	1.35	7.03	4.45	0	0.11	42.52	0	0.55
72	LO3	DS	5.93	0	25.27	4.14	0.68	9.7	2.15	0	0.06	20.22	0	0.28
73	LO4	DS	21.9	0	0.31	7.35	2.53	4.75	0.13	0.1	0.06	53.66	0	1.01
74	PF01	DS	13.23	0.06	0.89	10.52	1.2	2.1	3.81	0.12	0.1	58.25	0.43	0.68
75	PF02	DS	0.39	0	5.09	32.71	0.07	5.61	11.38	0	0.05	27.46	0	0
76	PF03	DS	6.46	0.05	1.23	8.36	0.74	1.97	5.58	0	0.1	68.11	0.56	0.28
77	PFL01	DS	7.24	0	5.67	4.94	0.53	0.7	1.07	0	0	66.18	6.86	0.47
78	PRG01	DS	16.06	0.07	0.88	10.61	1.51	2.66	4.16	0	0.13	53.4	0	0.73
79	PRG02	DS	8.44	0	7.65	5.53	0.57	0.96	1.03	0	0.06	63.33	0	0.52
80	TC01	DS	14.27	0.06	5.44	9.65	1.44	3.69	3.59	0	0.46	46.83	0	0.63

					RepPCA					
Element	**PC1F**	**PC1**	**PC2F**	**PC2**	**PC3F**	**PC3**	**PC4F**	**PC4**	**PC5F**	**PC5**
Al	0.46023426	-0.46023426	-0.03301144	0.03301144	0.2732224	-0.2732224	-0.10622817	0.106228	0.05244178	-0.05244178
Ba	0.32335792	-0.32335792	-0.31200185	0.31200185	-0.1702524	0.1702524	0.0259502	-0.02595	-0.239518029	0.239518029
Ca	-0.41976999	0.41976999	-0.1202494	0.1202494	0.3180386	-0.3180386	-0.0864721	0.086472	-0.133233254	0.133233254
Fe	0.08190813	-0.08190813	-0.38589629	0.38589629	-0.2792824	0.2792824	0.24843703	-0.24844	0.398630372	-0.398630372
K	0.44315691	-0.44315691	-0.10896763	0.10896763	0.2273179	-0.2273179	-0.1387837	0.138784	-0.084084424	0.084084424
Mg	-0.25225333	0.25225333	-0.36854213	0.36854213	0.4223433	-0.4223433	-0.08860402	0.088604	0.004940489	-0.004940489
Mn	0.07613576	-0.07613576	-0.4605196	0.4605196	-0.4543618	0.4543618	0.07727934	-0.07728	-0.154796302	0.154796302
Na	-0.02499257	0.02499257	-0.03593409	0.03593409	-0.2187547	0.2187547	-0.59163115	0.591631	-0.593276679	0.593276679
P	-0.04571699	0.04571699	0.22638795	-0.22638795	0.0595178	-0.0595178	0.59344408	-0.59344	-0.463377236	0.463377236
Si	0.15012531	-0.15012531	0.52495252	-0.52495252	-0.2831844	0.2831844	0.02593522	-0.02594	-0.034265711	0.034265711
S	-0.13777125	0.13777125	0.19848439	-0.19848439	-0.2367094	0.2367094	-0.42114234	0.421142	0.395548964	-0.395548964
Ti	0.43664477	-0.43664477	0.10440175	-0.10440175	0.3051292	-0.3051292	-0.07431884	0.074319	0.088534755	-0.088534755

new_data

Number	Sample Name	Locality	Al2O3	CaO	Fe2O3	K2O	MgO	MnO	P2O5	SiO2	TiO2
1	DF1	DF	16.39	1.55	10.69	1.72	2.79	4.41	0.27	52.67	0.75
2	DF2	DF	16.97	1.18	10.15	1.75	2.42	3.66	0.19	54.23	0.81
3	DF3	DF	15.65	1.22	10.49	1.61	2.66	4.25	0.37	54.69	0.75
4	DF4	DF	16.09	1.17	10.33	1.68	2.67	4.32	0.27	53.11	0.76
5	DF5	DF	16.23	1.21	10.51	1.68	2.51	4.3	0.29	53.89	0.75
6	DF6	DF	16.02	1.21	10.46	1.67	2.59	4.29	0.25	54.1	0.77
7	DF7	DF	16.47	1.58	10.09	1.71	2.73	3.98	0.27	53.34	0.77
8	DF8	DF	14.38	6.9	8.95	1.52	3.08	3.45	0.57	48.09	0.69
9	DF9	DF	15.63	1.04	10.42	1.62	2.51	4.51	0.34	54.9	0.73
10	DF10	DF	16.09	1.17	10.66	1.67	2.56	4.53	0.35	53.33	0.74
11	DF11	DF	17.45	0.86	10.38	1.8	2.13	3.7	0.18	53.75	0.81
12	DF12	DF	16.91	1.3	10.42	1.74	2.2	4.09	0.48	52.89	0.78
13	DF13	DF	15.82	0.92	10.7	1.68	2.31	4.52	0.27	55.15	0.75
14	DF14	DF	16.45	0.76	10.08	1.68	2.08	3.7	0.21	56.3	0.78
15	DF15	DF	15.15	1	10.79	1.7	2.61	5.28	0.23	53.78	0.71
16	DF16	DF	16.09	0.88	10.69	1.71	2.39	4.6	0.23	53.82	0.76
17	DF17	DF	15.35	0.88	10.36	1.6	2.33	4.35	0.25	56.1	0.73
18	DF18	DF	15.48	0.95	10.46	1.61	2.27	4.41	0.27	55.39	0.73
19	DF19	DF	16.73	0.8	10.07	1.71	2.25	3.62	0.16	55.6	0.81
20	DF20	DF	17.3	0.97	10.13	1.72	2.22	3.49	0.2	54.3	0.8
21	DF21	DF	14.57	0.89	9.55	1.49	2	3.59	0.33	59.28	0.72
22	DF22	DF	14.85	0.89	10.22	1.54	2.07	4.13	0.32	57.61	0.72
23	DF23	DF	14.13	0.96	9.78	1.42	2.32	3.86	0.34	58.71	0.7
24	DF24	DF	14.69	1	9.5	1.42	2.33	3.45	0.39	58.44	0.72
25	DF25	DF	15.02	0.91	9.51	1.44	2.36	3.5	0.29	58.57	0.74
26	DF26	DF	14.78	1.08	9.28	1.43	2.32	3.2	0.4	58.76	0.76
27	DF27	DF	15.18	0.98	9.54	1.52	2.12	3.74	0.36	57.51	0.76
28	DF28	DF	13.71	1.01	9.31	1.35	2.18	3.78	0.31	60.38	0.7
29	DF29	DF	14.8	1.55	9.96	1.52	2.22	4.6	0.75	55.51	0.7
30	DF30	DF	14.26	1.18	9.64	1.47	2.02	4.02	0.51	58.44	0.71
31	DF31	DF	16.19	0.88	10.1	1.69	1.95	3.88	0.3	56.21	0.78
32	DF32	DF	14.88	1.36	9.8	1.53	1.94	3.9	0.63	57.03	0.73
33	DF33	DF	14.1	2.11	9.45	1.49	1.91	3.92	1.16	57.55	0.69
34	DF34	DF	16.09	2.03	10.19	1.68	2.01	3.54	1.14	54.58	0.78
35	A1a	A	14.02	4.7	9.12	1.44	4.29	3.6	0.75	48.99	0.67
36	A1b	A	17.95	1.18	10.77	1.44	2.08	6.57	0.12	48.76	0.65
37	A2a	A	15.12	0.81	10.52	1.56	2.48	5.14	0.16	54.71	0.7
38	A2b	A	15.69	0.82	8.53	1.35	1.69	4.34	0.09	59.01	0.55
39	A3	A	13	5.05	9.03	1.36	4.67	4.19	0.68	47.76	0.62
40	A4	A	15.46	0.88	12.84	2.01	2.59	7.06	0.19	48.44	0.65
41	A5	A	13.34	3.71	8.88	1.37	3.94	3.75	0.47	52.66	0.66
42	A6	A	15.32	0.81	10.99	1.76	2.45	6.24	0.14	51.72	0.7
43	A7	A	13.19	4.85	8.99	1.37	4.52	3.94	0.55	48.99	0.64
44	A8	A	14.29	3.16	10.22	1.52	3.75	4.4	0.41	49.87	0.71
45	B1a	B	14.85	0.82	8.99	1.58	1.52	4.53	0.14	58.77	0.65
46	B1b	B	14.49	1.2	9.92	1.42	2.18	4.31	0.46	56.52	0.68
47	B2	B	16.65	0.72	8.83	1.5	1.68	3.48	0.09	57.65	0.71
48	C1	C	15.32	0.76	8.25	1.69	1.38	2.68	0.14	61.98	0.77
49	C2a	C	17.1	0.54	9.3	1.74	1.59	3.24	0.1	56.77	0.83
50	C2b	C	12.03	0.69	7.45	1.42	1.37	3.72	0.1	65.79	0.56

51	C3	C	15.43	0.95	10.57	1.64	1.86	5.24	0.35	53.63	0.72
52	E1	E	15.03	0.86	10.31	1.59	2.11	4.83	0.23	55.68	0.72
53	E2	E	14.17	0.76	10.03	1.47	2.08	4.5	0.17	58.16	0.67
54	E3	E	16.01	0.33	7.35	1.54	1.58	0.5	0.1	65.01	0.96
55	E4	E	15.3	0.73	10.36	1.55	2.28	4.7	0.15	55.66	0.73
56	E5	E	15	0.69	10.27	1.55	2.39	4.88	0.15	55.38	0.71
57	LBL1	L	9.87	4.33	7.16	1.25	2.14	4.89	0.1	58.93	0.44
58	LBL2	L	6.15	6.22	6.51	1.05	1.59	6.16	0.09	60.83	0.25
59	LBL3	L	7.66	1.62	7.42	1.35	2.08	7.13	0.11	64.47	0.33
60	LFP1a	L	6.84	14.1	4.18	0.68	1.61	1.43	0.76	51.82	0.4
61	LFP1b	L	7.53	2.01	4.75	0.66	0.72	1.35	0.77	72.56	0.5
62	LFP2	L	6.49	3.61	4.19	0.56	0.63	1.35	2.05	71.92	0.44
63	LFP3	L	8.57	1.76	5.49	0.76	0.78	1.63	0.65	70.14	0.56
64	LFP-cmp	L	8.97	2.29	5.84	0.96	1.13	2.46	0.67	68.2	0.49
65	2280	Y	15.16	1.17	9.07	1.6	2.17	16.05	0.17	41.21	0.66
66	HAP1	DS	16.57	0.28	8.67	1.23	0.68	0.95	0.08	63.08	0.9
67	HD01	DS	12.82	0.54	9.07	0.88	3.2	1.89	0.07	63.48	0.77
68	HD02	DS	12.74	0.87	9.88	1.24	2.45	3.59	0.12	59.79	0.67
69	HD03	DS	5.47	16.79	5.05	0.56	12.66	2.48	0.08	28.41	0.27
70	LO1	DS	15.38	0.62	9.96	1.65	2.36	4.48	0.11	55.96	0.73
71	LO2	DS	12.11	6.1	9.14	1.35	7.03	4.45	0.11	42.52	0.55
72	LO3	DS	5.93	25.27	4.14	0.68	9.7	2.15	0.06	20.22	0.28
73	LO4	DS	21.9	0.31	7.35	2.53	4.75	0.13	0.06	53.66	1.01
74	PF01	DS	13.23	0.89	10.52	1.2	2.1	3.81	0.1	58.25	0.68
75	PF02	DS	0.39	5.09	32.71	0.07	5.61	11.38	0.05	27.46	0.025
76	PF03	DS	6.46	1.23	8.36	0.74	1.97	5.58	0.1	68.11	0.28
77	PFL01	DS	7.24	5.67	4.94	0.53	0.7	1.07	0.005	66.18	0.47
78	PRG01	DS	16.06	0.88	10.61	1.51	2.66	4.16	0.13	53.4	0.73
79	PRG02	DS	8.44	7.65	5.53	0.57	0.96	1.03	0.06	63.33	0.52
80	TC01	DS	14.27	5.44	9.65	1.44	3.69	3.59	0.46	46.83	0.63

	NewPCA									
Element	**PC1F**	**PC1**	**PC2F**	**PC2**	**PC3F**	**PC3**	**PC4F**	**PC4**	**PC5F**	**PC5**
Al	0.462803311	-0.462803311	-0.213469988	0.213469988	0.260951824	-0.260951824	-0.06913998	0.06913998	0.04089521	-0.04089521
Ca	-0.450271582	0.450271582	0.007784742	-0.007784742	0.37138566	-0.37138566	-0.02390633	0.02390633	0.1275189	-0.1275189
Fe	0.009139457	-0.009139457	-0.456480179	0.456480179	-0.431579154	0.431579154	-0.17840876	0.17840876	-0.66857395	0.66857395
K	0.425423929	-0.425423929	-0.270356596	0.270356596	0.227838383	-0.227838383	-0.09879663	0.09879663	0.27626944	-0.27626944
Mg	-0.329943613	0.329943613	-0.326347938	0.326347938	0.418817157	-0.418817157	-0.0623457	0.0623457	-0.12393447	0.12393447
Mn	-0.044088562	0.044088562	-0.43254571	0.43254571	-0.481757231	0.481757231	-0.13017842	0.13017842	0.64205499	-0.64205499
P	-0.018075491	0.018075491	0.330353136	-0.330353136	-0.008724634	0.008724634	-0.94061582	0.94061582	0.0214979	-0.0214979
Si	0.263482497	-0.263482497	0.514478945	-0.514478945	-0.252474355	0.252474355	0.20641409	-0.20641409	-0.01076752	0.01076752
Ti	0.470577527	-0.470577527	-0.074044391	0.074044391	0.29066937	-0.29066937	-0.06970937	0.06970937	-0.17486597	0.17486597

			RepScores			
Sample	Sample Name	Locality	PC1F	PC1	PC2F	PC2
1	DF1	DF	1.17096849	-1.17096849	-0.692846302	0.692846302
2	DF2	DF	1.43766875	-1.43766875	-0.218963906	0.218963906
3	DF3	DF	0.92343516	-0.92343516	-0.267237841	0.267237841
4	DF4	DF	1.16897632	-1.16897632	-0.54448208	0.54448208
5	DF5	DF	1.09945282	-1.09945282	-0.382473753	0.382473753
6	DF6	DF	1.11112867	-1.11112867	-0.389942836	0.389942836
7	DF7	DF	1.11514656	-1.11514656	-0.366815732	0.366815732
8	DF8	DF	-0.5035958	0.5035958	-0.352696851	0.352696851
9	DF9	DF	1.03081764	-1.03081764	-0.393723929	0.393723929
10	DF10	DF	1.12836015	-1.12836015	-0.544479441	0.544479441
11	DF11	DF	1.63327366	-1.63327366	-0.23985265	0.23985265
12	DF12	DF	1.31267571	-1.31267571	-0.189855065	0.189855065
13	DF13	DF	1.24109848	-1.24109848	-0.425212672	0.425212672
14	DF14	DF	1.2474657	-1.2474657	0.106234112	-0.106234112
15	DF15	DF	1.03138322	-1.03138322	-0.809006251	0.809006251
16	DF16	DF	1.31384687	-1.31384687	-0.57437353	0.57437353
17	DF17	DF	0.94956758	-0.94956758	-0.200250334	0.200250334
18	DF18	DF	1.06158978	-1.06158978	-0.339691385	0.339691385
19	DF19	DF	1.35977204	-1.35977204	0.015442418	-0.015442418
20	DF20	DF	1.36995592	-1.36995592	-0.028671468	0.028671468
21	DF21	DF	0.83612742	-0.83612742	0.332075524	-0.332075524
22	DF22	DF	0.92682327	-0.92682327	-0.01044384	0.01044384
23	DF23	DF	0.5973188	-0.5973188	0.157894481	-0.157894481
24	DF24	DF	0.58729418	-0.58729418	0.396664021	-0.396664021
25	DF25	DF	0.63595004	-0.63595004	0.410666268	-0.410666268
26	DF26	DF	0.6044467	-0.6044467	0.617751788	-0.617751788
27	DF27	DF	1.09015022	-1.09015022	0.103949332	-0.103949332
28	DF28	DF	0.49836056	-0.49836056	0.365901312	-0.365901312
29	DF29	DF	0.65833079	-0.65833079	0.04279607	-0.04279607
30	DF30	DF	0.59413014	-0.59413014	0.385964429	-0.385964429
31	DF31	DF	1.41170547	-1.41170547	-0.033842648	0.033842648
32	DF32	DF	0.74260222	-0.74260222	0.394406132	-0.394406132
33	DF33	DF	0.33474862	-0.33474862	0.829560191	-0.829560191
34	DF34	DF	0.99276177	-0.99276177	0.590746969	-0.590746969
35	A1a	A	-0.62413066	0.62413066	-0.389451017	0.389451017
36	A1b	A	0.77230814	-0.77230814	-1.1884293	1.1884293
37	A2a	A	0.99077677	-0.99077677	-0.763302035	0.763302035
38	A2b	A	0.16852421	-0.16852421	0.357743438	-0.357743438
39	A3	A	-0.96998065	0.96998065	-0.819077968	0.819077968
40	A4	A	1.59016212	-1.59016212	-2.203059472	2.203059472
41	A5	A	-0.45526798	0.45526798	-0.335630189	0.335630189
42	A6	A	1.34378106	-1.34378106	-1.405902063	1.405902063
43	A7	A	-0.80608597	0.80608597	-0.731661443	0.731661443
44	A8	A	0.07469921	-0.07469921	-0.81974504	0.81974504
45	B1a	B	0.71543219	-0.71543219	0.234231485	-0.234231485
46	B1b	B	0.54620253	-0.54620253	-0.000912987	0.000912987
47	B2	B	0.85172633	-0.85172633	0.481838671	-0.481838671
48	C1	C	1.12380538	-1.12380538	1.094446506	-1.094446506
49	C2a	C	1.70896568	-1.70896568	0.27827491	-0.27827491
50	C2b	C	0.0344858	-0.0344858	1.056730883	-1.056730883

51	C3	C	1.29992507	-1.29992507	-0.696375235	0.696375235
52	E1	E	0.91649712	-0.91649712	-0.294339032	0.294339032
53	E2	E	0.5871973	-0.5871973	-0.057805654	0.057805654
54	E3	E	1.05240065	-1.05240065	2.424768232	-2.424768232
55	E4	E	1.0241011	-1.0241011	-0.439349032	0.439349032
56	E5	E	0.92055806	-0.92055806	-0.517521636	0.517521636
57	LBL1	L	-1.75998274	1.75998274	0.16961992	-0.16961992
58	LBL2	L	-2.82909209	2.82909209	0.088982905	-0.088982905
59	LBL3	L	-1.32061123	1.32061123	-0.03062336	0.03062336
60	LFP1a	L	-4.51348479	4.51348479	1.801351925	-1.801351925
61	LFP1b	L	-2.31378781	2.31378781	3.674804191	-3.674804191
62	LFP2	L	-3.11821384	3.11821384	4.635973509	-4.635973509
63	LFP3	L	-1.88540321	1.88540321	3.280505405	-3.280505405
64	LFP-cmp	L	-1.9191787	1.9191787	2.780012428	-2.780012428
65	2280	Y	2.31856409	-2.31856409	-5.160562302	5.160562302
66	HAP1	DS	0.7648989	-0.7648989	2.266348443	-2.266348443
67	HD01	DS	-0.2303866	0.2303866	0.993730335	-0.993730335
68	HD02	DS	-0.01645011	0.01645011	0.312317697	-0.312317697
69	HD03	DS	-7.30992828	7.30992828	-2.97042784	2.97042784
70	LO1	DS	1.14190608	-1.14190608	-0.395575416	0.395575416
71	LO2	DS	-1.73523915	1.73523915	-2.201379913	2.201379913
72	LO3	DS	-7.7841696	7.7841696	-2.993772587	2.993772587
73	LO4	DS	2.31478982	-2.31478982	0.684122278	-0.684122278
74	PF01	DS	-0.09770527	0.09770527	0.134502726	-0.134502726
75	PF02	DS	-5.89444138	5.89444138	-6.464340896	6.464340896
76	PF03	DS	-2.40089539	2.40089539	0.837672506	-0.837672506
77	PFL01	DS	-4.21097167	4.21097167	4.416687163	-4.416687163
78	PRG01	DS	0.8586411	-0.8586411	-0.496744441	0.496744441
79	PRG02	DS	-2.96159699	2.96159699	2.350431934	-2.350431934
80	TC01	DS	-0.67708257	0.67708257	-0.724299163	0.724299163

			NewScores			
Sample	**Sample Name**	**Locality**	**PC1F**	**PC1**	**PC2F**	**PC2**
1	DF1	DF	0.88358739	-0.88358739	-0.90910694	0.90910694
2	DF2	DF	1.34591878	-1.34591878	-0.68152581	0.68152581
3	DF3	DF	0.79320249	-0.79320249	-0.47274817	0.47274817
4	DF4	DF	0.91318495	-0.91318495	-0.74975602	0.74975602
5	DF5	DF	0.95187103	-0.95187103	-0.67565933	0.67565933
6	DF6	DF	0.96583758	-0.96583758	-0.70122114	0.70122114
7	DF7	DF	0.97683205	-0.97683205	-0.68944011	0.68944011
8	DF8	DF	-0.60526117	0.60526117	-0.18099527	0.18099527
9	DF9	DF	0.79627081	-0.79627081	-0.50478201	0.50478201
10	DF10	DF	0.86395218	-0.86395218	-0.70414799	0.70414799
11	DF11	DF	1.54016436	-1.54016436	-0.77223107	0.77223107
12	DF12	DF	1.20038497	-1.20038497	-0.51434185	0.51434185
13	DF13	DF	1.00856837	-1.00856837	-0.63132612	0.63132612
14	DF14	DF	1.2934614	-1.2934614	-0.37579096	0.37579096
15	DF15	DF	0.7065628	-0.7065628	-0.94006217	0.94006217
16	DF16	DF	1.05326212	-1.05326212	-0.82727755	0.82727755
17	DF17	DF	0.837926	-0.837926	-0.4224631	0.4224631
18	DF18	DF	0.84396167	-0.84396167	-0.474456	0.474456
19	DF19	DF	1.3944554	-1.3944554	-0.53710657	0.53710657
20	DF20	DF	1.3943613	-1.3943613	-0.58572149	0.58572149
21	DF21	DF	0.75919386	-0.75919386	0.31924138	-0.31924138
22	DF22	DF	0.77503831	-0.77503831	-0.0650945	0.0650945
23	DF23	DF	0.47637109	-0.47637109	0.23055971	-0.23055971
24	DF24	DF	0.59547337	-0.59547337	0.34822584	-0.34822584
25	DF25	DF	0.73132352	-0.73132352	0.18894495	-0.18894495
26	DF26	DF	0.73996006	-0.73996006	0.43309735	-0.43309735
27	DF27	DF	0.89155616	-0.89155616	0.11606055	-0.11606055
28	DF28	DF	0.42126644	-0.42126644	0.48388323	-0.48388323
29	DF29	DF	0.47996016	-0.47996016	0.2066695	-0.2066695
30	DF30	DF	0.5846526	-0.5846526	0.39282781	-0.39282781
31	DF31	DF	1.26953611	-1.26953611	-0.2918482	0.2918482
32	DF32	DF	0.73246869	-0.73246869	0.3650424	-0.3650424
33	DF33	DF	0.37337629	-0.37337629	1.11039791	-1.11039791
34	DF34	DF	1.00401856	-1.00401856	0.57076258	-0.57076258
35	A1a	A	-0.74711231	0.74711231	-0.13238203	0.13238203
36	A1b	A	0.50677741	-0.50677741	-1.48743114	1.48743114
37	A2a	A	0.6035823	-0.6035823	-0.76334151	0.76334151
38	A2b	A	0.31170706	-0.31170706	0.20181341	-0.20181341
39	A3	A	-1.27014623	1.27014623	-0.32376492	0.32376492
40	A4	A	0.73250605	-0.73250605	-2.17266434	2.17266434
41	A5	A	-0.6271321	0.6271321	-0.04781586	0.04781586
42	A6	A	0.73874808	-0.73874808	-1.40732595	1.40732595
43	A7	A	-1.07348864	1.07348864	-0.3301073	0.3301073
44	A8	A	-0.18977955	0.18977955	-0.75686544	0.75686544
45	B1a	B	0.76370757	-0.76370757	0.01208047	-0.01208047
46	B1b	B	0.37737132	-0.37737132	0.12661192	-0.12661192
47	B2	B	1.05080463	-1.05080463	0.02128788	-0.02128788
48	C1	C	1.46213901	-1.46213901	0.56360114	-0.56360114
49	C2a	C	1.73406823	-1.73406823	-0.27069107	0.27069107
50	C2b	C	0.24790071	-0.24790071	1.13236878	-1.13236878

51	C3	C	0.84168364	-0.84168364	-0.62039279	0.62039279
52	E1	E	0.77885729	-0.77885729	-0.49026622	0.49026622
53	E2	E	0.4985382	-0.4985382	-0.1323117	0.1323117
54	E3	E	2.09007237	-2.09007237	1.22355197	-1.22355197
55	E4	E	0.7889279	-0.7889279	-0.58230618	0.58230618
56	E5	E	0.66395352	-0.66395352	-0.61767879	0.61767879
57	LBL1	L	-1.38188045	1.38188045	0.67479819	-0.67479819
58	LBL2	L	-2.71510761	2.71510761	1.16221278	-1.16221278
59	LBL3	L	-1.41077924	1.41077924	0.64264881	-0.64264881
60	LFP1a	L	-3.7722685	3.7722685	2.79657733	-2.79657733
61	LFP1b	L	-1.15033836	1.15033836	4.08458921	-4.08458921
62	LFP2	L	-1.83689015	1.83689015	5.67652331	-5.67652331
63	LFP3	L	-0.78901771	0.78901771	3.47444552	-3.47444552
64	LFP-cmp	L	-0.92967591	0.92967591	2.96082254	-2.96082254
65	2280	Y	-0.1062752	0.1062752	-3.57993776	3.57993776
66	HAP1	DS	1.76009365	-1.76009365	1.18040609	-1.18040609
67	HD01	DS	0.01046329	-0.01046329	0.99648558	-0.99648558
68	HD02	DS	0.05438663	-0.05438663	0.29840132	-0.29840132
69	HD03	DS	-7.57699258	7.57699258	-1.54486116	1.54486116
70	LO1	DS	0.92173179	-0.92173179	-0.59380065	0.59380065
71	LO2	DS	-2.30444206	2.30444206	-1.67352935	1.67352935
72	LO3	DS	-8.06408869	8.06408869	-1.41616083	1.41616083
73	LO4	DS	3.1263768	-3.1263768	-1.08894882	1.08894882
74	PF01	DS	0.11583291	-0.11583291	0.10567346	-0.10567346
75	PF02	DS	-6.87802314	6.87802314	-5.36569818	5.36569818
76	PF03	DS	-2.15760735	2.15760735	1.57828553	-1.57828553
77	PFL01	DS	-1.99871351	1.99871351	3.03526271	-3.03526271
78	PRG01	DS	0.69487982	-0.69487982	-0.7542553	0.7542553
79	PRG02	DS	-2.03299557	2.03299557	2.67793801	-2.67793801
80	TC01	DS	-0.85505501	0.85505501	-0.53245953	0.53245953

extradata

Number	Sample Name	Locality	Al2O3	BaO	CaO	Fe2O3	K2O	MgO	MnO	P2O5	SiO2	TiO2
1	DF1	DF	16.39	0.08	1.55	10.69	1.72	2.79	4.41	0.27	52.67	0.75
2	DF2	DF	16.97	0.07	1.18	10.15	1.75	2.42	3.66	0.19	54.23	0.81
3	DF3	DF	15.65	0.07	1.22	10.49	1.61	2.66	4.25	0.37	54.69	0.75
4	DF4	DF	16.09	0.08	1.17	10.33	1.68	2.67	4.32	0.27	53.11	0.76
5	DF5	DF	16.23	0.07	1.21	10.51	1.68	2.51	4.3	0.29	53.89	0.75
6	DF6	DF	16.02	0.07	1.21	10.46	1.67	2.59	4.29	0.25	54.1	0.77
7	DF7	DF	16.47	0.07	1.58	10.09	1.71	2.73	3.98	0.27	53.34	0.77
8	DF8	DF	14.38	0.06	6.9	8.95	1.52	3.08	3.45	0.57	48.09	0.69
9	DF9	DF	15.63	0.08	1.04	10.42	1.62	2.51	4.51	0.34	54.9	0.73
10	DF10	DF	16.09	0.08	1.17	10.66	1.67	2.56	4.53	0.35	53.33	0.74
11	DF11	DF	17.45	0.07	0.86	10.38	1.8	2.13	3.7	0.18	53.75	0.81
12	DF12	DF	16.91	0.07	1.3	10.42	1.74	2.2	4.09	0.48	52.89	0.78
13	DF13	DF	15.82	0.08	0.92	10.7	1.68	2.31	4.52	0.27	55.15	0.75
14	DF14	DF	16.45	0.06	0.76	10.08	1.68	2.08	3.7	0.21	56.3	0.78
15	DF15	DF	15.15	0.08	1	10.79	1.7	2.61	5.28	0.23	53.78	0.71
16	DF16	DF	16.09	0.08	0.88	10.69	1.71	2.39	4.6	0.23	53.82	0.76
17	DF17	DF	15.35	0.07	0.88	10.36	1.6	2.33	4.35	0.25	56.1	0.73
18	DF18	DF	15.48	0.08	0.95	10.46	1.61	2.27	4.41	0.27	55.39	0.73
19	DF19	DF	16.73	0.06	0.8	10.07	1.71	2.25	3.62	0.16	55.6	0.81
20	DF20	DF	17.3	0.06	0.97	10.13	1.72	2.22	3.49	0.2	54.3	0.8
21	DF21	DF	14.57	0.08	0.89	9.55	1.49	2	3.59	0.33	59.28	0.72
22	DF22	DF	14.85	0.08	0.89	10.22	1.54	2.07	4.13	0.32	57.61	0.72
23	DF23	DF	14.13	0.08	0.96	9.78	1.42	2.32	3.86	0.34	58.71	0.7
24	DF24	DF	14.69	0.07	1	9.5	1.42	2.33	3.45	0.39	58.44	0.72
25	DF25	DF	15.02	0.06	0.91	9.51	1.44	2.36	3.5	0.29	58.57	0.74
26	DF26	DF	14.78	0.06	1.08	9.28	1.43	2.32	3.2	0.4	58.76	0.76
27	DF27	DF	15.18	0.09	0.98	9.54	1.52	2.12	3.74	0.36	57.51	0.76
28	DF28	DF	13.71	0.08	1.01	9.31	1.35	2.18	3.78	0.31	60.38	0.7
29	DF29	DF	14.8	0.08	1.55	9.96	1.52	2.22	4.6	0.75	55.51	0.7
30	DF30	DF	14.26	0.07	1.18	9.64	1.47	2.02	4.02	0.51	58.44	0.71
31	DF31	DF	16.19	0.08	0.88	10.1	1.69	1.95	3.88	0.3	56.21	0.78
32	DF32	DF	14.88	0.07	1.36	9.8	1.53	1.94	3.9	0.63	57.03	0.73
33	DF33	DF	14.1	0.07	2.11	9.45	1.49	1.91	3.92	1.16	57.55	0.69
34	DF34	DF	16.09	0.07	2.03	10.19	1.68	2.01	3.54	1.14	54.58	0.78
35	A1a	A	14.02	0.06	4.7	9.12	1.44	4.29	3.6	0.75	48.99	0.67
36	A1b	A	17.95	0.06	1.18	10.77	1.44	2.08	6.57	0.12	48.76	0.65
37	A2a	A	15.12	0.09	0.81	10.52	1.56	2.48	5.14	0.16	54.71	0.7
38	A2b	A	15.69	0.05	0.82	8.53	1.35	1.69	4.34	0.09	59.01	0.55
39	A3	A	13	0.07	5.05	9.03	1.36	4.67	4.19	0.68	47.76	0.62
40	A4	A	15.46	0.11	0.88	12.84	2.01	2.59	7.06	0.19	48.44	0.65
41	A5	A	13.34	0.07	3.71	8.88	1.37	3.94	3.75	0.47	52.66	0.66
42	A6	A	15.32	0.1	0.81	10.99	1.76	2.45	6.24	0.14	51.72	0.7
43	A7	A	13.19	0.07	4.85	8.99	1.37	4.52	3.94	0.55	48.99	0.64
44	A8	A	14.29	0.07	3.16	10.22	1.52	3.75	4.4	0.41	49.87	0.71
45	B1a	B	14.85	0.06	0.82	8.99	1.58	1.52	4.53	0.14	58.77	0.65
46	B1b	B	14.49	0.08	1.2	9.92	1.42	2.18	4.31	0.46	56.52	0.68
47	B2	B	16.65	0.05	0.72	8.83	1.5	1.68	3.48	0.09	57.65	0.71
48	C1	C	15.32	0.05	0.76	8.25	1.69	1.38	2.68	0.14	61.98	0.77
49	C2a	C	17.1	0.07	0.54	9.3	1.74	1.59	3.24	0.1	56.77	0.83
50	C2b	C	12.03	0.06	0.69	7.45	1.42	1.37	3.72	0.1	65.79	0.56

51	C3	C	15.43	0.1	0.95	10.57	1.64	1.86	5.24	0.35	53.63	0.72
52	E1	E	15.03	0.07	0.86	10.31	1.59	2.11	4.83	0.23	55.68	0.72
53	E2	E	14.17	0.07	0.76	10.03	1.47	2.08	4.5	0.17	58.16	0.67
54	E3	E	16.01	0.005	0.33	7.35	1.54	1.58	0.5	0.1	65.01	0.96
55	E4	E	15.3	0.08	0.73	10.36	1.55	2.28	4.7	0.15	55.66	0.73
56	E5	E	15	0.08	0.69	10.27	1.55	2.39	4.88	0.15	55.38	0.71

ExtraPCARep

Element	PC1F	PC1	PC2F	PC2	PC3F	PC3	PC4F	PC4	PC5F	PC5
Al	0.151237789	-0.151237789	-0.4142678	0.4142678	-0.336007994	0.336007994	0.17574096	-0.17574096	-0.50257327	0.50257327
Ba	-0.362910814	0.362910814	-0.2508614	0.2508614	0.281572261	-0.281572261	-0.34535849	0.34535849	0.40138678	-0.40138678
Ca	-0.323776971	0.323776971	0.34488083	-0.34488083	-0.336952181	0.336952181	0.11146742	-0.11146742	-0.05910421	0.05910421
Fe	-0.292703256	0.292703256	-0.44004679	0.44004679	-0.001274647	0.001274647	-0.14746943	0.14746943	0.03061098	-0.03061098
K	-0.006737253	0.006737253	-0.46338557	0.46338557	-0.254445452	0.254445452	-0.08283761	0.08283761	0.1631844	-0.1631844
Mg	-0.401318803	0.401318803	0.2072339	-0.2072339	-0.302253049	0.302253049	0.25481651	-0.25481651	0.40728052	-0.40728052
Mn	-0.381390173	0.381390173	-0.27752891	0.27752891	0.346001552	-0.346001552	0.13012128	-0.13012128	-0.27364689	0.27364689
P	-0.21104615	0.21104615	0.24890632	-0.24890632	-0.219177458	0.219177458	-0.78968848	0.78968848	-0.38612775	0.38612775
Si	0.467465389	-0.467465389	0.09539909	-0.09539909	0.331994653	-0.331994653	-0.23767378	0.23767378	0.17858725	-0.17858725
Ti	0.29204648	-0.29204648	-0.21706464	0.21706464	-0.510099615	0.510099615	-0.2164454	0.2164454	0.36537815	-0.36537815

ExtraRepScores

Sample	Sample Name	Locality	PC1F	PC1	PC2F	PC2
1	DF1	DF	-0.880710234	0.880710234	-1.51508127	1.51508127
2	DF2	DF	0.764499758	-0.764499758	-1.62558828	1.62558828
3	DF3	DF	-0.282435013	0.282435013	-0.54304648	0.54304648
4	DF4	DF	-0.49431247	0.49431247	-1.2322984	1.2322984
5	DF5	DF	-0.173781557	0.173781557	-1.16299709	1.16299709
6	DF6	DF	-0.07325831	0.07325831	-1.10885837	1.10885837
7	DF7	DF	-0.057904351	0.057904351	-0.97969352	0.97969352
8	DF8	DF	-2.348420817	2.348420817	3.30571596	-3.30571596
9	DF9	DF	-0.508726203	0.508726203	-0.83171714	0.83171714
10	DF10	DF	-0.761351029	0.761351029	-1.29822828	1.29822828
11	DF11	DF	0.932599705	-0.932599705	-2.28660273	2.28660273
12	DF12	DF	0.019165699	-0.019165699	-1.48366332	1.48366332
13	DF13	DF	-0.250181344	0.250181344	-1.47215269	1.47215269
14	DF14	DF	1.355016127	-1.355016127	-1.06340699	1.06340699
15	DF15	DF	-1.188113531	1.188113531	-1.40808297	1.40808297
16	DF16	DF	-0.366245515	0.366245515	-1.78471908	1.78471908
17	DF17	DF	0.157560103	-0.157560103	-0.59036233	0.59036233
18	DF18	DF	-0.21066435	0.21066435	-0.896174	0.896174
19	DF19	DF	1.410454719	-1.410454719	-1.34441388	1.34441388
20	DF20	DF	1.247070922	-1.247070922	-1.48769717	1.48769717
21	DF21	DF	0.871086279	-0.871086279	0.62335143	-0.62335143
22	DF22	DF	0.222783025	-0.222783025	-0.16884138	0.16884138
23	DF23	DF	0.256439182	-0.256439182	0.99791093	-0.99791093
24	DF24	DF	0.820244125	-0.820244125	1.22098487	-1.22098487
25	DF25	DF	1.279219668	-1.279219668	0.99324981	-0.99324981
26	DF26	DF	1.439390247	-1.439390247	1.40747378	-1.40747378
27	DF27	DF	0.491528627	-0.491528627	0.01897234	-0.01897234
28	DF28	DF	0.697782527	-0.697782527	1.61891172	-1.61891172
29	DF29	DF	-0.896467783	0.896467783	0.61318699	-0.61318699
30	DF30	DF	0.460703495	-0.460703495	1.08445332	-1.08445332
31	DF31	DF	0.716880123	-0.716880123	-1.30749146	1.30749146
32	DF32	DF	0.338099081	-0.338099081	0.67474823	-0.67474823
33	DF33	DF	-0.434302968	0.434302968	2.17290269	-2.17290269
34	DF34	DF	-0.259042659	0.259042659	0.19111222	-0.19111222
35	A1a	A	-2.793762882	2.793762882	3.6209091	-3.6209091
36	A1b	A	-1.394371678	1.394371678	-1.72346493	1.72346493
37	A2a	A	-1.015635205	1.015635205	-1.02539518	1.02539518
38	A2b	A	1.383332385	-1.383332385	1.65987144	-1.65987144
39	A3	A	-3.995580435	3.995580435	4.22291541	-4.22291541
40	A4	A	-4.135764444	4.135764444	-4.61678864	4.61678864
41	A5	A	-1.968322346	1.968322346	3.44991463	-3.44991463
42	A6	A	-2.179424166	2.179424166	-2.6010819	2.6010819
43	A7	A	-3.353586956	3.353586956	3.93945773	-3.93945773
44	A8	A	-2.376210118	2.376210118	1.24180068	-1.24180068
45	B1a	B	1.270514228	-1.270514228	0.39579064	-0.39579064
46	B1b	B	-0.381667987	0.381667987	0.8332308	-0.8332308
47	B2	B	2.336392684	-2.336392684	0.32635653	-0.32635653
48	C1	C	3.602809179	-3.602809179	0.56566254	-0.56566254
49	C2a	C	2.37216928	-2.37216928	-1.61722805	1.61722805
50	C2b	C	2.381952445	-2.381952445	3.28532055	-3.28532055

51	C3	C	-1.16869863	1.16869863	-1.6575041	1.6575041
52	E1	E	-0.009045538	0.009045538	-0.63383765	0.63383765
53	E2	E	0.296296126	-0.296296126	0.43791847	-0.43791847
54	E3	E	7.339112291	-7.339112291	2.08534227	-2.08534227
55	E4	E	-0.12177231	0.12177231	-0.84962315	0.84962315
56	E5	E	-0.383341202	0.383341202	-0.67142464	0.67142464

ExtraNewScores

Sample	Sample Name	Locality	PC1F	PC1	PC2F	PC2
1	DF1	DF	-0.93868611	0.93868611	-1.4850712	1.4850712
2	DF2	DF	0.7067536	-0.7067536	-1.6480512	1.6480512
3	DF3	DF	-0.30031233	0.30031233	-0.52980585	0.52980585
4	DF4	DF	-0.54172765	0.54172765	-1.21692951	1.21692951
5	DF5	DF	-0.21373358	0.21373358	-1.1522747	1.1522747
6	DF6	DF	-0.11171731	0.11171731	-1.10212869	1.10212869
7	DF7	DF	-0.09247612	0.09247612	-0.97330199	0.97330199
8	DF8	DF	-2.2280827	2.2280827	3.39619366	-3.39619366
9	DF9	DF	-0.54037639	0.54037639	-0.81663542	0.81663542
10	DF10	DF	-0.81057394	0.81057394	-1.27306743	1.27306743
11	DF11	DF	0.85162626	-0.85162626	-2.31388995	2.31388995
12	DF12	DF	-0.03320437	0.03320437	-1.47930307	1.47930307
13	DF13	DF	-0.30488024	0.30488024	-1.46554819	1.46554819
14	DF14	DF	1.32387799	-1.32387799	-1.10130763	1.10130763
15	DF15	DF	-1.24020552	1.24020552	-1.36763626	1.36763626
16	DF16	DF	-0.43266986	0.43266986	-1.77325787	1.77325787
17	DF17	DF	0.13975797	-0.13975797	-0.59293808	0.59293808
18	DF18	DF	-0.24398934	0.24398934	-0.89182265	0.89182265
19	DF19	DF	1.36814899	-1.36814899	-1.38391858	1.38391858
20	DF20	DF	1.19945571	-1.19945571	-1.52056675	1.52056675
21	DF21	DF	0.89366409	-0.89366409	0.58575192	-0.58575192
22	DF22	DF	0.21650463	-0.21650463	-0.18167099	0.18167099
23	DF23	DF	0.29240422	-0.29240422	0.98185199	-0.98185199
24	DF24	DF	0.8679832	-0.8679832	1.19137543	-1.19137543
25	DF25	DF	1.323033	-1.323033	0.95443335	-0.95443335
26	DF26	DF	1.49730382	-1.49730382	1.36189721	-1.36189721
27	DF27	DF	0.48655989	-0.48655989	-0.01081369	0.01081369
28	DF28	DF	0.75686086	-0.75686086	1.58578206	-1.58578206
29	DF29	DF	-0.87579286	0.87579286	0.63975952	-0.63975952
30	DF30	DF	0.50395197	-0.50395197	1.0678186	-1.0678186
31	DF31	DF	0.66808015	-0.66808015	-1.33606486	1.33606486
32	DF32	DF	0.36554063	-0.36554063	0.66335178	-0.66335178
33	DF33	DF	-0.35350703	0.35350703	2.18677051	-2.18677051
34	DF34	DF	-0.25262058	0.25262058	0.20201461	-0.20201461
35	A1a	A	-2.66243726	2.66243726	3.72612168	-3.72612168
36	A1b	A	-1.44545692	1.44545692	-1.6580758	1.6580758
37	A2a	A	-1.05709309	1.05709309	-0.99853938	0.99853938
38	A2b	A	1.46246159	-1.46246159	1.62584519	-1.62584519
39	A3	A	-3.84653671	3.84653671	4.36374653	-4.36374653
40	A4	A	-4.31641487	4.31641487	-4.48527452	4.48527452
41	A5	A	-1.84465339	1.84465339	3.51819599	-3.51819599
42	A6	A	-2.28251499	2.28251499	-2.53652727	2.53652727
43	A7	A	-3.2143931	3.2143931	4.05745584	-4.05745584
44	A8	A	-2.33297496	2.33297496	1.3281546	-1.3281546
45	B1a	B	1.29685872	-1.29685872	0.35919695	-0.35919695
46	B1b	B	-0.3514749	0.3514749	0.84100635	-0.84100635
47	B2	B	2.36315001	-2.36315001	0.25901776	-0.25901776
48	C1	C	3.6369091	-3.6369091	0.45051702	-0.45051702
49	C2a	C	2.31681079	-2.31681079	-1.69780545	1.69780545
50	C2b	C	2.51568064	-2.51568064	3.20311021	-3.20311021

51	C3	C	-1.23749272	1.23749272	-1.63109505	1.63109505
52	E1	E	-0.02760789	0.02760789	-0.63030745	0.63030745
53	E2	E	0.31812499	-0.31812499	0.42864654	-0.42864654
54	E3	E	7.32235314	-7.32235314	1.78531883	-1.78531883
55	E4	E	-0.1526758	0.1526758	-0.84854948	0.84854948
56	E5	E	-0.40757343	0.40757343	-0.66115517	0.66115517

ExtraPCANew

Element	PC1F	PC1	PC2F	PC2	PC3F	PC3	PC4F	PC4	PC5F	PC5
Al	0.13660612	-0.13660612	-0.4183793	0.4183793	-0.3382135	3.38E-01	0.18203386	-0.18203386	-0.49458888	0.49458888
Ba	-0.36841827	0.36841827	-0.2412894	0.2412894	0.2804413	-2.80E-01	-0.35196219	0.35196219	0.40644211	-0.40644211
Ca	-0.31212512	0.31212512	0.3562948	-0.3562948	-0.3361704	3.36E-01	0.11114952	-0.11114952	-0.05468395	0.05468395
Fe	-0.30873281	0.30873281	-0.4290178	0.4290178	5.40E-05	-5.40E-05	-0.14612716	0.14612716	0.02241856	-0.02241856
K	-0.02382462	0.02382462	-0.4625234	0.4625234	-0.2546468	2.55E-01	-0.08219364	0.08219364	0.15401911	-0.15401911
Mg	-0.39505288	0.39505288	0.2213042	-0.2213042	-0.300278	3.00E-01	0.2497503	-0.2497503	0.40900433	-0.40900433
Mn	-0.3908589	0.3908589	-0.2632697	0.2632697	0.347742	-3.48E-01	0.13308728	-0.13308728	-0.27402697	0.27402697
P	-0.2025794	0.2025794	0.2559614	-0.2559614	-0.218725	2.19E-01	-0.78513116	0.78513116	-0.39671529	0.39671529
Si	0.47161953	-0.47161953	0.0780635	-0.0780635	0.3307166	-3.31E-01	-0.23919247	0.23919247	0.17324375	-0.17324375
Ti	0.28284314	-0.28284314	-0.2278408	0.2278408	-0.510689	5.11E-01	-0.22088849	0.22088849	0.36496589	-0.36496589